Flow Measurement Concepts applied to Silicon Sensors

Dissertation

submitted to the Faculty of Sciences, University of Neuchâtel
to obtain the degree of Doctor of Science

by

Appo J. van der Wiel

Institute of Microtechnology
University of Neuchâtel
Rue A.L. Breguet 2
CH 2000 Neuchâtel
Switzerland

1994

IMPRIMATUR POUR LA THÈSE

Flow Measurement Concepts applied to Silicon Sensors

de Monsieur Appolonius van der Wiel

UNIVERSITÉ DE NEUCHÂTEL

FACULTÉ DES SCIENCES

La Faculté des sciences de l'Université de Neuchâtel
sur le rapport des membres du jury,

Messieurs N.F. de Rooij, M. Degrauwe,
J.H. Huising (Delft) et A.C. Hoogerwerf
(Micronas Semiconductor, Bevaix)

autorise l'impression de la présente thèse.

Neuchâtel, le le 24 novembre 1994

Le doyen :

H.-H. Nägeli

In remembrance of

Gersom and Eliëzer

the sons of Moses

To my parents,

my sisters

and

Hetta

Printed by
'Trias College'
Leeuwarden, The Netherlands

CONTENTS

POSTULATES

Orifice flow sensors for gases can neither be regarded as volume-flow nor as mass-flow sensors.

Silicon hot-wire flow sensors need temperature compensation.

Calorimetric and Coriolis flow sensors form Wheatstone bridges in respectively the thermal and mechanical domain.

Calorimetric flow sensors measuring the ratio of the fluid heat transport and the heat conduction in the tube, suppress the influence of boundary layers entirely.

Silicon flow sensors provide a much better matching of heat flows than conventional flow sensors, due to the precision of micro-machining.

Application of a constant supply for the reference quantity in a thermal Sigma-Delta converter suppresses cross-talk in the thermal feedback loop.

The modern Dutch Psalter is far more similar to the original version that Calvin published in 1562, than the one used in Switzerland today.

In the canton of Neuchâtel cycle paths end where you start to need them.

'Publier ou oublier' That's the question when unexpected results appear.

1 INTRODUCTION

The objective of this thesis is the analysis and application of flow measurement concepts that are essential for successful production of silicon mass-flow sensors for biomedical, automotive and domestic applications.
Flow monitoring and flow control is rapidly gaining importance in many fields. In the biomedical field a strong demand for cheap disposable sensors is present since sterilisation of used medical equipment is expensive. The automotive industry is a second field where it is necessary to measure the air and fuel flow for optimal engine performance. A third field for flow control is the market for domestic apparatus such as dishwashers, washing machines, air conditioning systems or water supply systems. Hence, a strong potential exists for flow sensors to monitor and control gas and liquid flows for biomedical, automotive and domestic applications.
The flow sensors for the applications mentioned above have to be produced in large quantities for low prices, since they are either disposable or they only form a small part of a total product: The production costs of disposable sensors have to be less expensive than the sterilisation of a sensor, whereas the production costs of a car or dishwasher cannot be increased by several percent because of the addition of one flow sensor. IC-technology offers a production method to produce low-cost electrical circuits in large quantities on silicon wafers. Hence, sensor design based on IC-technology enables the production of low-cost silicon sensors in large quantities. Furthermore, electronics can be integrated on-chip if the production process of the sensor is compatible with a process for integrated circuits. However, despite the wide applicability of flow sensors, low-cost silicon realisations of flow sensors are hardly available on the market today, although silicon sensors for monitoring and control of temperature, time, voltage and pressure are widely spread.
In this thesis, the influence of fluid pressure and ambient temperature is regarded as the main difficulty to realise silicon flow sensors. So far, this subject was not treated as a basic design constraint for silicon flow sensors. Focusing on this constraint, three measurement principles were investigated by realisation, characterisation and comparison of two thermal sensors and a novel bi-directional mechanical sensor. Furthermore, as nowadays digital read-out is almost indispensable, it is applied to all sensors as the basic sensor output.
The art of flow measurement embodies the conversion of the magnitude of a flow into an information signal *and* the comparison of this signal with a reference. Flow is defined as an amount of matter that traverses a cross-section per unit time. Examples of matter are mass, heat and electrical charge which respectively result in mass flow (kg/sec), heat flow (J/sec) and current (Coulomb/sec). Although volumetric flow (m^3/sec) is a unit that is commonly used to calibrate gas and liquid flow meters, volume is not a matter that flows.

Volumetric flow refers indirectly to an amount of fluid that is determined by its mass or the number of molecules that traverses. The relation between volumetric flow and mass flow is given by the density (kg/m^3). Hence, the density of the fluid is an indispensable constant to interpret volumetric flow. So, in this thesis we refer directly to the mass of the fluid that traversed the sensor and sensor responses are depicted as function of a mass flow.
A flow meter or flow sensor is a device that converts the magnitude of a mass flow into an information signal. So, a flow sensor is a transducer which produces an information signal as function of the magnitude of the flow. The transfer function describes the relation between the input, the magnitude of flow, and the output, the information signal, of the sensor. This output can be visual, electric, thermal or otherwise: The level of a float in a vertical conic glass tube of a rotameter is a visual sign of flow, as well as the level of a river. A thermal indication of air flow is obtained by putting a wetted finger in the air and electric or digital read-out is offered by many industrial flow sensors.
Conversion of the magnitude of flow into an information signal is only one part of measuring flow. Comparing this signal with a reference has to be executed in order to obtain a certain value for the flow. A pole in the river with painted marks of former levels is such a reference, as well as the ruler on the conic tube of the rotameter. In this way a quantitative value of the actual flow is obtained by comparing the information signal with the reference scale. This scale was calibrated before by marking the reference scale for known flows. Hence, the sensor compares the actual flow with reference flows which were applied to the sensor before.
After one is able to measure flow, one can proceed to regulate flow, as flow control is based on flow measurement. Locks are built in rivers to regulate the water level, but the essential action for this regulation is taking the reading from the measurement pole. One closes or opens the lock only when the level of the river is higher or lower than the required level which is indicated by a mark on the measurement pole. In general, the actual flow value is indicated by the output of the sensor, whereas the required flow value is indicated by a fixed point on the reference scale. The difference between this point and the actual value is defined as the error signal. Control is realised by an actuator that changes the flow in such a way that the error signal is minimised and the flow is under control when the sensor signal equals the required value on the reference scale. An example of such an actuator is the lock in the river and in general, flow controllers consist of a flow sensor in connection with a pump or regulation valve.

1.1 Concepts of Flow Measurement

This section focuses on the conversion of the magnitude of a flow into an information signal. This results in a classification for sensors that distinguishes direct measurement from indirect measurement. Intrinsic compensation is introduced as compensation method for errors which is effected by the sensor construction.

1.1.1 Direct and Indirect Measurement

The most important difference between flow and quantities like voltage, pressure and temperature, is that for the latter the output is measured directly, whereas flow has to be measured indirectly by means of another quantity. Indirect measurement is defined as measurement of a quantity by means of an intermediate quantity with different units, which is not used as the final information carrier. Indirect sensors are also called 'tandem transducers', since two conversions are used in tandem [15]. The following example illustrates the indirect way of flow measurement: Going outdoors without a coat directly gives an indication of the outside temperature. However, one has to use a wetted finger as an indirect sensor to determine the direction and force of a light breeze which causes a certain *cooling* of the finger. Hence, the cooling is used as a measure for flow and our temperature scale is 're-calibrated' as a scale for wind. Indirect measurement can be formalised by defining x the quantity to be measured, y the information carrier and z the intermediate quantity. Figure 1.1 shows a block diagram of an indirect sensor with the transfer functions f and g. Each transfer function consists of two functional blocks, the sensitivity function S and the bias function O (offset). The sum of these functions determines the magnitude of the output quantity. The functions S and O are basically different, since O is independent of the input quantity whereas S equals zero when the input quantity is zero. Therefore, S defines the modulation of the input quantity, whereas O defines its bias component.

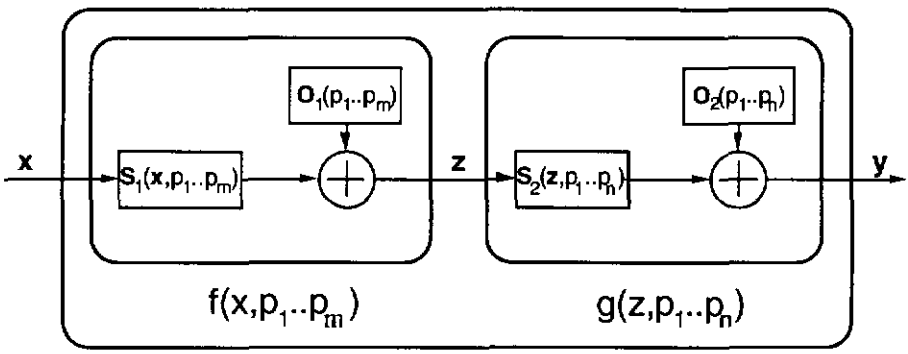

Figure 1.1: General block diagram of an indirect sensor with x the input quantity, z the intermediate quantity, y the output signal and $p_{1..}p_{m,n}$ the perturbing quantities.

The output of most sensors depends on perturbing quantities such as ambient temperature and fluid pressure. These quantities are denoted by $p_{1..m,n}$. The functions f and g are differently affected by the perturbations as these functions are based on different physical functions. Therefore, each function has its own set of disturbing quantities as is indicated by equation 1.1.

$$\textit{direct:} \quad y = f(x, p_1.. p_m)$$

$$\textit{indirect:} \quad y = g(z, p_1.. p_n) = g\big(f(x, p_1.. p_m), p_1.. p_n\big) \tag{1.1}$$

Indirect sensors normally have a smaller measurement range and suffer more from (offset) drift than direct sensors. Smaller measurement ranges are due to the fact that the output range of the first sensor function is normally different from the input range of the second one. Only when they are the same, measurement ranges comparable with sensors based on direct measurement can be achieved. E.g.: The force and direction of a storm has to be measured by leaning against the wind, since the method with the finger fails because it will be cooling at all sides due to turbulence. Nevertheless, the temperature sensing would still be accurate. More drift is expected by the fact that the two sensor functions are affected by different parasitic quantities or in different way by a same parasitic quantity. The reason is that the functions f and g are based on different physical principles and the offset of the first function is added to the offset of the second one.
Table 1.1 shows commercially available flow meters and lists the intermediate quantities and the measurement ranges of these sensors for which an accuracy of better than 1 % is realised.

Principle	*Sensor*	*Intermediate quantity*	*measurement range*
Mechanical	*Oval gear flow meter* *Paddle wheel sensor*	*none, direct sensor* *pressure drop*	*1:100* *1:10*
Hall effect	*Magnetic flow sensor*	*none, direct sensor*	*1:100*
Doppler effect	*Acoustic flow sensor*	*frequency shift of an ultrasonic wave*	*1:20*
Navier-Stokes	*Vortex meter* *Hot-wire sensor*	*resonating drag force* *heat convection and drag forces*	*1:10* *1:20*
Bernoulli	*Orifice flow meter* *Rotameter*	*pressure drop* *pressure drop, gravity and drag forces*	*1:10* *1:10*
Coriolis effect	*Coriolis mass-flow meter*	*differential resonance phase shift*	*1:100*
Calorimetric	*Thermal mass-flow meter*	*differential temperature shift*	*1:50*

Table 1.1: Principles of commercially available flow meters listing the intermediate quantity and the 1% resolution measurement range [13,21].

The measurement range of the flow meters based on direct measurement, the magnetic and the oval gear flow meter, are at least 5 times larger than the flow meters based on indirect measurement, except for the Coriolis and the calorimetric mass-flow meter. Hence, direct measurement for flow is in

principle better than indirect measurement. However, the two direct flow meters cannot be applied always, since oval gear flow meters are relatively slow and magnetic flow meters only work when the fluid has a certain electrical conductivity. The exceptional large measurement range of the Coriolis mass-flow meter and the calorimetric mass-flow meter is given by their differential measurement arrangement which results in an intrinsic compensation for parasitic quantities like ambient temperature. The next section discusses the common basic concept behind these high performance indirect mass-flow sensors.

1.1.2 Intrinsic Compensation

The Coriolis and the calorimetric mass-flow meter show much better performance than the other indirect flow sensors listed in table 1.1. Although these sensors are based on different physical phenomena, the excellent performance of both is based on differential measurement of the intermediate quantity with two carefully matched sensors exposed to exactly the same flow.
Figure 1.2 shows the Coriolis measurement principle, which used in high precision mass-flow meters that appeared on the market around 1977 [21]. The sensor basically consists of an u-shaped tube which is clamped to a rigid base. An actuator impels a harmonic oscillation on the top-side of the tube, perpendicular to the plane of the tube and therefore the displacement sensors will oscillate exactly in phase in case no flow is present. However, when a flow is present, the tube twists because of opposite Coriolis forces caused by the moving fluid upstream and downstream from the actuator. Hence, one sensor will lead the resonance frequency whereas the other will lag. This results in a delay Δt between the two sensor signals which therefore becomes a measure for the mass-flow.

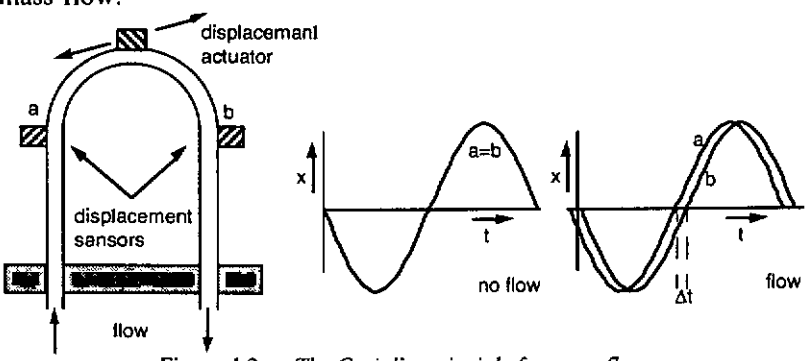

Figure 1.2: The Coriolis principle for mass-flow.

Figure 1.3 shows the calorimetric measurement principle used in high precision thermal mass-flow controllers which were introduced to the market in the early seventies. This sensor also consists of a u-shaped tube which is clamped to a metal base to force a same ambient temperature to both ends of the tube and the fluid.

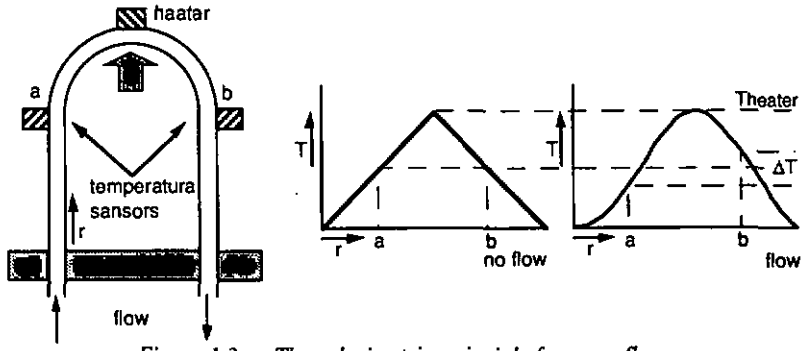

Figure 1.3: The calorimetric principle for mass-flow.

The top-side of the tube is heated and a constant temperature gradient is created towards both ends of the tube. However, when a flow is present, the temperature upstream from the heater will drop, since heat flows from the heated tube into the cold fluid. The temperature downstream from the heater will increase, since the now heated fluid gives heat away to the tube. Hence, the temperature shift ΔT between the two sensor signals becomes a direct measure for the mass-flow. Direct measurement of ΔT is applied in the Liqui-flow controller of Bronkhorst High-Tech which was introduced on the market in 1993. In this sensor ΔT is measured by a series of thermocouples between *a* and *b* .

Although the physical backgrounds of the Coriolis and the calorimetric flow meter are completely different, their similarity is striking. Both flow meters consist of a tube without obstructions containing two sensors which are mounted upstream and downstream from the actuator which is placed at the middle of the tube. Furthermore, both tube ends are fixed to a solid construction which insures that the flow conditions at the tube exit equal the conditions at the entrance.

The success of these flow meters is based on the fact that the flow modulates the intermediate quantity upstream and downstream from the actuator with the same amplitude, *but with opposite sign*. In this way the intermediate quantities z_{up} and z_{down} are formed which have an equal bias component z_o but an opposite signal component Δz which is caused by the flow x. Hence, differential measurement of the two signals results in cancelling of the common bias component z_o. Therefore all dependencies of parasitic quantities are cancelled as shown in equation 1.2 with O_1 and S_1 referring to the model presented in figure 1.1:

$$z_{up} = f_{up}(x) = O_1 - S_1(x) = z_o - \Delta z(x)$$

$$z_{down} = f_{down}(x) = O_1 + S_1(x) = z_o + \Delta z(x) \qquad (1.2)$$

$$y = g\left(z_{down} - z_{up}\right) = g\left(2 \cdot S_1(x)\right) = g\left(2\Delta z(x)\right)$$

Now the expected high level of offset and drift, which is normally introduced by application of indirect measurement is effectively suppressed. This compensation can be defined as *intrinsic* compensation, as it is entirely effected by the intermediate quantity and not by modulation of the sensor output signal.

1.2 Concepts of Signal Conditioning

Measurement of a quantity consists of converting its magnitude into an information carrier and comparing it with a reference scale. Whereas the *conversion* of a magnitude of a quantity into a sensor output signal was discussed in the previous section, this section focuses on the *comparison* of the magnitude of a quantity with a reference. This comparison is a crucial design consideration for successful sensor development [4]. Distinction between absolute and relative measurement leads to differential measurement which cancels drift and offset effectively by the use of an active reference source. Application of differential measurement in Sigma-Delta converters results in two practical circuits for silicon sensors, which offer digital sensor read-out.

1.2.1 Absolute and Relative Measurement

An absolute way and a relative way of comparing a measured quantity with a reference are distinguished. The precision of absolute measurement is determined by the stability and invariance of the sensor function, whereas relative measurement depends on the stability of the reference. Relative measurement is often preferred since stable references can be implemented more easily than stable transfer functions.
Absolute measurement is defined as the comparison of the information signal with a reference scale that once had been calibrated in units of the measured quantity. An example of an absolute measurement instrument is the analog voltmeter that converts the measured voltage into an angle of the indicator. The sensitivity factor of such a voltmeter can be expressed in V/rad. The accuracy of this absolute measurement is given by the stability of this factor. Position of the meter and the temperature dependence of the spring constant or magnetic flux affect the precision of the measurement. For proper operation, the conditions of the meter have to equal the conditions during calibration.
Relative measurement is defined as the comparison of two information signals that are generated at the same time and where one signal serves as reference. The signals and their difference have the same dimension and determination of the ratio of these signals results in a dimensionless number. An example of a relative measurement instrument is the digital voltmeter which compares the charging time of a capacitor with the discharging time that are respectively a function of the input voltage and the internal reference voltage. The input voltage and the reference voltage are both converted to an information signal of the same dimension (time) at the same time by one sensor or two carefully matched sensors. Now a change in the measurement conditions becomes a common mode effect for both the signal *and* the reference. Therefore the precision is entirely determined by the stability of the reference voltage.

1.2.2 Differential Measurement

When the output of a relative sensor is affected by a perturbing quantity like ambient temperature, compensation can be achieved by using an active reference which is perturbed in the same manner as the sensor output. Although

realisation of active reference sources might seem difficult, such reference sources are normally formed by a complementary sensor which is either not affected by the quantity to be measured or affected in the opposite way. The use of complementary signal sources is called differential measurement since subtraction of the two sensor signals gives the information signal by elimination of the common mode bias components of the sensor. Furthermore the sensitivity is doubled when the complementary sensor has the opposite sensitivity in respect with the first one. One of the best examples of such differential measurement is the Wheatstone bridge.
Figure 1.4 illustrates the differences of absolute, relative and differential measurement based on temperature dependent piezoresistors, which are commonly used for silicon pressure sensors. The quantity to be measured is the pressure P and the perturbing quantity is the ambient temperature T. Now R(P,T) and R(-P,T) define piezoresistors which resistivity respectively increase and decrease with pressure. The resistors have the same temperature dependence and a same absolute piezoresistive effect. For reasons of simplicity the assumption is made that the piezoresistivity of the resistors does not depend on temperature. Therefore R(P,T) and R(-P,T) can be decomposed as $R_o(T)+\Delta R(P)$ and $R_o(T)-\Delta R(P)$, as shown in figure 1.1. R_o defines the bias component O and ΔR the sensitivity S.

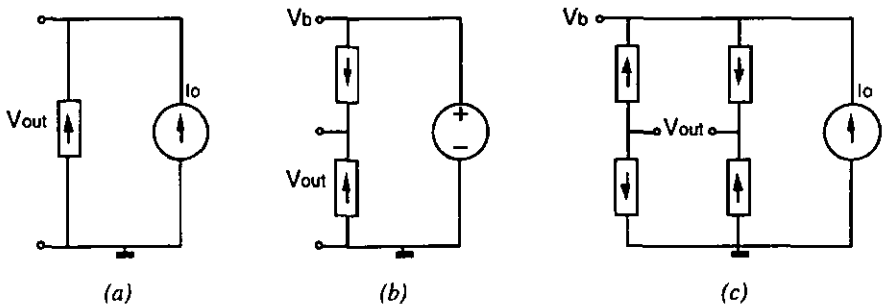

Figure 1.4: (a) Absolute measurement (b) Relative measurement with a passive reference (c) Differential measurement.

Figure 1.4a shows an absolute sensor with one piezoresistor which is supplied by a constant current and its sensor output V_{out} is given by equation 1.3:

$$V_{out} = I_o \cdot (R_o(T) + \Delta R(P)) \qquad (1.3)$$

The signal $\Delta R(P)$ is added to a bias component $R_o(T)$. For silicon piezoresistors ΔR is normally smaller than 3 % of R_o in order to have a linear transfer function. However, the temperature dependence of such resistors is at least 0.18 %/°C and therefore a 15 °C increase in ambient temperature has the same effect as applying the maximum pressure. Hence, this absolute sensor is not of practical importance. The bias component cannot be kept constant by using a temperature dependent current source, since the sensitivity is linear proportional to the current source. Hence, the temperature dependence of the bias component would be transferred to the sensitivity.
Figure 1.4b shows a sensor based on relative measurement with a passive

reference V_b. This measurement is called relative since the sensor output V_{out} is compared with the passive reference V_b which is generated at the same time. V_{out} is given by equation 1.4:

$$V_{out} = \left(1 + \frac{\Delta R(P)}{R_o(T)}\right) \cdot \frac{V_b}{2} \qquad (1.4)$$

Here, the signal component is added to a temperature independent bias component $V_b/2$. Therefore, this bias component does not change with ambient temperature. Although the bias component is temperature independent, the sensitivity is not, since it is inversely proportional to $R_o(T)$, which is temperature dependent. The sensor can still not be used over a wide temperature range since it has a temperature dependent sensitivity. Again, in this case application of a temperature dependent voltage source cannot be used, since it would cause a large temperature drift of the bias component.
Figure 1.4c shows the Wheatstone bridge as differential measurement method which is normally used for silicon pressure sensors. The total bridge consists of two complementary sensors as shown in figure 1.4b and they are supplied with the same bridge voltage V_b. Here, differential measurement is applied since two voltages are compared which have an opposite pressure dependence. A current source is used in order to create an active reference voltage $V_b = R_o(T) \cdot I_o$ which depends on the bridge resistance $R_o(T)$. In this way V_b depends in exactly the same way on temperature as the piezoresistors, even when the temperature dependence is non-linear. Equation 1.5 shows the Wheatstone bridge transfer function:

$$V_{out} = \left(\frac{\Delta R(P)}{R_o(T)}\right) \cdot V_b = \Delta R(P) \cdot I_o \qquad (1.5)$$

V_{out} only depends on the pressure dependence of the resistors and no bias component is present. For reasons of simplicity it was assumed that the piezo resistivity of the resistors is independent of temperature, which is normally not the case. However, the use of a temperature dependent current source can compensate for such a temperature dependent sensitivity. Note that the success of differential measurement depends on carefully matching the bias components of the two sensors, since the perturbing quantities have to affect the complementary sensors in exactly the same way to achieve total compensation.
The example above illustrates differential measurement with a Wheatstone bridge of electrical resistors that are pressure dependent. However, Wheatstone bridges can also be constructed with other kind of resistors and conductors. Figure 1.3 described the calorimetric flow meter as a sensor based on differential measurement. This flow meter consists of two complementary sensors, that are separated by the heater in the middle of the tube: The first sensor is formed by the tube section upstream from the heater, whereas the second sensor is formed by the tube section downstream from the heater. Each sensor consists of two equal heat conductors in series that acts as a temperature divider for the heater temperature and the temperature across the colder

conductor forms the sensor information signal. Hence, each sensor has an output temperature which has a bias temperature of half the heater temperature and is modulated by flow. So, the calorimetric mass-flow meter can be regarded as a chain of four equal heat conductors. A constant temperature is kept between the middle of the chain and both the chain ends. The temperature difference between one quarter and three quarters is the output temperature, which is modulated by flow. Hence, this sensor can be regarded as a thermal Wheatstone bridge. In the same way, the Coriolis mass-flow meter, which is depicted in figure 1.2, can be regarded as a Wheatstone bridge with a mechanical oscillation as bridge actuator.
From the illustrations above it is concluded that not only the physical conversion of a quantity into a information signal is important as discussed in 1.1, but that the way of comparing the sensor signal with the reference is crucial also. The next section describes two Sigma-Delta converters which are based on differential measurement and give a robust digital output. The first converter was built and successfully applied not only for the sensors described in this thesis, but also for standard pressure sensors produced by ASCOM Microelectronics.

1.2.3 Sigma-Delta conversion

With the increasing demand for digital sensor read-out, Sigma-Delta conversion becomes more and more important, since it has several advantages above the application of other A/D converters. Conventional A/D converters can be regarded as an amplifier or a voltmeter. They read the information signal from the sensor, but do not interact with the sensor. Therefore, they form a separate function block in the system with only an incoming signal from the sensor. In contrast, Sigma-Delta converters are a part of the sensor function since they act as a feedback amplifier for the sensor output. Hence, Sigma-Delta conversion normally results in a much more robust sensor signal than is provided by A/D converters [5].
Equation 1.5 shows that the output voltage of a Wheatstone bridge is given by the *difference* of the bridge resistors divided by the total bridge resistance in case the bridge is supplied with a constant voltage. A similar method is shown in figure 1.5a which depicts a circuit that measures the *ratio* of two resistors. By application of feedback, the voltages $I_2 \cdot R_{up}$ and $I_1 \cdot R_{down}$ are kept at V_{ref} by means of two current amplifiers, which results in the following equation:

$$\frac{R_{up}}{R_{down}} = \frac{I_1}{I_2} \tag{1.6}$$

Figure 1.5b represents an implementation of equation 1.6 which is based on Sigma-Delta conversion. The voltage across R_{down} is kept at the reference voltage $I_o \cdot R_{up}$ by means of the current switch and the capacitor. When the voltage across R_{down} is not high enough, the comparator becomes high and the current $2 \cdot I_o$ is switched on, whereas the current is switched off when the comparator has become low again. The switching is synchronised with the clock by using a D flip-flop. The clock is transmitted to the output F_1, when the

current is switched on, and otherwise to F_2. Hence, F_1 expresses the number of pulses per second when current is fed to R_{down}, whereas F_2 expresses the number of pulses when no current is fed to R_{down}. F_{clock} expresses the total number of clock pulses per second and can be written as $F_1 + F_2$. If the switch current is twice the current through R_{up}, F_1 equals F_2 when R_{down} equals R_{up} and the following expression can be derived:

$$I_o \cdot R_{up} = 2 \cdot I_o \cdot R_{down} \cdot \frac{F_1}{F_{clock}} \tag{1.7}$$

The clock frequency is much higher than the relaxation frequency of the feedback loop. Therefore, the circuit acts as a pulse-width modulator and for high clock frequencies, the clock does not affect the linear transfer function.

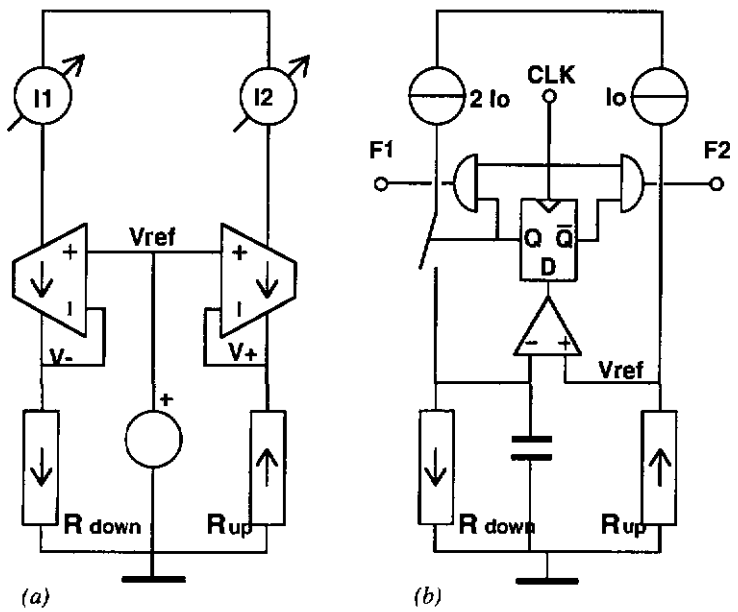

Figure 1.5: Analog and digital circuit to determine the ratio of two piezoresistors.

The frequencies are expressed as the number of pulses per second. However, F_2 will have produced N pulses in a certain time period T. Hence, F_2 equals N/T, F_1 equals (N+S)/T and F_{clock} equals (2N+S)/T, with S/T the difference of F_1 and F_2. Rearranging (1.7) and substitution of the above expressions results in the following expression:

$$\frac{R_{up}}{R_{down}} = \frac{N+S}{\left(N+\frac{S}{2}\right)} \tag{1.8}$$

Equation 1.8 can be approximated by equation 1.9 which shows a linear relation ship between the resistor ratio and S.

$$\frac{R_{up}}{R_{down}} = \frac{R_o + \Delta R}{R_o - \Delta R} \approx 1 + \frac{2\Delta R}{R_o} = 1 + \frac{S}{2 \cdot N} \Rightarrow \frac{\Delta R}{R_o} = \frac{S}{4 \cdot N} \qquad (1.9)$$

Figure 1.6 shows the difference between the approximation 1.9 and equation 1.8. The error is smaller than 0.1 % if R_{down} differs from R_{up} by less than 3%.

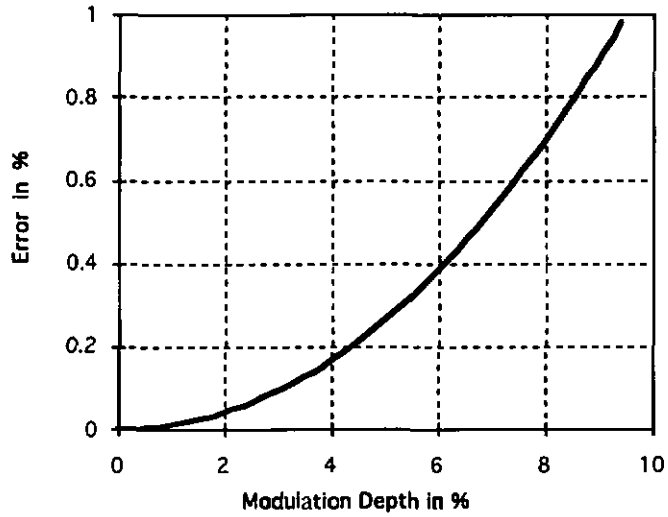

Figure 1.6: Non-linearity of the Sigma-Delta converter versus modulation depth.

Figure 1.7 depicts the circuit that was built to determine S in a very simple way.

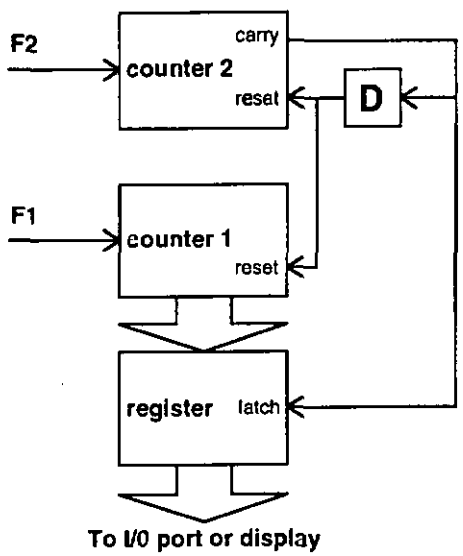

Figure 1.7: Low-cost circuit to determine the difference of two frequencies.

The lower frequency F_2 is fed to a n-bit counter, which gives a carry after N pulses. At this moment, the register or display is loaded with the value of

another n-bit counter, which is clocked by F_1. At the moment the counter of F_2 reaches N, the counter of F_1 should arrive at N+S, since F_1 is larger than F_2. However, it had reset itself already at N and therefore the value clocked into the register represents S directly. One delay after the carry signal got high, both counters are reset and a next value is measured immediately.Figure 1.7 depicts the circuit that was built to determine S in a very simple way. The lower frequency F_2 is fed to a n-bit counter, which gives a carry after N pulses. At this moment, the register or display is loaded with the value of another n-bit counter, which is clocked by F_1. At the moment the counter of F_2 reaches N, the counter of F_1 should arrive at N+S, since F_1 is larger than F_2. However, it had reset itself already at N and therefore the value clocked into the register represents S directly. One delay after the carry signal got high, both counters are reset and a next value is measured immediately.

The Sigma-Delta converter needs temperature compensation, since the signal output S is temperature dependent. S is proportional to the nominal resistance R_o, which typically shows a temperature dependence of at least 0.18 %/°C. Compensation cannot be achieved by modulation of the current I_o and the reference voltage V_{ref}, since they do not appear in the transfer function. Hence, external compensation has to be carried out, although this circuit has the advantage that the transfer function is independent of the supply voltage and drift of the current sources. Compensation is easily achieved by multiplication of S by a number that represents R_o, since S has already a digital representation. A Sigma-Delta converter that can compensate for ambient temperature, is presented in figure 1.8. The circuit produces not only the number S, representing the resistors ratio, but also the number G, representing the conductance $1/R_o$.

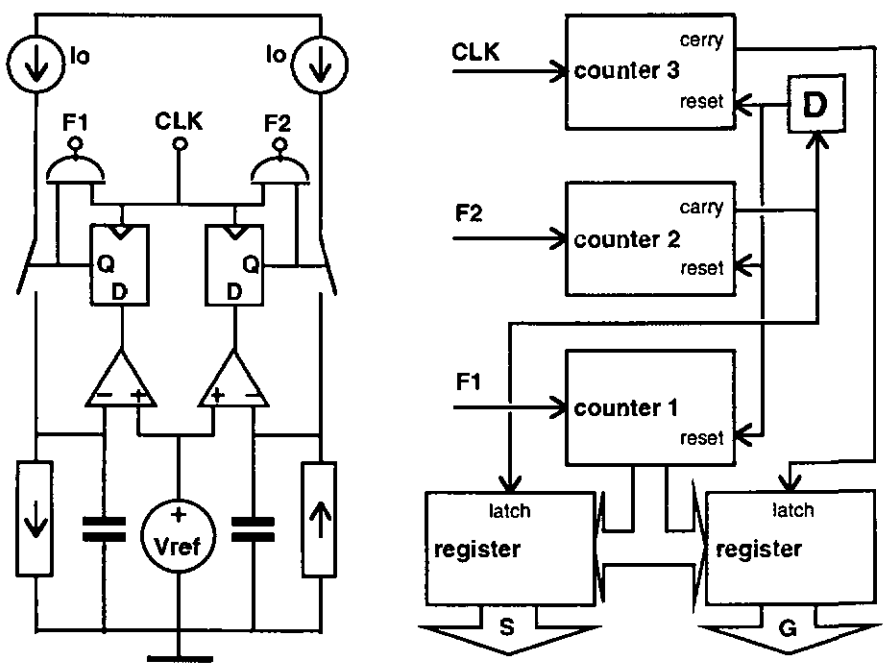

Figure 1.8: Sigma-Delta configuration which offers the ratio S of two sensing resistors and the number G which represents the conductance of one of these resistors.

In a similar way as before, the following relations can be found with N the number of pulses which triggers the carry of the counter for F_2:

$$\frac{R_{up}}{R_{down}} = 1 + \frac{2 \cdot \Delta R}{R_{down}} = 1 + \frac{S}{N} \Rightarrow \frac{\Delta R}{R_{down}} = \frac{S}{2 \cdot N}$$
$$R_{down} = \frac{V_{ref} \cdot N}{I_o \cdot G} \qquad (1.10)$$

Substitution of R_{down} in the upper equation results in the following expression for ΔR, which is independent of the ambient temperature:

$$\Delta R = \frac{S}{2 \cdot G} \cdot \frac{V_{ref}}{I_o} \qquad (1.11)$$

Expression 1.11 shows that the difference of the resistors is linear proportional to S and that the output is corrected for perturbing influences by G. Furthermore, the relation between S and ΔR is exact and no approximation is made. Hence, equation 1.11 is also valid if ΔR is much larger than 3 % of R_o. Note that the sensitivity can be set by trimming the ratio V_{ref}/I_o. Furthermore, the circuit becomes independent of the supply voltage in case V_{ref} is made linear proportional to I_o.

1.3 Realisation of Silicon Flow Sensors

To build silicon sensors that are more successful than conventional sensors, one has to fully exploit the advantages of IC-technology. By using this technology, sensors can be made very small, the sensor dimensions can be controlled extremely well, the sensor output is always electrical and signal conditioning can be integrated on-chip.
Small dimensions are required for biomedical sensors that are used on catheter tips. Catheters basically consist of a 1 - 3 mm thick flexible tubes, that can be moved through a blood channel in living bodies. They are used in hospitals to monitor temperature, blood pressure and gas concentrations of patients during operations or medical examinations. A flow sensor mounted on a catheter tip, acts as a probe, and the sensor has to monitor the flow which is outside the sensor. Such flow sensor should be very small, should have a minimum of electrical contacts and has to monitor flow outside the sensor. These requirements were achieved by the realisation of a silicon flow sensor which measures 2.0 x 1.5 x 0.4 mm only. The functioning of the chip was based on hot-wire principle. The chip contains a membrane which is aligned to the flow and is heated in the middle. Hence, a convective heat flow is established from this membrane into the fluid. This heat flow is modulated by the fluid velocity and the temperature of the membrane drops when a flow becomes present. This temperature drop is measured by on-chip temperature sensors.
The advantage of the excellent dimension control has been exploited by the realisation of the silicon calorimetric sensor. Conventional calorimetric flow

sensors consist of a small tube of stainless steel, which has a diameter of about 1 mm and a length of a few centimetres. The heat resistor and the temperature sensors are realised with platinum resistors that are wound around the tube. The positioning of these resistors determine the offset and offset drift of the sensor. However, the positioning of the temperature sensors and heating elements is precise within 2 μm for silicon sensors. Furthermore, the regulation circuit that is needed to bias calorimetric flow sensors, can be integrated on-chip, whereas these circuits occupy most volume of the package for conventional flow sensors. The silicon calorimetric sensor and the hot-wire sensor need typically 250 mW heating power for proper operation. Hence, a mechanical silicon sensor has been realised that only needs an operation power of less than 5 mW. This silicon sensor consists of two silicon cantilevers suspended in an orifice. These cantilevers bend when a flow is present. The bending is detected by piezoresistors integrated on the silicon cantilevers. Hence, the output of this sensor is a voltage, whereas conventional mechanical flow sensors always need additional sensors to obtain an electrical read-out.

1.4 Outline

The design, fabrication and characterisation of the three different silicon flow sensors are discussed in the next three chapters. The last chapter discusses the differences between the silicon sensors.

Chapter 2 describes the indirect bi-directional gas-flow sensor which measures the pressure drop across an orifice by means of two thin cantilevers suspended in that orifice. Piezoresistors integrated on the cantilevers provide the conversion from the pressure drop into the electrical domain. Based on Bernoulli's law, an analytic sensor model was found which describes the sensor response effectively. Characterisation was carried out for air flow at different pressures and ambient temperatures. Sigma-Delta modulation offered digital read-out and high resolution.

Chapter 3 describes the hot-wire flow sensor for liquids which measures the heat convection as function of the flow. On-chip diodes that serve as temperature sensors, provide the conversion from the thermal domain into an electrical signal. Based on King's law, an analytic sensor model was found which was in agreement with measurements taken with water flows up to 0.8 kg/sec in a test conduit with a diameter of 20 mm. Characterisation for ambient temperature was carried out in a narrow conduit with a diameter of 2 mm. Temperature compensation was achieved by differential measurement based on Sigma-Delta modulation that also offered digital read-out .

Chapter 4 describes the calorimetric flow sensor which measures a temperature distribution as function of the flow. Diodes provide the conversion from the thermal domain into an electrical signal and an on-chip feedback amplifier regulates the heater temperature to a constant value. An analytic sensor model was found which predicts a linear sensor response for small flows independent of boundary layers in the sensor tube. Characterisation for ambient temperature was carried out for both water and air. Differential measurement based on Sigma-Delta modulation offered digital read-out and temperature compensation by using two integrated heaters in a feedback configuration.

Chapter 5 not only discusses the different physical backgrounds of the sensors that are analysed, but also the concepts of measurement. Furthermore, possible applications are reviewed. The chapter closes with a summary of the results presented in this dissertation.

2 THE ORIFICE FLOW SENSOR

2.1 Introduction

Orifice flow sensors consist of an obstruction in a conduit. The aperture that remains in the conduit, is called orifice or venturi. When a flow is present, a pressure drop across this obstruction is created proportional to the magnitude of the flow. Detection of the pressure drop with an external pressure sensor results in a measure for flow. A well known example is the carburettor of a car engine. This device consists of a venturi in the air inlet of the engine and regulates the fuel injection. When air flows towards the cylinders, the pressure in the venturi becomes lower than the atmospheric pressure. This pressure difference pushes the fuel from the fuel reservoir, which is at atmospheric pressure, into the air stream through a conduit with a small sprinkler head. The amount of fuel is proportional to the pressure in the venturi. Hence, the air flow causes a pressure that determines the amount of fuel injected. Sensors that measure the pressure in the orifice are established as consumption meters or vacuum meters, although they can be regarded as air flow meters.
In this chapter an orifice flow sensor is presented which is formed by two 15 μm thin flexible cantilevers, suspended in an orifice. These cantilevers bend proportionally to the differential pressure that is caused by a flow perpendicular to these cantilevers. Integrated piezoresistors on these cantilevers directly detect this bending and internal connection of these resistors into a Wheatstone bridge configuration provides a differential sensor signal without using an external pressure sensor.
Not only the size of the orifice defines the sensor sensitivity, but also its shape. Hence, the orifice should have the same shape at both sides of the cantilevers in order to obtain the same sensitivity for both flow directions. Therefore, the silicon sensor consists of a sandwich of two symmetrical die, mounted face to face. Note, that in this way always a symmetrical orifice is formed which is independent of the shape of the aperture.
The fabrication of the sensor die was based on an industrial process. The sensor characterisation was performed with prototypes that were realised by gluing the sandwich of the symmetrical die to a standard ceramic substrate for pressure sensors. The sensor response showed excellent agreement with the sensor model which was based on Bernoulli's Law. The influence of ambient temperature and fluid pressure was investigated by using a Wheatstone bridge and a Sigma-Delta converter. It was found that the temperature dependence of the piezoresistors partially compensates for the temperature dependence of the transfer function which relates the pressure drop with a flow.

2.2 Principle

The physical background of the sensor is based on Bernoulli's Law, which is discussed in section 2.2.1. The relation between the sensor sensitivity and the sensor dimensions is discussed in section 2.2.2. This results in a directly applicable expression relating the change of the resistance with flow.

2.2.1 Bernoulli's Law

Bernoulli's Law gives the relationship between flow and the pressure drop in a venturi by considering the potential energy of the fluid traversing the venturi. The potential energy of a fluid is expressed by the static pressure which represents the kinetic energy of the fluid molecules that move in all directions. This energy is imposed by temperature. If the fluid flows in a certain direction, it gains kinetic energy in that direction and as a consequence, the kinetic energy in other directions decreases if no energy is added. Hence, the static pressure drops when a flow becomes present. Per unit volume this phenomena can be expressed by the following law of conservation:

$$P_{dyn} + \frac{1}{2}\rho \cdot u^2 = P_{stat} \qquad (2.1)$$

with p_{dyn} and p_{stat} the dynamic and static pressure, u the average velocity and ρ the density of the fluid. This equation can be applied to the sensor with u the fluid velocity in the orifice A, as shown in figure 2.1:

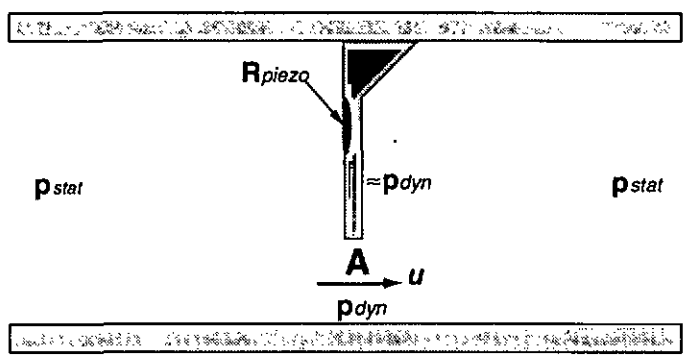

Figure 2.1 Schematic cross section of the silicon cantilever used as an orifice.

The velocity in front of the sensor can be neglected since the orifice diameter is much smaller than the tube diameter. Hence, the pressure difference ΔP between the static fluid pressure and the pressure in the orifice can be expressed as:

$$\Delta P = \frac{1}{2}\rho \cdot u^2 \qquad (2.2)$$

Rearranging 2.2 and substitution of the volumetric flow rate ϕ_v as the product of u and the orifice aperture A results in Bernoulli's Law:

$$\phi_v = A\sqrt{\frac{2 \cdot \Delta P}{\rho}} \tag{2.3}$$

An efficiency factor $\beta > 1$ has to be added to compensate for the Reynolds number and the shape and edges of the aperture [10]. This factor also takes into account the effect that the fluid densitity is not constant for compressable fluids. This constant is normally determined by measurement. When β equals 1, the pressure drop of the fluid is transferred into kinetic energy without any losses. However, normally the flow causes a smaller pressure drop than expected. For instance, the flow velocities parallel to the orifice are never zero and the pressure behind the cantilevers cannot reach the static pressure completely. The losses and the change of density are indicated by a value of β larger than 1.
The influence of the fluid pressure can be modelled by defining the density ρ as the product of the fluid pressure p_{stat} multiplied with the normal density ρ_o. Now equation (2.3) can be expressed in the following way:

$$\phi_v = \beta \cdot A\sqrt{\frac{2 \cdot \Delta P}{\rho_o \cdot P_{stat}}} \tag{2.4}$$

The pressure drop which is due to friction forces (Poiseuille friction) can be neglected, since the orifice edges are very thin. The friction between the fluid and these edges is too small to cause a significant pressure drop.

2.2.2 Sensor Sensitivity

The relation between the pressure drop and the bending of the sensor cantilever is discussed. A schematic sketch of the cantilever is depicted in figure 2.2. A hole is made in the cantilever at the side where it is clamped to the chip. In this way two bridges are formed which have a length a and a width b. Over the entire length of these bridges piezoresistors are realised, as the surface stress is the largest at the bridges.
The resistance change of the piezoresistors can be expressed as a function of the average surface stress σ_{avg} and the longitudinal piezoresistive constant π_l:

$$\frac{\Delta R}{R} = \pi_l \cdot \sigma_{avg} \tag{2.5}$$

The average stress at the surface of the two bridges can be expressed by the momentum M_x and thickness d as follows [24,30]:

$$\sigma_{avg} = \frac{1}{a}\int_0^a \frac{3 \cdot M_x}{b \cdot d^2} d(x) \tag{2.6}$$

As depicted in figure 2.2, the momentum M at x can be considered as the sum of three torque's, the torque T_a in a and the torque $(a\text{-}x)\cdot F_a$, both due to the pressure ΔP on the cantilever at the right side from a and the torque T_x due to ΔP on the

bridges at the right from x and at the left from a. Now the following linear relation for the momentum at x can be derived with c the cantilever length from the end of the bridges and e the cantilever width:

$$M_x = \Delta P \cdot \left(\frac{1}{2} e \cdot c^2 + e \cdot c \cdot (a - x) + b \cdot (a - x)^2 \right) \tag{2.7}$$

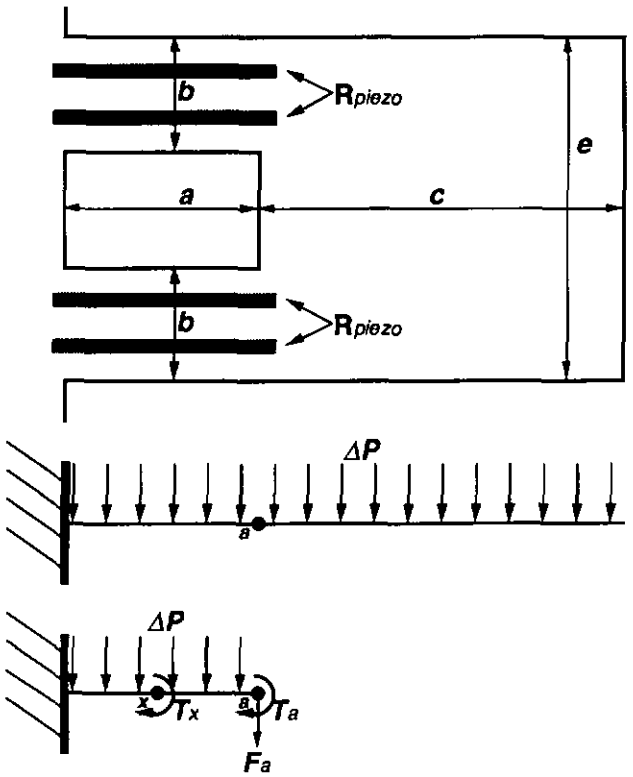

Figure 2.2 Top side of the silicon cantilever with the dimensions and the corresponding calculation model.

Substitution of equation 2.7 in equation 2.6 results after integrating in an equation for σ_{avg}. Now the relation between ΔR and ΔP is found in combination with equation 2.5. In combination with equation 2.4 the relation between ΔR and the flow is found which is shown in expression 2.8 for the volumetric flow ϕ_v and the mass flow ϕ_m with the number C depending on the cantilever dimensions:

$$\phi_v = \beta \cdot A \sqrt{\frac{C}{\pi_l \cdot \rho_o \cdot P_{stat}} \cdot \frac{\Delta R}{R}}$$

$$\phi_m = \rho_o \cdot P_{stat} \cdot \phi_v = \beta \cdot A \sqrt{\frac{C \cdot \rho_o \cdot P_{stat}}{\pi_l} \cdot \frac{\Delta R}{R}} \qquad \text{with} \tag{2.8}$$

$$C = \frac{4 \cdot b \cdot d^2}{3 \cdot c \cdot e \cdot (c + a) + 2 \cdot b \cdot a^2}$$

Although orifice flow sensors are known as volumetric flow meters, equation 2.8 shows that the square root of the fluid density appears in the expressions for both volumetric flow and mass flow. Hence, based on the principle, no preference can be found to define such sensors as either volumetric flow sensors or as mass flow sensors.

2.3 Realisation

The layout of the sensor die and the wafer are discussed in this section, as well as the wafer processing and the packaging. Section 2.3.1 presents the symmetric design which is optimised for high sensitivity combined with a high resonant frequency. Section 2.3.2 describes the wafer fabrication process which was based on a standard Micronas process. Section 2.3.3 describes the hybrid packaging which was based on a standard package for pressure sensors and was used for characterisation of the chip. The electrical interconnect was made by thick-film technology in combination with standard connectors for plastic tubing.

2.3.1 Design

The sensor die basically consists of a rectangular aperture of which one quarter is covered by a 15 µm thick cantilever which is clamped at one corner of the aperture. A hole in the cantilever is etched at the clamped side. In this way, two bridges form the connection between the rest of the cantilever and the chip rim. Now the surface stress becomes concentrated on these bridges during bending. Piezoresistors are implanted over the total length of these bridges in order to obtain a maximum sensor output, as well as a minimum influence of mismatch errors due to the fabrication process (See figure 2.2 for a schematic view).
The sensitivity of the device is determined by the constant C in equation 2.8 and it depends on sensor dimensions only. In order to obtain a stable flow around the cantilevers, oscillation of the cantilevers has to be avoided. Cantilevers with a high resonant frequency need more effort to oscillate than cantilevers with a low resonant frequency. Hence, the design was optimised for a high theoretical resonant frequency. Decreasing the bridge length c and the cantilever width e increases the resonant frequency, but decreases the sensitivity. However, the sensitivity can also be improved by minimising b. The minimum width for b is 100 µm, since each bridge contains two 30 µm wide piezoresistors that are separated with a distance of about 20 µm for isolation. In order to combine high sensitivity with a resonant frequency higher than 20 kHz, the following cantilever dimensions were chosen: a, b, 100 µm, c: 700 µm and e: 300 µm [24].
Figure 2.3 depicts the layout of two versions of the chip which measures 3.5 x 5.5 mm. Each version contains two resistors which are implanted on the bridges of the cantilevers at equivalent places. However, the metal patterning differs in order to obtain a complete Wheatstone bridge when the two different dies are bonded together face to face. To make electrical interconnect, large internal bonding pads were realised with a second aluminium layer. Contact apertures were realised on each chip to access the external contact pads for wire-bonding,

after bonding the die together. Apertures can be chosen in-between 0.43 mm^2 and 1.1 mm^2 by changing the position the sensors in-between the outer positions which are indicated by figure 2.4. A photograph of an aperture is shown in figure 2.7a. The light grey sensor is shown with its back side, whereas the dark grey chip is shown with its top side. Both cantilevers will bend in the same direction when a flow is present. This results in compressive surface stress for one cantilever and in tensile stress for the other. Hence, two resistors will decrease, whereas the two others will increase. In this way, a maximum output signal is achieved from the Wheatstone bridge.

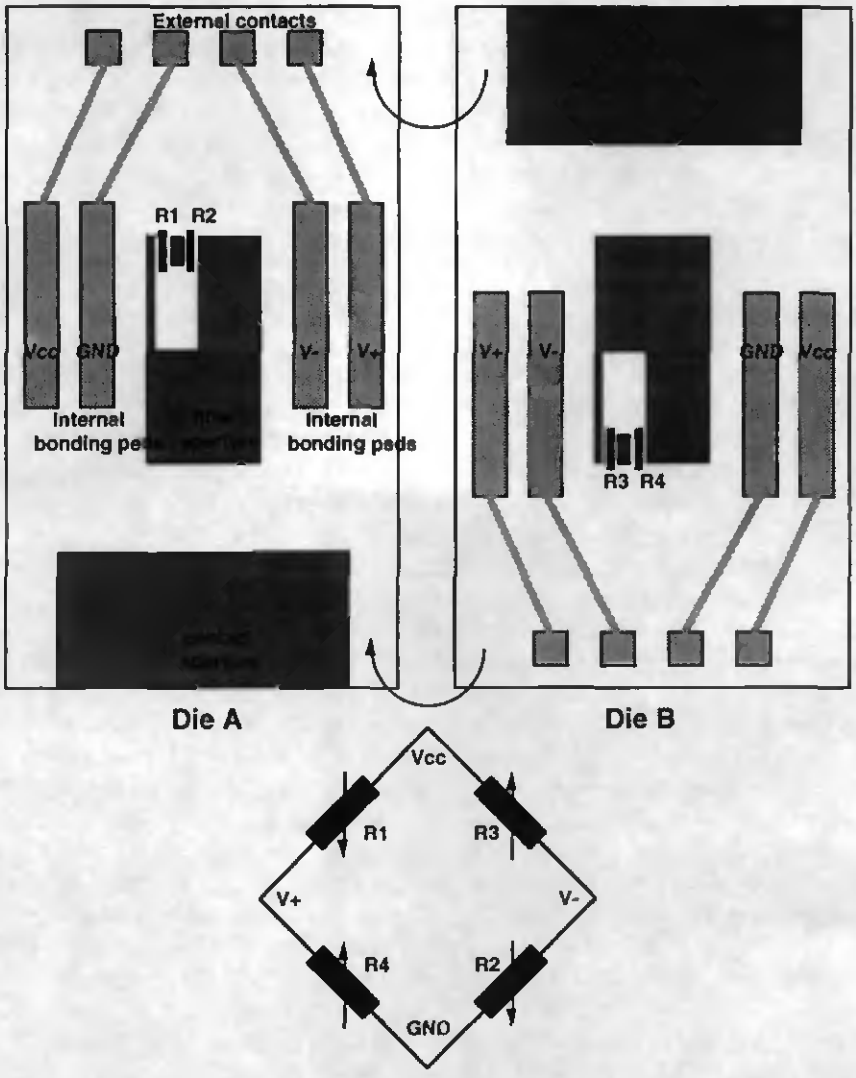

Figure 2.3 Two complementary sensor die and the electric circuit which is created by bonding die A to die B, face to face

Special attention was given to the wafer layout in order to achieve wafer to wafer bonding. The two versions are distributed over the wafer in such a way

that when two of such wafers are bonded face to face, version A always faces version B. This was achieved by placing the different versions in a chess board pattern on the wafer with an even number of rows and columns.

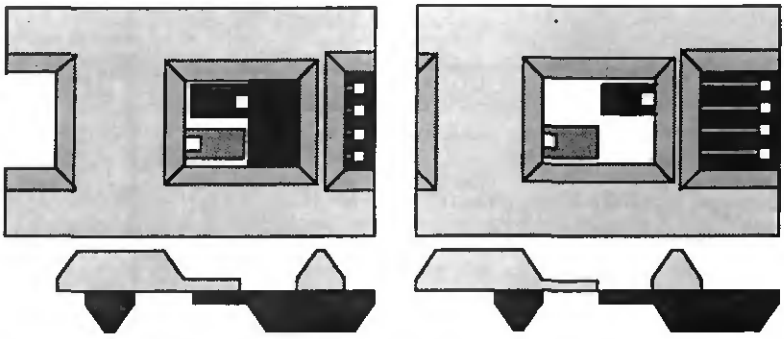

Figure 2.4 Schematic top-view and cross-section of the orifice sensor for minimum ond maximum orifice aperture.

2.3.2 Wafer Processing

The low-cost basic wafer process which was based on the standard sensor process of ASCOM Microelectronics, is shown in figure 2.5.

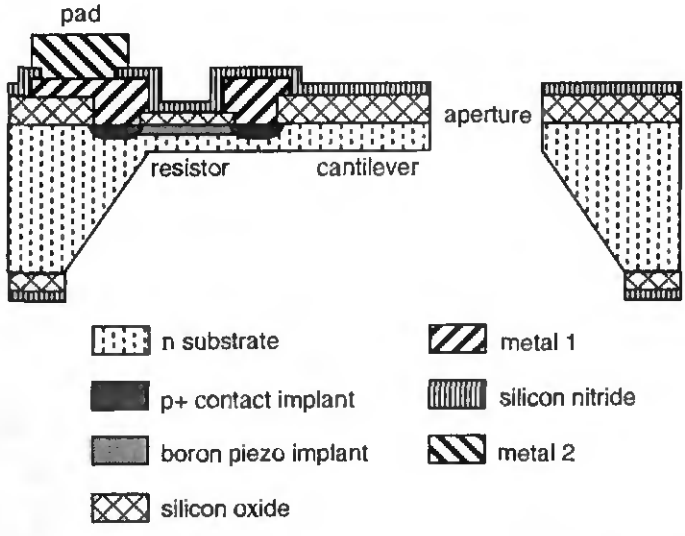

Figure 2.5: Schematic cross-section of the sensor showing the wafer fabricotion

Openings were etched for both the p+ areas and the piezo resistors after thermal oxidation of the n-type double polished wafers. An implant oxide was grown and the piezo implantation was carried out with a dose of $6 \cdot 10^{14}$ Boron/cm^2 at 100 KeV. After the second photolithography, only the p+ areas were not covered by photoresist and a second dose of $1 \cdot 10^{16}$ Boron/cm^2 was implanted at 100 KeV and a drive-in diffusion with oxidation was carried out. Contact openings were etched and the first metal was formed by a layer of 0.56 µm aluminium, sputtered on top of a 0.14 µm thick Ti-W layer. This layer was used

as a diffusion barrier for the aluminium. After patterning the first metal and deposition of 1 µm of silicon nitride at both sides, pad openings at the front and membrane openings at the back were formed. Aluminium was sputtered to a thickness of 1.5 µm and patterned to form the second metal. Membranes were etched to a thickness of 15 µm by anisotropic KOH etching and the cantilevers were liberated by a RIE etch from the front using 10 µm thick resist as protection mask which was coated on to the wafer and patterned before the KOH etch. The wafer processing was carried out by CSEM, Neuchâtel, Switzerland, except for the KOH and the RIE etching which were respectivily performed at ASCOM Microelectronics and IMT.
Leakage currents were observed that were probably caused by surface stress after the deposition of the Ti-W layer, since production runs without this step did not show significant leakage currents.

2.3.3 Hybrid Packaging

Metal-metal bonding was carried out with square pieces of silicon with a surface of 1.5 cm^2 and covered with an aluminium layer with a thickness of 0.5 µm. Pressing two of such pieces together at 580 °C for about one minute results in a rigid mechanical die attach. The resistance of such a metallic bond was only three times higher than the resistance of the aluminium surface before bonding [24]. Due to time constrains, this way of metal-metal bonding has not yet been performed with sensor chips. Sensor mounting was achieved by gluing a chip of version B on top of a chip of version A. The latter was glued to a ceramic substrate and electrically connected by standard wire bonding to the metal leads on the ceramic. Standard pins for electrical connections were soldered onto the edge of the ceramic. Plastic nozzles were glued onto the ceramic in order to protect the chips and to provide the fluid interconnect by means of plastic tubing, as shown in figure 2.7b. Due to the gluing, no electrical connection was achieved in-between the two die. As a consequence, only the two resistors of dic A were contacted. However, a complete Wheatstone bridge was realised with a combination of two devices of which a cross-section is shown in figure 2.6.

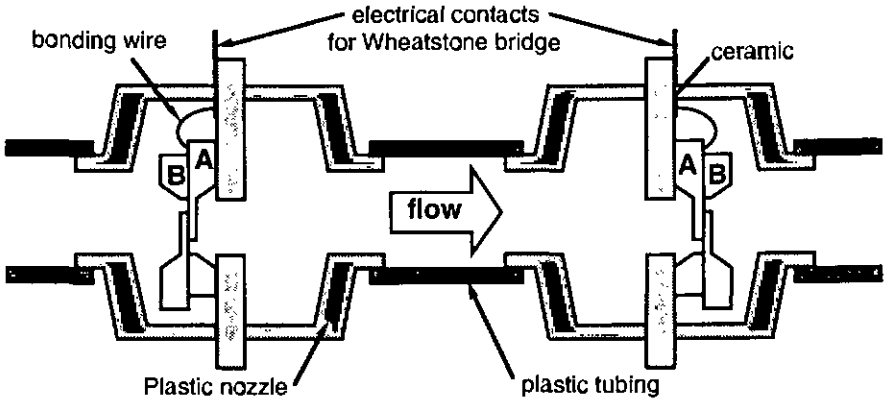

Figure 2.6: Cross section of a sensor set-up with two devices in order to form a complete Wheatstone bridge.

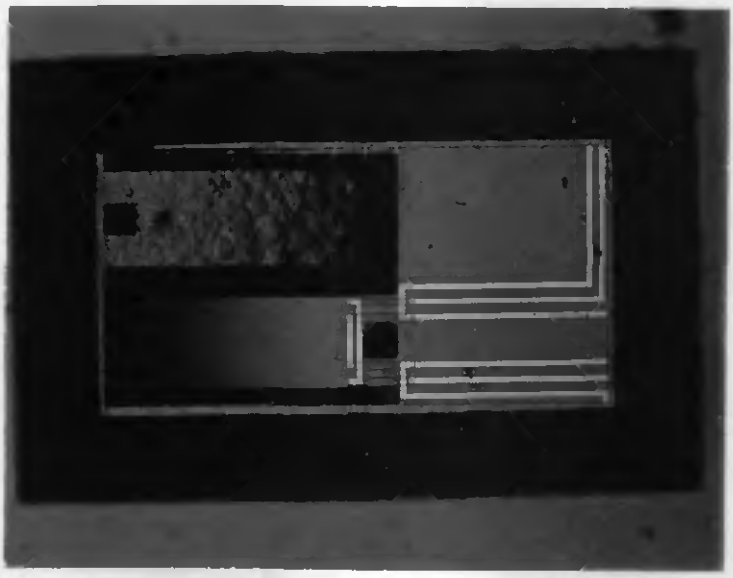

Figure 2.7a: Top view of the sensor sandwich showing the orifice with the cantilevers and the piezoresistors.

Figure 2.7b: Side view of the completed orifice flow sensor showing the plastic nozzles glued to the ceramic.

When a flow is applied, the piezoresistors of die A increase for the sensor at the left and decrease for the sensor at the right. Since both devices have an identical aperture, the total structure can be regarded as one symmetrical sensor. Offset and drift are not considered in the next sections, since they were mainly caused by leakage currents and the double sensor arrangement. Analysis of these issues only becomes important when the leakage currents are eliminated and the final package of the sensor is realised.

2.4 Characterisation

The sensor characterisation was performed with an automatic test bench. The Wheatstone bridge configuration was read out with a voltage meter and with the Sigma-Delta converter depicted in figure 1.5b. The frequency F_1 was counted by a HP frequency counter which was triggered after 2^{15} pulses of F_2. This trigger pulse was generated by a programmable frequency divider SN74292. The clock frequency was set at 150 kHz. The sensor was only characterised for air, since exposure to water resulted in a too large drift of the sensor output.

2.4.1 Automatic Test Set-up

A fully automatic measurement set-up was developed in order to characterise the sensors for flow at different temperatures and different fluid pressures. Figure 2.8 depicts a schematic view of this set-up. To compare the sensor responses for these different conditions, good repeatability is necessary and was achieved by computer control. The sensor was placed in series with a mass-flow controller which regulates either an air flow or a water flow through the sensor. Air flow was regulated with a Brooks Mass-flow controller with a range from 0.1 to 5 l_n/min or a Bronkhorst High-tech mass-flow controller with a range from 0.004 to 0.2 l_n/min. Water flow was regulated with Bronkhorst Liqui-Flow controllers, one with a range from 0.004 to 20 g/hour and one with a range of 20 to 1000 gram/hour. The setpoint of the flow controllers was set by a voltage from a computer controlled DAC (HP 59501B). Mass-flow controllers have the advantage that they control flow independent of the fluid pressure. Therefore, the fluid pressure in the device could be set by a computer controlled pressure regulator (DPI 500 or DPI 510 from Druck Ltd.), connected to the outlet of the sensor. In this way, the fluid pressure in the sensor was regulated from 0.1 to 2 bar absolute, independent of the flow.
A closed system was developed for water that consisted of two 50 liter beer kegs. Flow was achieved by applying a pressure to the air inlet of one keg. From this keg water flowed to one of the liquid flow controllers which was connected to the inlet of the sensor. After passing the sensor, this flow was led to the keg with the lowest pressure. The water pressure in the sensor was controlled by the pressure controller connected to the air inlet of this keg.
In addition to the automatic flow and pressure control, the ambient temperature was regulated by a computer controlled climate chamber (Heraeus Vötch VMT 04/35) from 5 to 95 °C. The sensor and a 3 m long brass conduit were placed inside this chamber. The brass conduit connected the flow controller with the sensor and served as a heat exchanger. By this construction, the fluid was heated

or cooled to the required ambient temperature before reaching the sensor.
The sensor control electronics were mounted on standard PCB's, placed in a shielded box outside the climate chamber. The sensor signals were measured by a Keithley scanning multimeter (199 DMM) and a Gould oscilloscope, both linked to the computer. The connections from the box to the sensor and to the multimeter were all shielded. Hence, flow, pressure and temperature were controlled by the computer which also stored the measurement data from the multimeter and the oscilloscope.

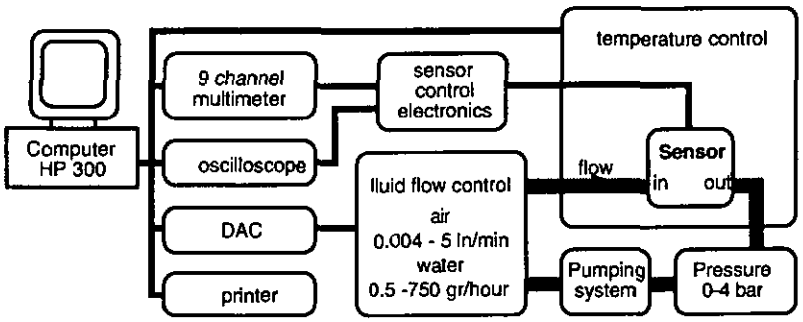

Figure 2.8 Block diagram of the test set-up with flow, pressure and temperature control.

2.4.2 Sensitivity to Differential Pressure and Mass-Flow

Figure 2.9 depicts the linear sensor output as function of a differential pressure across the sensor combination (depicted in figure 2.6). The resistors were connected in a Wheatstone bridge and supplied with a constant voltage of 5 V. A sensitivity was measured of 0.25 mV/V·mbar. Substitution of this value in equation 2.5 resulted in a value of $44 \cdot 10^{-11}$ Pa^{-1} for π_l, the piezoresistive constant. (σ_{avg} was calculated from the equations 2.6 and 2.7). The measured value for π_l is lower than the theoretical value of $71 \cdot 10^{-11}$ Pa^{-1} [11], since the piezoresistors were badly isolated from rest of the chip. The leakage currents, parallel to the piezo resistors, are not modulated by the pressure. Hence, the sensitivity was less than expected.
Figure 2.10 depicts the sensor output as function of a mass flow through the sensor. A sensitivity was measured of 0.008 mV/V(mg/sec)^2 with an aperture of 0.425 mm^2. Since the sensor shows a quadratic response, the sensitivity is given for the square of the flow. Substitution of this sensitivity in equation 2.8 results in a value of 1.15 for β, the efficiency factor. From the discussion in section 2.2.1 it is concluded that the kinetic energy of the fluid flow is transferred into a pressure drop with high efficiency. Figure 2.10 also shows that the response of the symmetric sensor is almost independent of the direction of flow (up to 25 mg/sec), although preliminary measurements with an asymmetric sensor (four beam accelerometer) showed that changing the flow direction changed the sensitivity by a factor 2 [24,28]. For one direction, the sensor response deviates strongly from the predicted curve for flows higher than 25 mg/sec, since the beams started to oscillate strongly at a frequency of 21.1 kHz. This oscillation added a sinusoidal voltage to the output up to 40 mV/V RMS. The resonant frequency only slightly deviates from the calculated value of 20.5 kHz [24].

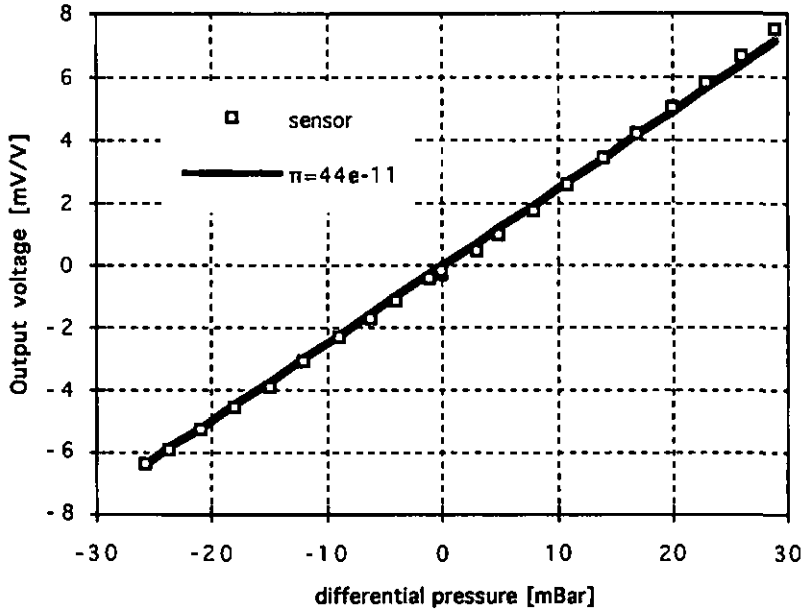

Figure 2.9: Response of the orifice flow sensor for differential pressure (Wheatstone bridge, corrected for offset).

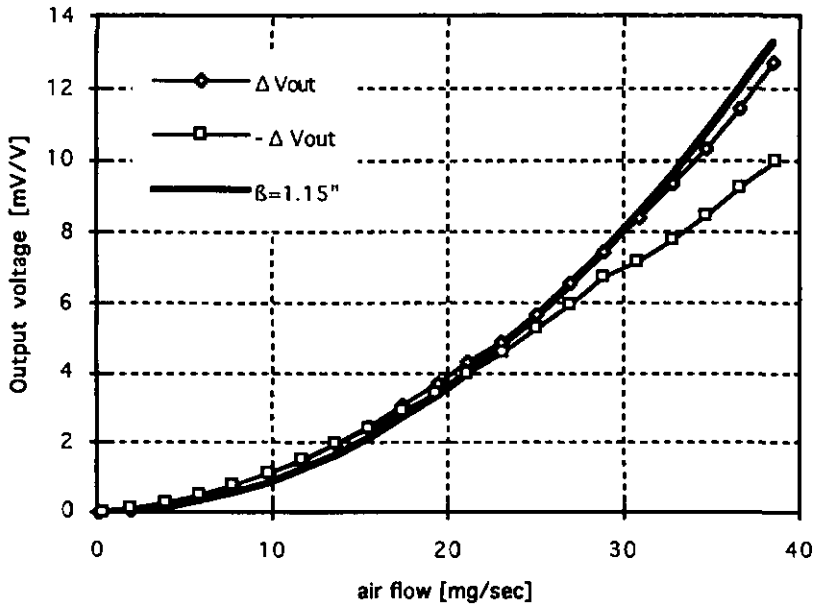

Figure 2.10: Response of the orifice flow sensor for two flow directions (Wheatstone bridge, corrected for offset).

2.4.3 Dependence on Fluid Pressure

Figure 2.11 depicts the sensor response which was measured with the Sigma-Delta converter for a pressure range of 800 and 1500 mbar. The sensitivity of the sensor varied -0.15%/mbar for this pressure range. As expected from equation (2.8), the sensitivity decreases when the fluid pressure increases. However, the predicted linear relation between resistor change $\Delta R/R_o$ and fluid pressure p_{stat} was not measured. Explanation is found by the fact that the flow profile around the irregular orifice changes with the fluid pressure. Hence, the efficiency factor β also depends on the fluid pressure. Therefore, an additional dependence on the fluid pressure is introduced.
At 800 mbar, oscillation starts already for flows smaller than 7 mg/sec. This low value can be explained by the low fluid pressure. The damping of the cantilevers is much less for small fluid pressures than for high fluid pressures, since the damping is proportional to the fluid pressure [28].

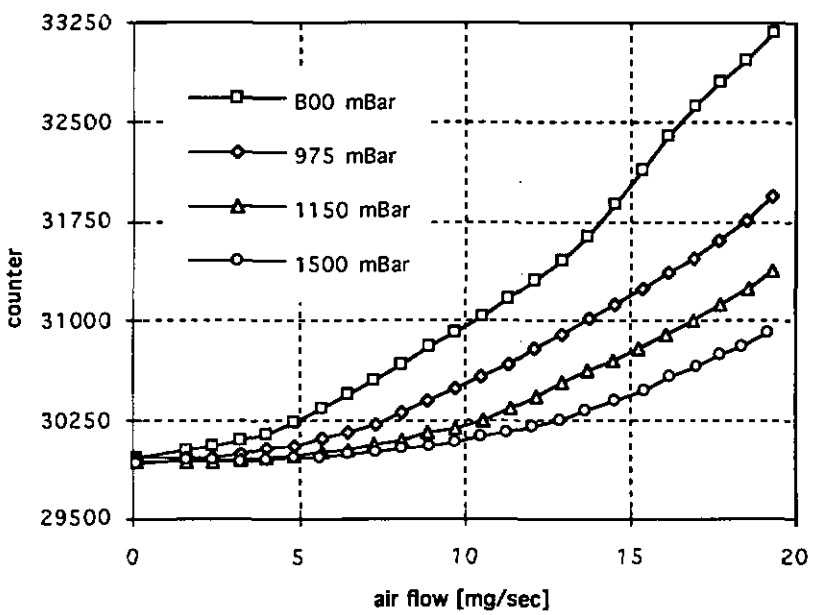

Figure 2.11: Response orifice flow sensor for different ambient outlet pressures (Sigma-Delta converter).

2.4.4 Dependence on Ambient Temperature

Figure 2.12 depicts the temperature dependence of the orifice flow sensor which was measured with the Sigma-Delta converter and with a voltmeter directly. The temperature was varied in between 10 and 55 °C. At room temperature a sensitivity of 5.7 counts/(mg/sec)^2 or 0.044 mV/V/(mg/sec)^2 was found for respectively the Sigma Delta converter and the Wheatstone bridge. For both measurement methods the temperature dependence of the sensitivity (TCS) measured 0.5 %/°C. In accordance with equation (2.8), the sensitivity increases

with the temperature, since the density decreases with temperature. Furthermore, the graph shows that the transfer functions have exactly the same shape. This is explained by the fact that both measurement methods give a representation of $\Delta R/R_0$, although the signal treatment is completely different (see equations 1.5 and 1.9).

Since the orifice flow sensor is an indirect sensor, the total TCS is the sum of the TCS of the transfer function from flow to pressure and the TCS of the transfer function from pressure to output signal. The last one has a negative TCS and is normally about 20 % smaller than the temperature dependence of the nominal bridge resistance R_0 and negative. As R_0 showed a positive temperature dependence of 0.46 %/°C, a TCS of about - 0.38 %/°C is expected. Hence, the negative TCS of the Wheatstone bridge partially compensates for the positive TCS of the first transfer function (from flow to differential pressure). Hence, the TCS of the first transfer function can be estimated at about 0.5 + 0.38 = 0.88 %/°C. To verify this value, measurements were performed with a Wheatstone bridge supplied with a constant bridge current of 5 mA. As shown in section 1.2.2, the output of a Wheatstone bridge supplied with a constant current does not depend on the bridge resistance R_0. The resulting sensor response is depicted in figure 2.13. A sensitivity was measured of 0.031 mV/mA/(mg/sec)^2 and a TCS was found of 0.93 %/°C, which now only depends on the first transfer function from flow to pressure. This TCS is in close agreement with the expected value of 0.88 %/°C.

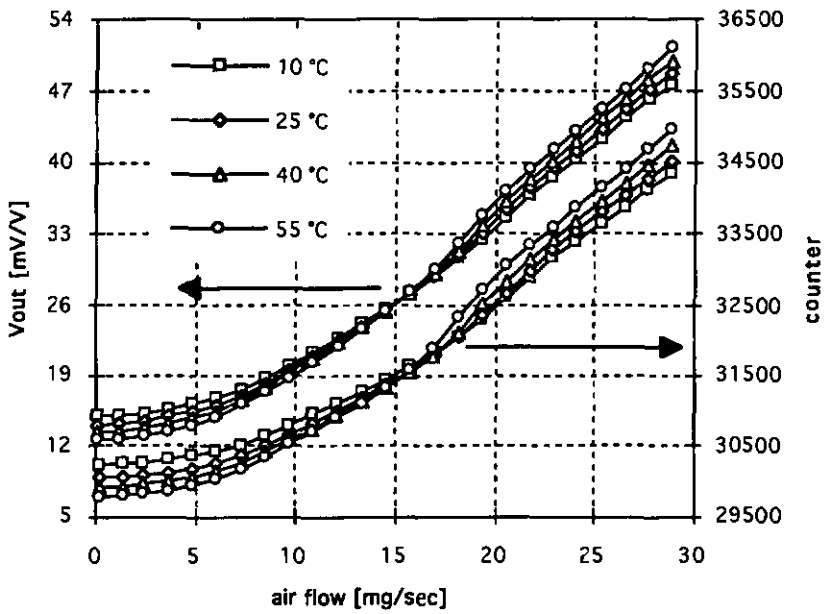

Figure 2.12: Response of the orifice flow sensor for different temperatures (Wheatstone bridge and Sigma-Delta converter).

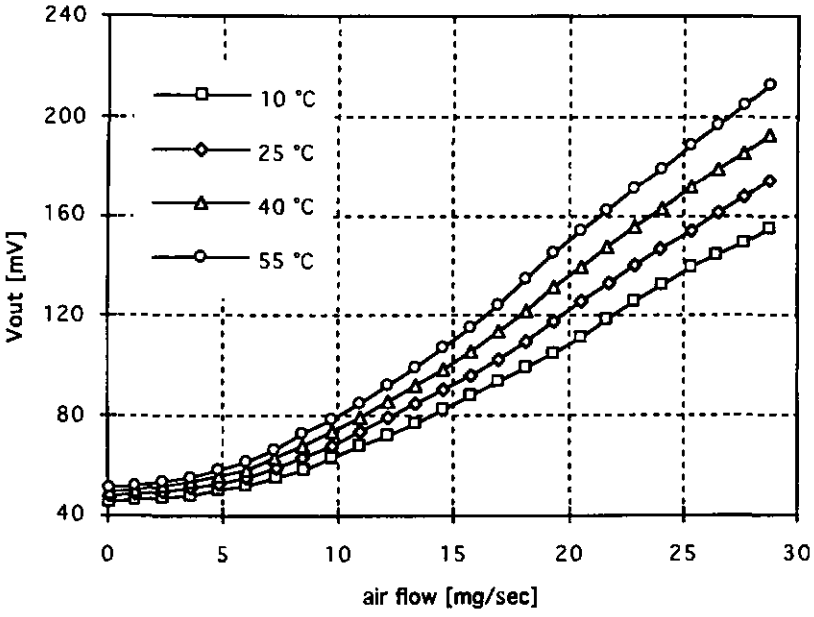

Figure 2.13: Response orifice flow sensor for different temperatures (Wheatstone bridge with constant bridge current).

2.5 Summary

A bi-directional silicon orifice flow sensor has been realised using an industrial wafer process in combination with wafer bonding. Characterisation was performed by using the sensor in a Wheatstone bridge configuration and with a (15 bit, 150 kHz) Sigma-Delta converter, which provided digital read-out. Sensitivities of respectively 0.044 mV/V/(mg/sec)^2 and 5.7 counts/(mg/sec)^2 were obtained. Due to the symmetric design, the sensitivity does not depend on the flow direction for flows up to 20 mg/sec. At higher flows the sensor starts to oscillate with a frequency of 21 kHz. Comparison of the measured response with the presented analytic model resulted in a piezoresistive coefficient for the piezoresistors of $44 \cdot 10^{-11}$ Pa^{-1} and an efficiency constant β of 1.15.
The temperature dependence is 0.93 %/°C and is reduced to 0.50 %/°C if the output is modulated by the temperature dependent bridge resistance, e.g. when a Wheatstone bridge is used that is supplied with a constant voltage or when a Sigma-Delta converter is applied. The sensor dependence on the outlet pressure is about -0.15 %/mbar.

3 THE HOT-WIRE FLOW SENSOR

3.1 Introduction

The principle of hot-wire sensors is based on heat transfer from a heated object into a moving fluid. An example of such a sensor is the finger putted in the air to measure wind: The air stream cools the finger. Therefore, the cooling is regarded as a measure for flow. Industrial hot-wire sensors consist of a very thin heated metal wire which is mounted in-between two needles and heated by an electrical current. When the hot-wire is placed in a flow, heat convection takes place from the wire into the fluid and the hot-wire temperature decreases. The hot-wire resistance is a function of its temperature, since the hot-wire has a large positive temperature dependence. Hence, not only the hot-wire temperature decreases, but also the hot-wire resistance. Therefore, the resistance of the heated wire is used as an indirect measure for flow.
Many silicon hot-wire sensors have been developed over the last twenty years for gases [16,17,19,25,26] and some for liquids [27]. The silicon sensor which is presented in this chapter is based on a hot spot at the middle of a silicon membrane. By placing the sensor in the fluid parallel to the flow, heat convection takes place from the heated area into the passing fluid. The membrane area around the heated area provides the thermal isolation from the rest of the device. Both the heater temperature and the ambient temperature are measured by diodes integrated on-chip in the heater area and near the edge of the chip.
The fabrication of the sensor die was based on bipolar IC-technology and the fabrication of the two packages was also based on industrial production techniques. One package was based on a ceramic structure that approximated the shape of a wing. Experiments with this package, used as a probe in a large conduit, showed that the sensor response was in good agreement with the sensor model which was based on King's Law. The second package was based on a standard transistor housing and was used to characterise the sensor's dependence to ambient temperature. With two of these sensors an effective compensation for temperature has been realised by using differential measurement by using a Sigma-Delta converter. This resulted in high resolution and a digital output signal.

3.2 Sensor Model

An analytical heat flow model has been derived which relates the hot-wire principle with the sensor dimensions. In this way, the dissipated power of the

heater is related with the velocity of the fluid passing over the heater area. Consideration of the power balance of the sensor results in an expression that has the form of King's Law. As a result of this model, the optimal heater surface is found as a function of the membrane size (section 3.2.3).
Three heat flows are important for the power balance in the sensor, as is indicated in figure 3.1: The forced convective heat q_{conv} that flows from the membrane into the fluid, the conductive heat q_{cond1} from the membrane into the fluid and the conductive heat q_{cond2} from the heater into the substrate. The following equation is found for the total dissipated power P_{diss}:

$$P_{diss} = q_{cond1} + q_{cond2} + q_{conv} \quad [W] \tag{3.1}$$

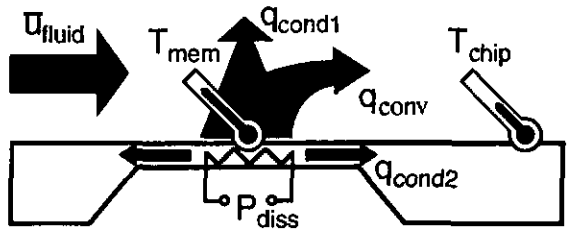

Figure 3.1: Cross section of the chip showing the conductive and convective heat flows and the differential temperature measurement.

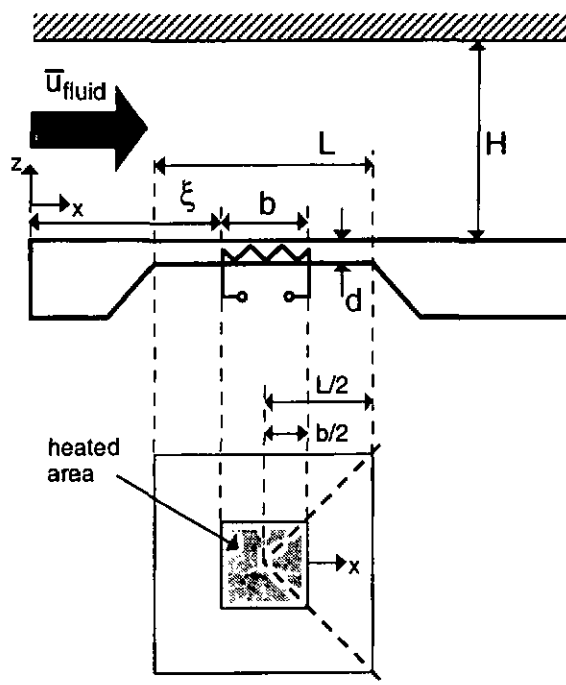

Figure 3.2: Geometrical dimensions for the heat flow model.

In figure 3.2 the important geometrical dimensions are given. L indicates the membrane length, b the length of the heated area, x the distance from the sensor edge to the heater, d the membrane thickness and H the distance from the membrane to the tube wall assumed to be at liquid temperature.
First the conductive heat flows are discussed which represent the static part of the model. The convective heat flow, the dynamic part of the model, is considered afterwards. Referring to section 1.1.1, the conductive heat flow is represented by the bias component O_I, whereas S_I represents the convective heat flow.

3.2.1 Conductive Heat Flow

In a three dimensional space the conductive heat flow q from a first isotherm (surface with constant temperature) S_r to a nearby second isotherm S_{r+dr} is expressed by:

$$q \cdot dr = -k \cdot S \cdot dT \quad [W] \tag{3.2}$$

k is the thermal conductivity of the material in W/mK and T the temperature in K. Note that $dr/(k \cdot S)$ is an expression for the thermal resistance between two isotherms. To find an expression for q, the surface S has to be written as a function of the vector r. Figure 3.3 shows a cross section for an isotherm S_{real}. The middle of the membrane is heated to a temperature ΔT above ambient temperature. The assumption is made that heat only diffuses away from the heated area through the material above the heater and that no heat is transferred from the chip to the fluid outside the heater area. Therefore, the isotherms have a curvature similar to diffusion contours. Directly above the heater the contours are approximately flat and just beside the heat source the ratio between the horizontal and the vertical dimension of the curvature is about 3 to 4 (verified with the finite element modelling program ANSYS).
In order to obtain an analytical expression, it is assumed that heat only flows in between the dotted lines of figure 3.3. The hatched areas are chosen to be equal, in order to insure that the thermal resistance of the volume indicated by the lower hatched area is approximately equal to the thermal resistance of the upper one. Hence, the dotted lines are chosen at an angle of 45° with respect to the heated surface. Now the isotherms are expressed as a function of z only.

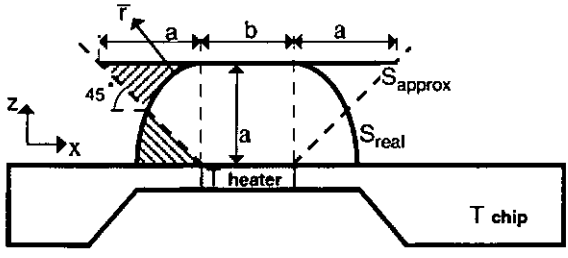

Figure 3.3: Sketch of a cross section of a real isotherm S_{real} and an approximated isotherm S_{approx}.

For q_{cond1} the surface $S_{approx.}$ at a distance a from the heated surface can be written as $(b + 2 \cdot a)^2$. Substitution of this surface in equation 3.2 and integrating z from $z = 0$ to $z = H$ gives:

$$q_{cond1} = k_{fl} \cdot b \cdot \left(2 + \frac{b}{H}\right) \cdot \Delta T \quad [W] \tag{3.3}$$

with k_{fl} the thermal conductivity of the fluid in W/mK.
q_{cond2} is found in a similar way. Figure 3.2 indicates that the membrane can be divided by the diagonals in four sectors. The surface $S_{approx.}$ for one sector at a distance a from the heated surface is then $d \cdot (b + 2 \cdot a)$ or $4 \cdot d \cdot (b + 2 \cdot a)$ for four sectors. Note that the approximated isotherms are continuous from one section to another. Substitution of $S_{approx.}$ in equation 3.2 and integrating x from $x = 0$ to $x = L/2 - b/2$ results in the following equation with k_{si} the thermal conductivity of the membrane (silicon):

$$q_{cond2} = 8 \cdot k_{si} \cdot \frac{d}{\ln\left(\frac{L}{b}\right)} \cdot \Delta T \quad [W] \tag{3.4}$$

The static behaviour of the sensor predicted by the equations 3.3 and 3.4 are in good agreement with simulations carried out with the finite element modelling program ANSYS. Depending on the mesh of the model, ANSYS gives values a few percent larger or smaller than the expressions above.

3.2.2 Convective Heat Flow

A dynamic analysis is carried out by applying the boundary layer theory in order to calculate the convective heat flow as function of the flow velocity. An in-depth study of this theory can be found in [6,19]. Finite element modelling of heat transfer in fluids is not possible with our facilities, since it demands the computation capacity of very large computers. In this paragraph only relevant formulas are introduced without referring to that theory.
For both laminar and turbulent flow the convective heat q_{conv} is described as:

$$q_{conv} = h_{avg} \cdot b^2 \cdot \Delta T \quad [W] \tag{3.5}$$

with h_{avg} the average heat transfer coefficient in W/m^2K, b^2 the heater surface and ΔT the temperature difference between the heater and the fluid.
For a hot plate the local heat transfer coefficient h_x is given as function of the fluid velocity u as well as x, the co-ordinate in the direction of the flow and the origin at the front of the hot plate (see figure 3.2) [6]:

$$h_x = 0.332 \cdot \frac{k_{fl}}{x} \cdot \sqrt[3]{\mathrm{Pr}} \cdot \sqrt{\mathrm{Re}} = 0.332 \cdot k_{fl} \cdot \sqrt[3]{\mathrm{Pr}} \cdot \sqrt{\frac{u}{\nu x}} \quad [W] \tag{3.6}$$

with Pr the Prandtl number, Re the Reynolds number and ν the fluid viscosity in m^2/s. However, this equation is only valid for a plate with a constant temperature. If there is an unheated area of length ξ from the leading edge to the heated area, the heat transfer starts at a distance ξ from the starting point of the velocity boundary layer. The unheated length ξ is important to interpret the measurement results. Therefore, equation 3.6 is expanded for respectively laminar and turbulent flow in the following way [6]:

$$\begin{aligned} h_x &= 0.332 \cdot k_{fl} \cdot \sqrt[3]{\frac{Pr}{1-\sqrt[4]{\left(\frac{x}{x}\right)^3}}} \cdot \sqrt{\frac{u}{\nu x}} && \text{Re} < 2300 \\ h_x &= 0.0296 \cdot k_{fl} \cdot \sqrt[9]{\frac{Pr^3}{1-\sqrt[10]{\left(\frac{x}{x}\right)^9}}} \cdot \sqrt[5]{\frac{1}{x} \cdot \left(\frac{u}{\nu}\right)^4} && \text{Re} > 500000 \end{aligned} \qquad (3.7)$$

No satisfying equation is known for Reynolds numbers in the range of 2300 to $5 \cdot 10^5$, since in this flow range, flows are very unstable. Locally, the character of the flow changes constantly from laminar to turbulent. Hence, flow meters are hardly exploited in this flow range. The following integral expresses h_{avg}.

$$h_{avg} = \frac{1}{b} \int_{x}^{x+b} h_x dx \quad [W] \qquad (3.8)$$

Substitution of equation 3.8 in equation 3.5 gives then the following expression for q_{conv}:

$$q_{conv} = b \cdot \Delta T \int_{\xi}^{\xi+b} h_x dx \quad [W] \qquad (3.9)$$

The conductive heat flows and the convective heat flow are all linear functions of ΔT as was stated by King's Law in 1906. For laminar flow King's Law is then expressed for the silicon sensor as:

$$P_{diss} = (O_1 + S_1(u)) \cdot \Delta T \qquad \textit{with}$$

$$\begin{aligned} O_1 &= k_{fl} \cdot b \cdot \left(2 + \frac{b}{H}\right) + 8 \cdot k_{si} \cdot \frac{d}{ln\left(\frac{t}{b}\right)} \\ S_1 &= 0.332 \cdot k_{fl} \cdot b \int_{\xi}^{\xi+b} \sqrt[3]{\frac{Pr}{1-\sqrt[4]{\left(\frac{\xi}{x}\right)^3}}} \cdot \sqrt{\frac{u}{\nu x}} dx \end{aligned} \qquad (3.10)$$

O_1 expresses the conductive thermal heat conductance, and S_1 the convective thermal heat conductance. Equation 3.10 describes the sensor behaviour as a function of the fluid velocity and the sensor properties. The next section

discusses the optimal heated membrane area for maximum convection with respect to the conductive heat flow.

3.2.3 Optimal Heater Area

The middle of the sensor membrane serves as the heater area and should be as large as possible in order to obtain maximum convection. However, the area left around the heater has to be as large as possible also, in order to achieve an optimal isolation between the heater and the rest of the chip.
An optimum is found for the ratio of the total membrane area and the heated part, since in the previous sections both the conductive heat flow and the convective heat flow are expressed in terms of sensor properties. The conductive heat flow is expressed as O_l and the convective heat flow is proportional to S_l, as expressed by King's Law. For optimal sensor behaviour, S_l has to be as large as possible with respect to O_l. In figure 3.4 the function S_l/O_l is plotted as function of *b*/L in arbitrary units and an optimal ratio S_l/O_l is found for *b*/L = 0.55. Hence, the surface of the heater should represent 27% of the membrane surface for optimal sensor sensitivity.

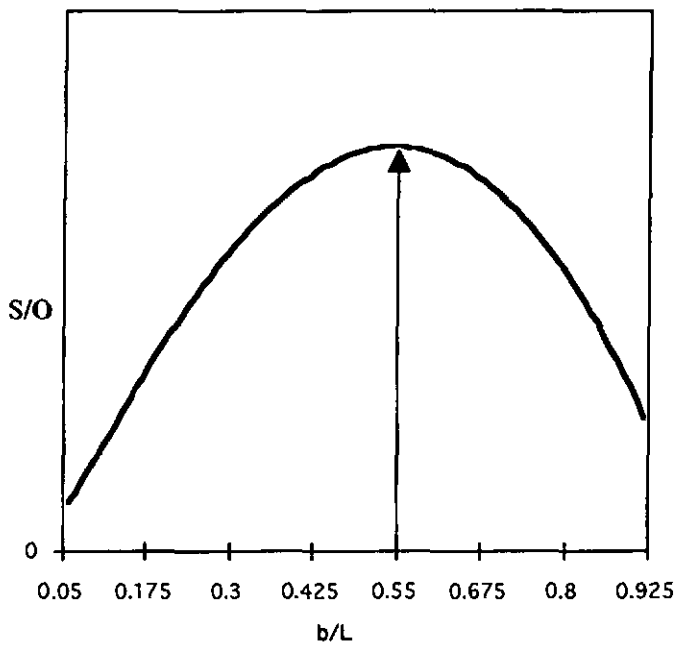

Figure 3.4: The ratio S_l/O_l, the ratio of convective and conductive heat flow as function of b/L, the heater length divided by the membrane length.

3.3 Realisation

This section discusses the design considerations of the sensor chip and of two different packages that have been used for sensor characterisation. The chip design focuses on the choice and layout of the temperature sensors and the

heater. The design of the two packages was based on standard encapsulation techniques in use at ASCOM Microelectronics in Bevaix, Switzerland.

3.3.1 Sensor Design

Original hot-wire sensors consist of a very thin metal wire mounted in-between two needles. This wire serves not only as heating element, but also as temperature sensor of the hot-wire. To fully exploit the possibilities of standard on-chip devices, the design of the silicon sensor is based on a heater with a separate temperature sensor. This separation of the actuator-sensor combination allows for sophisticated signal treatment and a second temperature sensor can be placed at the rim of the chip to measure the ambient temperature. In this way, the heater can be set at a constant temperature above ambient, whereas original hot-wires are set at a fixed absolute temperature. Hence, the influence of the ambient temperature is suppressed. The chip layout was designed to be as small as possible in order to be applicable for biomedical applications. Standard bipolar wafer processing and micro machining was used in order to allow for low cost batch processing.

3.3.1.1 Temperature Sensors

Three different on-chip temperature sensors are presented in table 3.1: Pn-junctions, diffused resistors, and thermocouples. The latter are based on the Seebeck coefficient of an aluminium-silicon junction.

Temperature Measurement	*Pn-junction*	*Resistor*	*Thermocouple*
Sensitivity	*1.5 - 2 mV/°C*	*0.15- 0.25 %/°C*	*0.5 - 1 mV/°C*
Non-linearity (0 - 100 °C)	*±0.5 %/°C*	*±1.5%/°C*	*probably considerable*
Impedance	*0.5 - 30 KΩ*	*0.5 - 30 KΩ*	*3 - 30 KΩ*
Process dependence	*small*	*moderate*	*high*
Chip surface	*moderate*	*moderate*	*large*

Table 3.1: Comparison on-chip temperature sensing based on standard wafer processing.

Pn-junctions are superior over resistors and thermocouples when non-linearity and process dependence is taken into account, while the sensitivities of these sensing elements do not show a large difference. Resistors have a non-linearity

which is three times larger then that of diodes. Furthermore, diodes are less sensitive to perturbations of the bias current, since the sensitivity of the voltage across the diodes only changes with the logarithm of the current, whereas the sensitivity of the voltage across the resistors is proportional with the bias current. The no-offset feature of thermocouples cannot be exploited for hot-wire sensors. The flow signal is added to a bias temperature that represents the heater temperature at zero flow. The circuit that sets the initial temperature normally causes offset and drift. Hence, the output signal will be affected by offset and drift, despite the no-offset feature of thermocouples. Furthermore, the sensitivity and the linearity of thermocouples are difficult to predict and depend heavily on the fabrication process [2]. Hence, diodes supplied with a constant current were chosen as temperature sensors.

3.3.1.2 Uniform Heating

The heated area of the membrane should measure 27 % of the membrane surface, as was found in section 3.2.3. On this part of the membrane not only a heater has to be implemented, but also a temperature sensor. Therefore, the heater can cover only a part of the heated area. If this area has an uniform temperature distribution, a temperature sensor, placed anywhere on this area, will represent the real heater temperature. In addition, a uniformly heated area allows for verifying the sensor model, for which a uniform heating was assumed. A ring of diffused resistors around the heated area was chosen as heating element, since the amount of heating along this ring of resistors can be set precisely by the position and the width of the resistors.
A two dimensional finite element model of the membrane was developed in order to determine the exact position and surface of the ring of resistors. The program ANSYS was used for modelling low resistive areas in the plane representing the membrane. The edges of the membrane were fixed at zero temperature and a current was defined through the low resistive areas resulting in local power dissipation. ANSYS calculated the temperature distribution of the membrane after determining the heat dissipation in the low resistive areas. The results are shown in figure 3.5. For the hatched area inside the heating structure, a uniform temperature was found with a variation of less than 1 % of the total temperature difference between the middle and the rim of the membrane.
Figure 3.6 shows the absolute difference of the temperature in the middle and in a corner of the heated area as was measured with the integrated diodes. The measured voltage change $-\Delta V$ of the diode placed in the centre and one of the diodes in the corner is depicted as function of the heat dissipated in the resistor. Also the difference between these diodes is shown as percentage of the voltage $-\Delta V$. For these measurements each diode was supplied with a constant current of 100 μA and heating was achieved by applying a voltage to the heat resistor. When more than 100 mW was dissipated, the difference between inner and outer diode is less than 1.5 %. Therefore, it is concluded that the area inside the heat resistor is homogeneous within 1.5 %, as is in close agreement with the modelling carried out with the finite element program ANSYS.
The voltage difference becomes less than 0.1 mV for heating powers smaller than 100 mW. Hence, below this heating power the differences become too small to measure properly and the deviation depends more on the measurement

error than on the temperature difference.

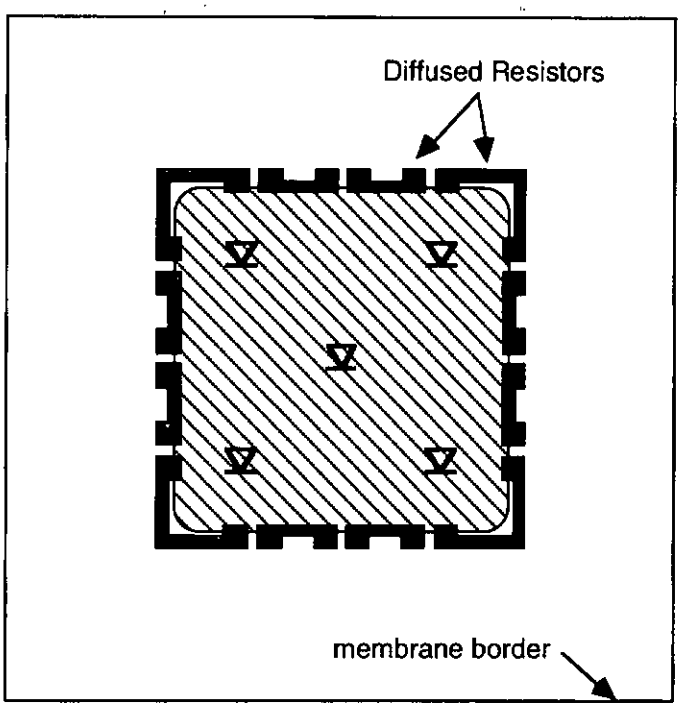

Figure 3.5: Uniform heating of the middle of a square membrane. The hatched area indicates where the temperature is uniform within 1 %. The grey structures indicate the heat dissipating resistors and the diode symbols mark the emitter areas of the diodes.

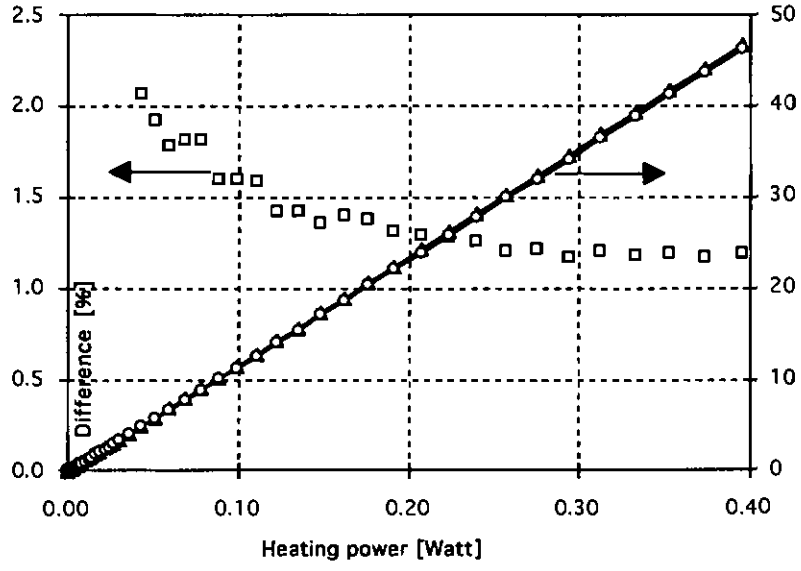

Figure 3.6: Measured temperature difference between the middle and a corner of the heated area as function of the heating power.

3.3.1.3 Chip layout

Figure 3.7 shows a sketch of the chip and its electrical equivalent. The membrane measures 600 μm by 600 μm and has a thickness of 12.7 microns. The temperature sensors are formed by a string of four diodes. One string is placed at the centre of the heater and the other one on the thick rim of the sensor. The diodes are formed by bipolar transistors with the base connected to the collector, since such diodes show better stability than single pn-junctions. Mismatch and first order voltage and temperature gradients are eliminated by using four transistors in common centroid geometry that is closely matched. Each string is supplied with a constant current of 100 μA from an external current source. This resulted in differential measurement of the temperature difference with a sensitivity of 7.00 mV/°C. The heat resistor is a high doped emitter n^+ diffusion and has a resistance of typically 130 Ω. The resistor forms a ring with a varying width around the temperature sensing diode string in the middle of the membrane (see figure 3.5). The square inside this resistor represents 27% of the membrane surface in order to obtain the largest possible sensitivity (see section 3.2.3). Bonding pads are located downstream on the chip to insure that the necessary electrical connections do not affect the flow profile over the heater area.

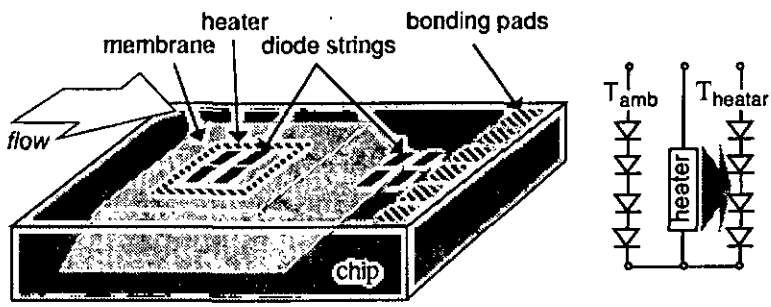

Figure 3.7: Schematic view of the liquid flow sensing chip and its equivalent schematic.

3.3.1.4 Wafer Processing

Standard bipolar wafer processing was used for the fabrication of the chip as is shown in figure 3.8. After the predeposition of an arsenic buried layer on a p-type double polished wafer, a n-type epitaxy of 11 microns was grown. The epitaxial layer was oxidised and patterned. Isolation between the different electrical components was achieved by a long boron diffusion traversing the epitaxial layer. The base was defined with a boron implantation and both the emitter and resistor diffusions were made by a phosphor predeposition, followed by a drive-in diffusion. After opening of the silicon oxide, electrical interconnect was realised by patterning an evaporated aluminium layer. Then a PECVD nitride layer was deposited, not only at the front side of the wafer in but also on the back side. At the front side, this layer served as a passivation of the circuitry, whereas at the back side, it served as a mask for the KOH etching. Electrical contact with the sensor was achieved by removing the nitride on the aluminium pads at the front side. The oxide and nitride layer at the back side

was patterned in order to define the membrane areas. The thickness of the membranes was determined by the etching time in KOH. The method of electrochemical etch-stop determines the membrane thickness by applying a voltage between the epitaxial layer and the substrate. This method could not be applied, since the KOH would etch away the p-type isolation diffusions in the epitaxial layer.

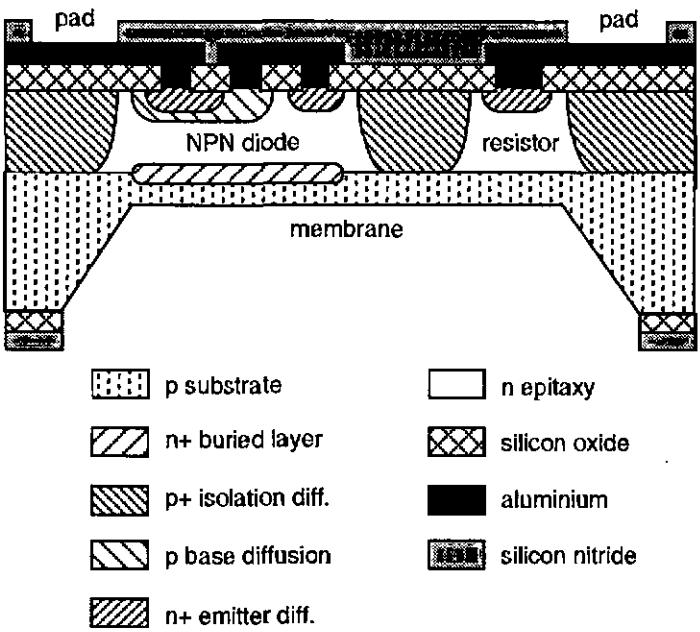

Figure 3.8: Schematic cross-section of the chip showing the fabrication process.

3.3.2 Packaging

Two ways of packaging were used for sensor characterisation: One to investigate the sensor behaviour at different temperatures and one to compare the response with the sensor model. For the latter purpose the sensor package should not disturb the flow profile along the test conduit. Therefore, a 0.6 mm thick wing shaped velocity probe was developed which was small in comparison with the 20 mm diameter test conduit. In this way, the obstruction caused by the sensor was minimal, but the flows needed for characterisation ranged from 2 to 800 g/sec. Since temperature control of such flows would require far too much energy, a low-cost package was developed based on a TO-5 housing that was used to study the temperature dependence of the sensor in a climate chamber. For this package, a high sensor response was found for flows up to 0.3 g/sec, small enough to allow temperature control. However, the irregular shape of this package determined the flow profile across the sensor, prohibiting comparison with the sensor model.

3.3.2.1 Low-Cost Mounting

A low-cost sensor package was developed in order to characterise the sensor for temperature influences. This package consists of a TO-5 housing without a cap. The sensor was glued onto the housing with a spacer chip in-between in order to make the level of the bonding pads of the housing lower than the sensor surface. The bonding wires were protected by an epoxy.
Figure 3.9 shows a cross section of the device and the mounting to the sensor housing was achieved by means of a single O-ring. The rim of the TO-5 housing, normally used as a support for the cap, was now used to transmit the force to the O-ring in order to provide tightness. An aluminium block was realised in which a 2 mm wide channel was drilled. The sensor was placed in the channel by means of an opening containing the O-ring fitting. Flow connections were provided by standard gas tubing. Figure 3.10a shows a photograph of the TO-5 package.

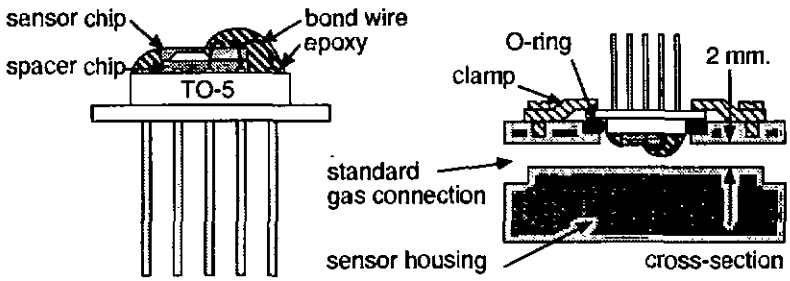

Figure 3.9: Cross section of the TO-5 housing and the mounting to the test tube.

3.3.2.2 Velocity Probe

A 0.6 mm. sensor package was developed to characterise the sensor response for a stable flow with a known flow profile. The form of this package is wing shaped. In this way, the disturbances caused by the package, are minimised. Therefore, the probe was made as thin as possible, although no compatibility was lost with the standard thick-film fabrication processing of ASCOM Microelectronics: Two 0.3 mm thick ceramic substrates of two square inches were glued on top of each other and the chips were inserted in the laser drilled openings of the upper ceramic, as is shown in the first cross section of figure 3.11. In this way, 14 devices were fabricated simultaneously with two substrates. The substrate at the top was patterned by using thick-film technology before the assembly of the sandwich. The interconnections and solder pads were printed with a silver-platinum paste, whereas gold pads were printed near the chip in order to exploit standard bonding techniques. The bonds were protected from the fluid by epoxy. Each device was glued in the top-end of a 8 mm thick plastic mounting tube. This tube was stuck into the measurement test tube with a 20 mm. diameter. Sealing was provided by two O-rings. This also allowed for changing the flow angle of the device by simply turning it. Furthermore, this construction provided an easy exchange for mounted sensors. Figure 3.10b shows a photograph of the ceramic device mounted in the plastic tube.

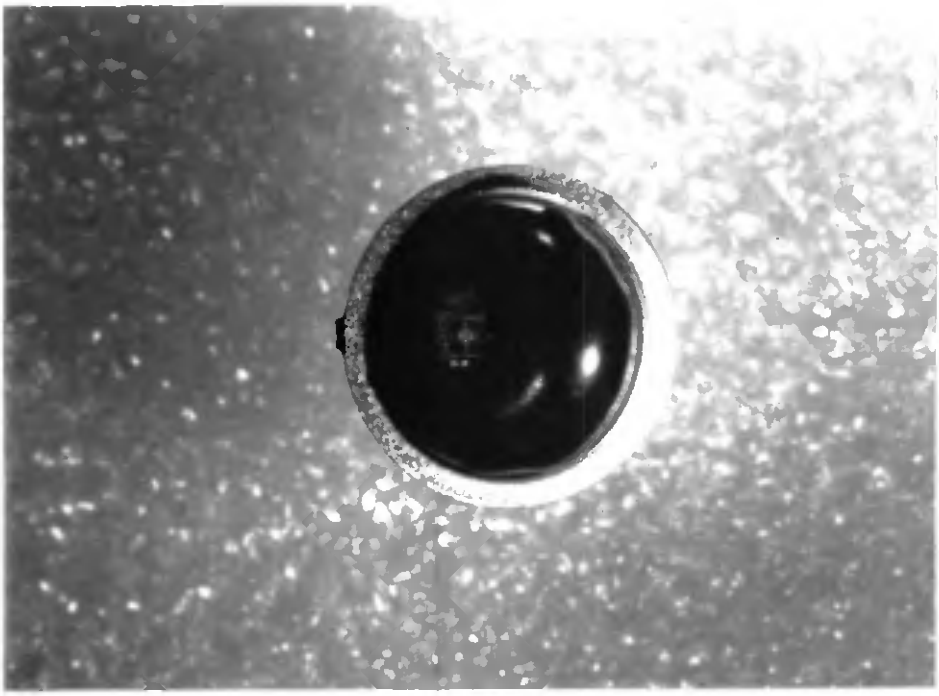

Figure 3.10a: Photograph of the hot-wire chip mounted on the TO - 5 housing.

Figure 3.10b: Photograph of the hot-wire chip on the ceramic velocity probe, mounted in a plostic tube.

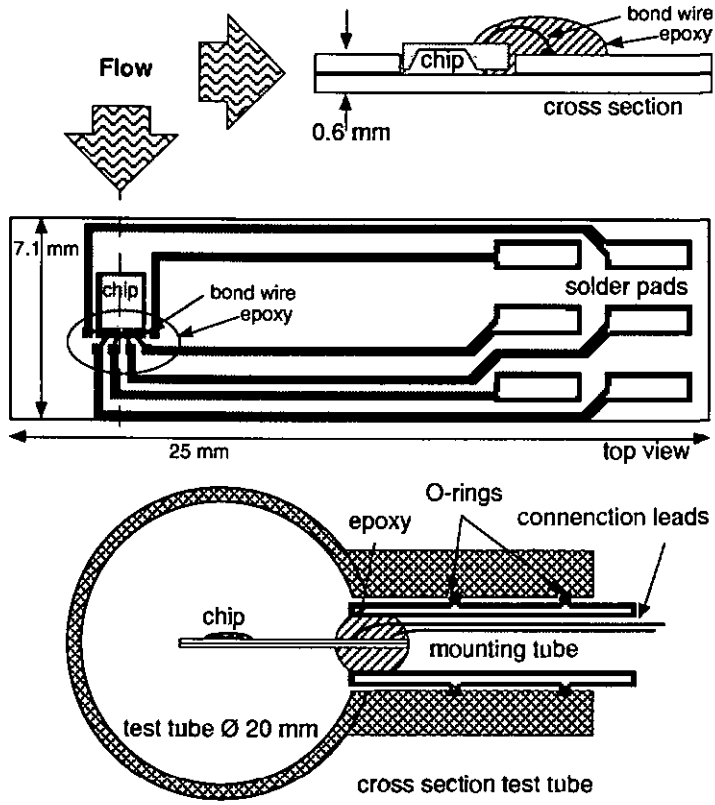

Figure 3.11: Cross section and top view of the ceramic and cross sectional view of the velocity probe mounted in the test tube.

3.4 Characterisation

This section reports on the signal conditioning and characterisation of the sensor. Measurements with the ceramic package were performed to verify the sensor model by using the principle of open loop. The principles of open loop, feedback and time modulated feedback are evaluated and these principles were applied to the sensor mounted on the TO-5 housing for different ambient temperatures.

3.4.1 Response Velocity Probe

This section presents the experiments carried out with the wing shaped velocity probe described in section 3.3.2.2. The 1.2 meter long measuring tube had a diameter of 20 mm in which a de-ionised water flow of 5 to 3000 litres per hour was regulated. This resulted in an average velocity from 0.005 to 2.65 m/s. The chip, mounted on top of a wing shaped ceramic, was not only positioned exactly parallel to the water flow in the middle of the tube, but also slightly tilted by 2° and 5°, in order to investigate the influence of the positioning. The heat resistor on the membrane was supplied with a constant voltage of 5 V which set a temperature difference of 10 °C between the heater and the chip rims.

The measured responses and the predicted laminar response of the chip are depicted in figure 3.12. From the graph it can be seen that the response predicted by the model is in good agreement with experimental results for Reynolds numbers up to 8000. This means that for our measurement set-up the model is valid for velocities up to 0.4 m/s by using the equation for the Reynolds number $Re = u_{avg} \cdot d/v$. Furthermore, the sensor is sensitive over almost three decades of flow velocity. The upper curve, measured with the sensor placed completely parallel to the flow, shows a peak for Reynolds numbers of about 2300. This peak is explained by the fact that the surface and the edges of the ceramic are not completely smooth, causing local turbulence which decreases the heat transfer. However, if the sensor is tilted a little, the flow profile over the sensor is stable and the heat transfer increases, as the boundary layer gets thinner. Hence, the graph shows no peaks for the tilted positions and the sensitivity is higher than predicted by the theory.

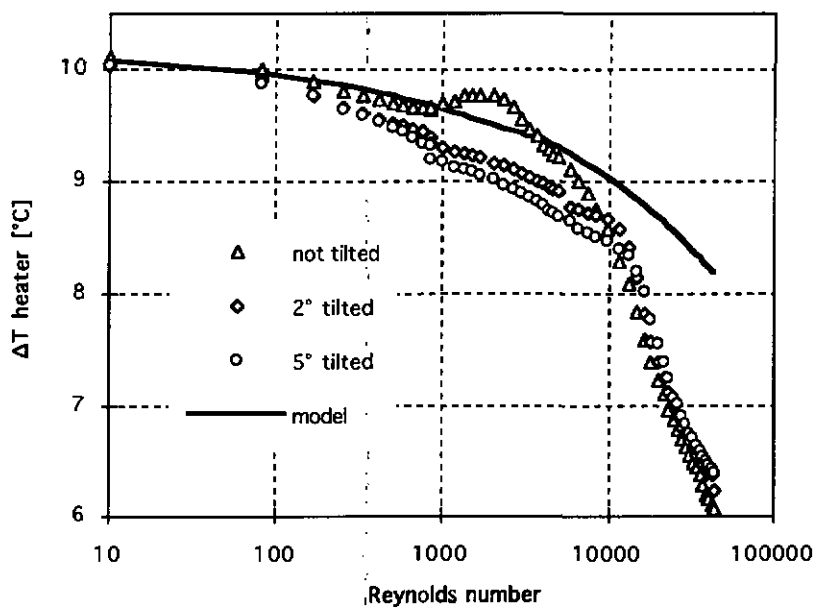

Figure 3.12: Sensar response and calculated laminar response as function of the Reynolds number.

In order to relate the sensor response properly with the sensor model, the following parameters were measured and used for the model: 145 W/mK for the thermal conductivity of silicon, 12.7 μm for the membrane thickness and 270 μm for the effective length of the heated area. Furthermore, the change of the velocity profile, heating of the chip and the entrance length ξ had to be taken into account. For laminar flow, the velocity in the middle of the tube is twice the average velocity. However, above 0.15 m/s (Re > 2300) the flow is not laminar anymore and the velocity becomes less than twice the average velocity [23]. The chip rims were heated up to 4 °C in comparison with the water temperature and this had a significant effect on the sensor response. Therefore, this additional

heating of the fluid was taken into account by considering the whole chip as a heated area of the ceramic. Hence, equation 3.10 was applied a second time with the whole chip surface as a heated area of 4 °C and ξ the distance from the edge of the ceramic to the front edge of the chip.
For each measurement point, both the diode voltages were measured 250 times within 40 seconds by a scanning multimeter and the voltage difference was calculated by the computer controlling the measurement. Averaging was necessary since the signal varied strongly because of turbulence in the flow. With maximum flow the noise is 60 dB (!) higher than for zero flow as was measured with a spectrum analyser connected to the sensor. The noise level was constant for frequencies ranging from 0.1 Hz to 200 Hz and the first 3 dB point was found at 200 Hz, resulting in a thermal time constant of 5 msec.
It is shown that theory fits well with the measurement results, although effects as positioning and turbulence had to be taken into account. Since the velocity profile of the flow changes with increasing velocities [23], the shape and smoothness of the measurement tube and package is important in order to relate the sensor signal to total flow. The accuracy is affected strongly by noise and filtering has to be applied. However, measurement of the RMS. output voltage can be used as a no-flow indicator in large conduits: The turbulence of the flow is indicated by the large RMS output voltage of the sensor, which becomes zero when no flow is present.

3.4.2 Signal Conditioning

The fluid velocity u can be derived from King's law in two different ways: u as function of the temperature difference ΔT when the heating power P is kept constant and u as function of P when ΔT is kept constant. Two different methods are discussed for the latter method, normal feedback and Sigma-Delta modulation.
The first method, open loop, is indicated in figure 3.13a. P is kept constant independently of ΔT by applying a fixed voltage to the heat resistor. The voltage across the diodes that measure the heater temperature T_{heater} causes V_{out} to decrease when a voltage is applied to the heater. Therefore, the potentiometer is regulated in such a way that V_{out} equals zero when no flow is present. The voltage across the potentiometer represents T_{heater} when no flow is present. However, when a flow is present, T_{heater} will decrease. Hence, V_{out} will rise. In this way V_{out} is a measure for the flow. Because of the differential measurement of the temperature difference, a change in ambient temperature has the same effect on both diode strings.
The second method is called feedback, since ΔT is kept constant by regulating the heater voltage. This is achieved by using an amplifier as shown in figure 3.13b. The input voltage of the amplifier is regulated to zero by increasing the heater voltage V_{out}. Due to the thermal feedback, the voltage drops across the diodes near the heater. When the input voltage of the amplifier approaches zero, the voltage across the potentiometer represents T_{heater}. A flow decreases the heater temperature. However, now the amplifier increases V_{out} in order to return to the required heater temperature. Hence, V_{out} becomes a measure for the flow and the heater temperature is kept constant and set by the potentiometer.

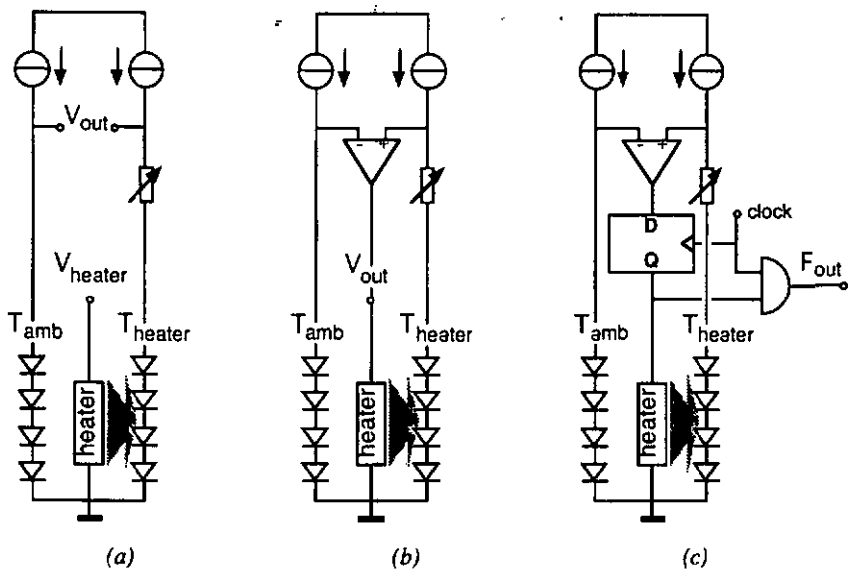

Figure 3.13: Circuit diagram showing (a) the open loop, (b) the feedbock and (c) the time modulation principle applied to the hot-wire sensor.

The third method, Sigma-Delta modulation, is shown in figure 3.13c. A Sigma-Delta modulator is build from a comparator, a switch and a D-flip-flop. When the temperature of the heater becomes to low, the output of the comparator becomes high and the heater is switched on at the next positive edge of the clock. When the heater reaches the required temperature, the output of the comparator becomes low and the heater is switched off at the next edge of the clock. Therefore, the frequency of clock pulses when the heater is on, F_{out}, is a measure for the flow, as the dissipated power is synchronised with the clock by the D-flip-flop. The clock period is chosen much smaller than the time constant of the sensor. In this way, 'Lock in' with the clock signal is avoided.

Table 3.2 gives a comparison between the different measuring methods. The simplest measurement method is the open loop configuration for which no additional circuitry is needed. However, for this arrangement an external voltmeter is necessary with an accuracy of 0.2 mV. With implementation of a high gain amplifier, the sensor can be used in the normal feedback configuration which results in a somewhat extended measurement range. Now an ordinary voltmeter can be used for accurate flow measurement. However, at the cost of only a little more hard-ware along with the sensor, a Sigma-Delta converter can be implemented. The main advantage of this configuration is that a voltmeter is not needed for the measurement, but a counter or PC. In addition, accuracy is not limited by the sensor noise or the voltmeter anymore, but by the measurement period. Therefore, this method is the most accurate, although the application has to allow for a measurement period that is much larger than the sensor relaxation time.

Measurement Principle	*Open loop*	*Feedback*	*Sigma-Delta modulation*
Measured signal	$\Delta T = \frac{P}{(O_1 + S_1)}$	$P = (O_1 + S_1)\Delta T$	$F = C \cdot (O_1 + S_1)\Delta T$
Range	*0 - 20 mV*	*3 - 4 V*	*pulses*
Resolution needed for 1 % accuracy	*0.2 mV*	*10 mV*	*±0.1 sec*
External detection	*Voltmeter (70 mV full scale)*	*Voltmeter (5 V full scale)*	*Counter or PC*
Additional circuitry	*none*	*amplifier 1000 x*	*Comparator, D flip-flop, AND gate and clock*

Table 3.2: Comparison of different electronic detection methods.

3.4.3 Response Low-Cost Mounting

In the following sections the measurement results are presented for the different measurement methods listed in table 3.2. The sensor was mounted on the TO-5 package. The measurements were carried out with the automatic measurement set-up which is described in section 2.4.1. Special attention was given to the temperature dependence of the sensor. All responses were found to be proportional to the square root of the flow, as was expected from King's Law.
Poor repeatability was observed due to the shape of the epoxy defining the flow profile across the sensor. Just behind the heated membrane a little bump of epoxy isolates the bonding wires and causes disturbances in the boundary layer which defines the sensitivity of the sensor. Even more important is the shape of the epoxy at the front end of the chip which cannot be controlled very well by the deposition method of the epoxy by a hollow needle. The second cause for the poor repeatability was the air that was dissolved in the water. It was observed that air bubbles are formed on top of the heater, even when the sensor is heated only a few degrees above ambient. These air bubbles can be very small and change the sensor response slightly so that no distinction can be made between the flow signal and the formation of small air bubbles. The third reason for drift and damage was due to bad electrical isolation from the fluid that affected all measurements. The isolation was achieved by epoxy covering the bonding wires. The black epoxy ISOL of Dexter showed a very good attachment to the silicon nitride layer on the chip. However, heating the device in water to 50 °C resulted in open contacts that were completely isolated from the water. Apparently, the bonding wires were pulled away from the bonding pads due to swelling of the epoxy, since the curing of the epoxy in a dry environment at 120 °C did never cause open contacts. The clear epoxy Araldit AY-105 in

combination with Araldit HY-991 did not show breaking of bonding wires. However, short cuts to the water were observed due to water flowing in-between the chip and the epoxy. Solutions could be found by using a combination of epoxies and pre-treatment of the chip surface to improve the interface of the epoxy and the chip.

3.4.3.1 Open Loop

Figure 3.14 shows the open loop sensor response for ambient temperatures varying from 10 °C to 40 °C. The sensor was connected as shown in figure 3.13a and the heater was supplied with an voltage of 3.6 volt, resulting in a dissipated power of 99.7 mW. The current through the diodes was set at 100 μA and resulted in a temperature sensitivity of 7 mV/°C and a voltage difference across the diode strings of 36.6 mV. Therefore, a heater temperature ΔT was found of 5.2 °C for an ambient temperature of 25 °C. By varying the flow from 0 to 85 mg/sec, the output voltage varied about 2 mV.

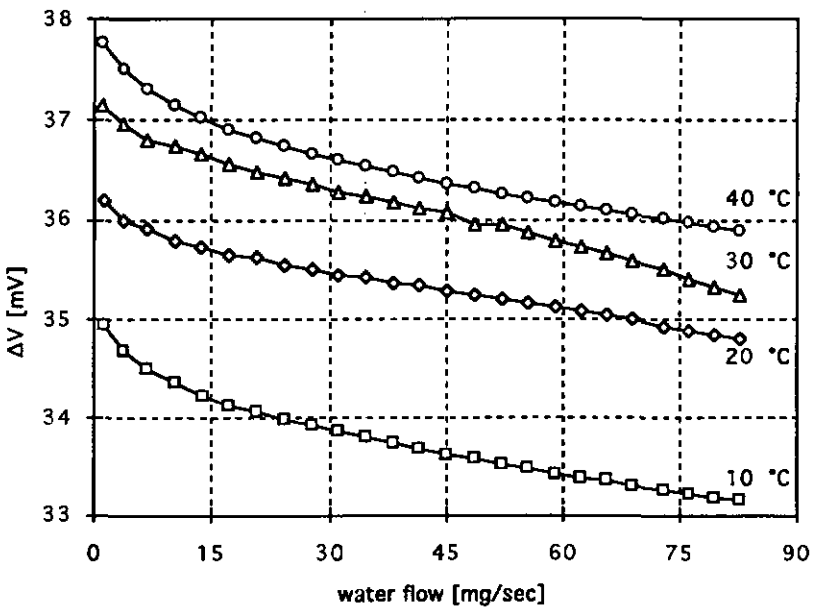

Figure 3.14: Open-loop sensor response of the hot-wire sensor for different ambient temperatures.

3.4.3.2 Feed-Back

Figure 3.15 shows the closed loop sensor response for different ambient temperatures. The sensor was connected as is shown in figure 3.13b and the temperature difference ΔT was set at 5 °C by means of an instrumentation amplifier built of 3 op-amps of a LM 324 integrated circuit. This resulted in a heating power of 98 mW for an ambient temperature of 25 °C. By varying the flow from 0 to 85 mg/sec, the heater voltage varied about 70 mV. A slightly better repeatability was found than for the open loop configuration. Furthermore, the signal voltages were about a factor 100 larger, reducing the

influence of noise and improving stability.

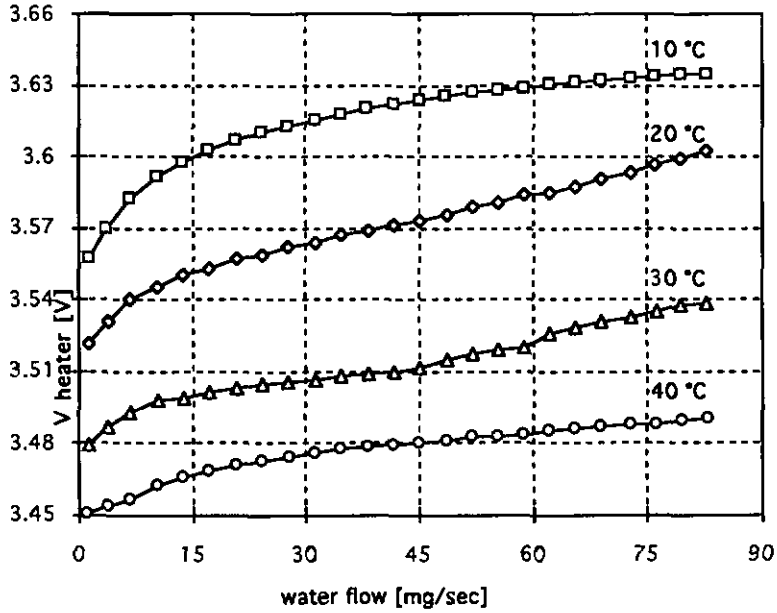

Figure 3.15: Closed-loop sensor response of the hot-wire sensor for different ambient temperatures.

3.4.3.3 Sigma-Delta Conversion

Figure 3.16 shows the digital sensor response for different ambient temperatures. The sensor was connected as is shown in figure 3.13c and the switch-on heater voltage was set at 6.2 V. This resulted in a heater temperature of 5 °C at which the heater was switched on for 52% of the time at an ambient temperature of 25 °C. The clock frequency was set at 300 kHz. By varying the flow from 0 to 85 mg/sec, the output frequency varied about 10 kHz. The crossing of the curves measured at 30 °C and 40 °C are due to the poor repeatability of the measurements due to air bubbles that are formed at the heated area. The sampling rate of the frequency counter was set at about three times per second, which resulted in a resolution better than 0.1 % full scale for the temperature measurement.

In order to investigate the absolute error of the frequency conversion, the effective output voltage of the heat resistor was measured by means of a low pass filter. Figure 3.17 compares the normalised frequency signal with the normalised measured effective voltage. A small and fairly random error distribution is found with a maximum of about 1 % full scale. These errors are partly due to noise caused by the flow, since the frequency and effective voltage were not measured exactly at the same time, but with a delay of one second. It is concluded that the Sigma-Delta modulator does not introduce significant non-linearity.

Comparing the responses of the three different excitation methods, the Sigma-Delta conversion offers highest resolution and stability, whereas the open loop

configuration needs special attention for noise reduction.

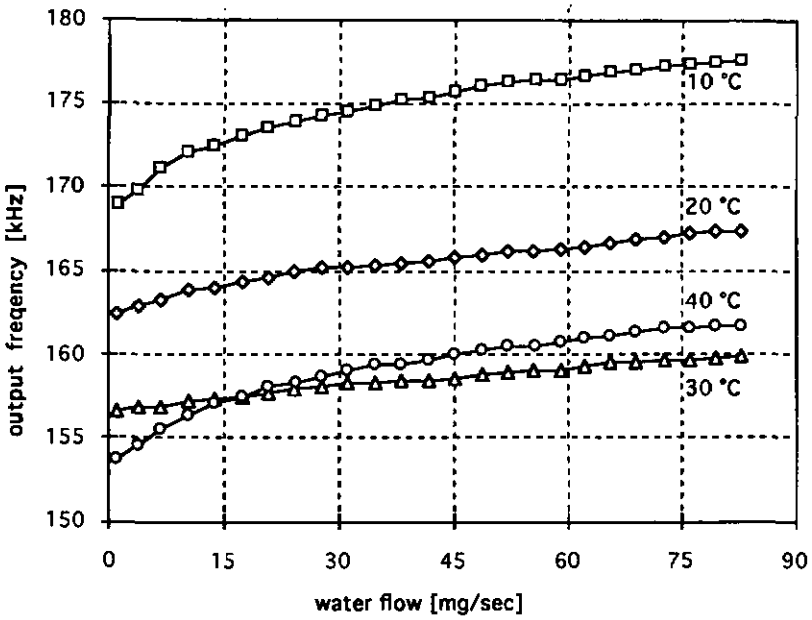

Figure 3.16: Sigma-Delta modulated sensor response of the hot-wire sensor for different ambient temperatures.

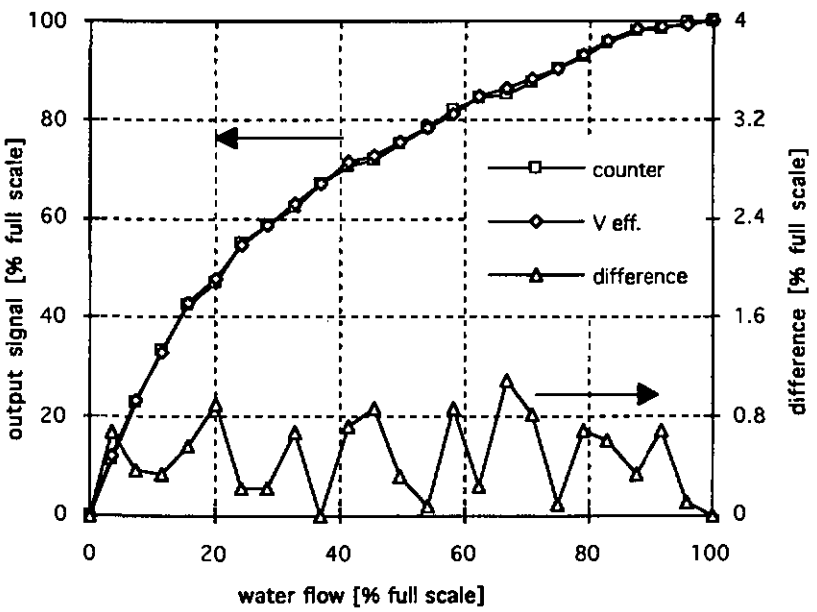

Figure 3.17: Normalised Sigma-Delta modulated sensor response of the hot-wire sensor in comparison with the effective voltage across the heater.

3.5 Temperature Dependence

The heat conductivity of silicon k_{si} was investigated since it determines the conductive heat flow in the sensor membrane, the bias component O_1 of the sensor signal. Much work has been done to characterise this property of silicon at low temperatures [22]. However, characterisation of k_{si} for different doping concentrations around room temperature was not found. Hence, experiments were performed in order to measure the temperature dependence of k_{si} which resulted in a large gradient of -0.35 %/°C. Therefore, the hot-wire sensor can be used only in a temperature range of a few degrees unless temperature compensation is applied. An effective compensation method has been found based on differential measurement with a two sensor arrangement where one sensor was exposed to the flow and the reference sensor was not. The sensors were driven by a Sigma-Delta modulator which increased the accuracy and offered digital output.

3.5.1 Heat Conductivity of Silicon

The heat transport in silicon is determined by phonons. At temperatures below 20 K, phonons are not disturbed by the crystal lattice and the heat conductivity is very large. However, for higher temperatures the phonon mobility is reduced strongly by the thermal activity of the crystal lattice, resulting in a negative temperature dependence of k_{si}. Free electrons or holes, created by doping atoms, should contribute to the heat conductivity. However, k_{si} decreases for higher doping concentrations since impurities reduce the phonon mobility in the crystal. Only at temperatures above 700 K the heat conduction by electrons contributes significantly to the total heat transport.
The heat conductivity of the silicon was not only measured for the hot-wire sensor, but also for the calorimetric sensor described in chapter 4. For the hot-wire sensor only the membrane was considered as a silicon heat conductance, whereas the entire calorimetric chip was considered as such. The chips were supplied with a heat flow P_{diss} by the on-chip heater and the temperature difference ΔT was measured with the on-chip temperature sensors for different ambient temperatures. The heat conductivity was calculated from the following formula with A the cross-section and L the length of the heat conductors:

$$k_{si} = \frac{L}{A} \cdot \frac{P_{diss}}{\Delta T} \tag{3.11}$$

Figure 3.18 depicts k_{si} as function of the ambient temperature. The square dots are measured with the hot-wire sensor, whereas the others represent measurements with the calorimetric sensor.
At room temperature the heat conductivity is 149 W/mK for the silicon chip with a membrane of 80 µm, whereas the other structures shows a smaller conductivity. All chips have a heavily doped boron 11 µm epitaxial layer that has a smaller heat conduction in comparison with the p-substrate which is only lightly doped. Therefore, k_{si} decreases with the membrane thickness, since structures with a thicker membrane have a larger portion of lightly doped

silicon. For the calorimetric sensor the heat resistance was measured for the entire chip including the lightly doped chip rims that conduct 80 - 90 % of the heat. Since only the heavily doped membrane area was taken into account for the hot-wire sensor, the difference between the 13 µm membrane and the 20 µm membrane is fairly large. Although the absolute value of k_{si} decreases with the doping concentration, its temperature dependence can be approximated by a gradient of -0.35 %/°C, independent of the doping concentration.

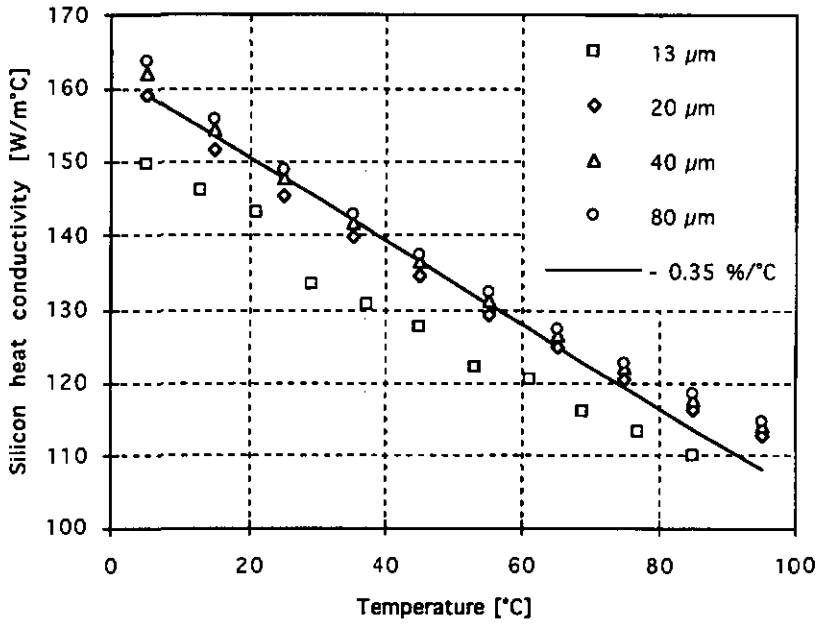

Figure 3.18: Measured heat conductivity of silicon k_{Si} as function of the ambient temperature and membrane thickness.

3.5.2 Temperature Compensation

The principle of differential measurement was elaborated with a Sigma-Delta converter in order to compensate for the influence of ambient temperature. Two sensors were used, one sensor exposed to the flow and the reference sensor placed in a side branch where no flow was present. Figure 3.19 shows the electric schematic of the double sensor arrangement. The signals F_{ref} and F_{sens} were realised with the circuit shown in figure 3.13c and applied to the circuit presented in figure 1.7. This resulted in a number representing ΔP, the difference in power dissipated in the two heaters.

Applying a same heater temperature to the two sensors, the heater of the first will dissipate both the static heat flow $O_1 \cdot \Delta T$ through the membrane and a dynamic heat flow $S_1 \cdot \Delta T$ which depends on the fluid flow. However, the heater of the second sensor will only dissipate the static heat flow, $O_1 \cdot \Delta T$, which equals that of the first sensor since they operate at the same (ambient) temperature. Subtraction of the two heat flows will result in a signal that

represents the dynamic heat flow of the first sensor, $S_1 \cdot \Delta T$. Note that the output signal equals zero when no flow is present, whereas with a single sensor in feedback mode the output signal is modulated on top of a large temperature dependent initial value, as was shown in section 3.4.

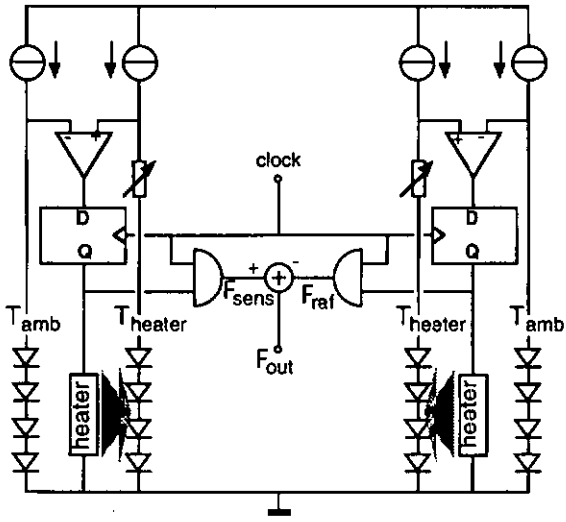

Figure 3.19: Double sensor arrangement for temperature compensation also offering digital output.

Figure 3.20 shows the output response of the double sensor arrangement which resulted in a sensitivity of 115 counts/√(mg/sec).

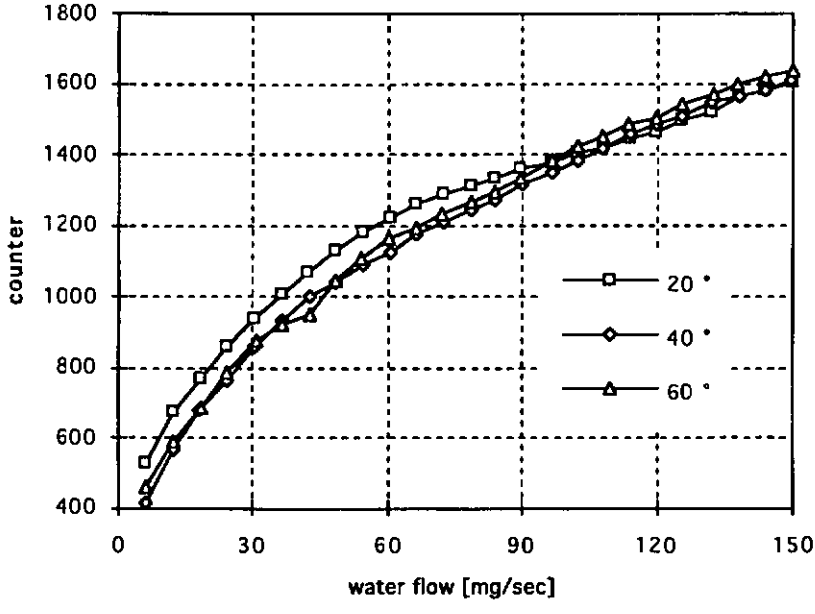

Figure 3.20: Response of the double sensor arrangement for different temperatures.

From the graph is observed that the compensation method is very effective and an error of only 4% full scale was observed for a temperature range from 20 °C to 60 °C. The offset shown in figure 3.21 was caused by the mismatch of the heat resistors and can be eliminated by two small resistors in series with the heaters.

3.6 Summary

A small silicon hot-wire flow sensor chip has been realised using an industrial bipolar process. In addition two packages have been developed and evaluated which were fabricated with industrial mass production techniques.
With the first package, a wing shaped ceramic, measurements were performed in a 20 mm conduit that justified the sensor model although turbulence affected the accuracy of the device strongly.
With the second package, based on a TO-5 housing, the measurement principles open loop, feedback and Sigma-Delta conversion have been applied for different ambient temperatures.
The dependence of ambient temperature has been characterised and an effective compensation method has been realised which was based on a differential measurement of two sensors where one sensor was not exposed to the flow. Here, the sensors were driven using Sigma-Delta conversion, resulting in high accuracy and digital output.

4 THE CALORIMETRIC FLOW SENSOR

4.1 Introduction

One of the most important challenges in flow measurement is the realisation of linear mass-flow sensors which are independent of fluid pressure and fluid temperature. Calorimetric flow meters [3,8] satisfy these goals well for both liquids and gases. Over the last 10 years, calorimetric flow sensors were also fabricated using integrated circuit technology [1,7,12,18]. These sensors consist of a flow channel in which one or three thin bridge structures are realised containing a heater and two temperature sensors. One sensor is placed upstream from the heater, whereas the other is placed downstream. A flow decreases the temperature of the first sensor, whereas it increases the temperature of the second and proportional to flow, a differential temperature signal is obtained.
A first drawback of the probe structure is that the thin sensing bridge is in direct contact with the fluid. This type of flow sensors is unsuitable for applications in hostile environments, since particle deposition or chemical attack will impede proper sensor operation. In this chapter the problem is solved by presenting the flow to the backside of a 50 μm thick silicon membrane, whereas the heater and temperature sensors are placed at the front side of this membrane.
A second drawback of the probe structure is that the sensor response is perturbed by the heat conduction in the probe supports and the heat transfer from the probe into the channel walls. Hence, the response of these sensors is affected by the ambient temperature and the fluid pressure. However, conventional calorimetric flow sensors are not perturbed by these quantities, since the entire capillary tube is used as measurement element instead of a probe structure. Hence, the design of the sensor presented in this chapter is based on a 7 mm long and 0.8 mm wide channel, conform conventional design.
The sensor was made by a bipolar process which allowed for the integration of a temperature controller, current sources and temperature sensors. The membrane was formed by micro machining. The chip was glued to a ceramic substrate with adjustable resistors for offset elimination.
A linear analytic model of the linear sensor response is presented and a qualitative explanation is given for the sensitivity and the temperature dependence which were both better than expected from the model.
The sensor was characterised using the on-chip temperature regulator and a dedicated Sigma-Delta converter. The measurements were performed for both water and air at different ambient temperatures and fluid pressures. As expected from the sensor model, the sensor responses were not affected by the ambient temperature and the fluid pressure.

4.2 Principle

The sensor principle is shown in figure 4.1. The sensor consists of a silicon chip in which a groove is formed. The groove forms a flow channel that is completed by gluing the chip to a substrate in which inlet and outlet holes are realised. The middle of the sensor channel is heated to a temperature T_{heater}. The heat flows from the middle of the tube to both ends which are clamped at ambient temperature. Hence a linear temperature gradient is created along the tube from the heater towards the ends. The presence of a fluid flow in the channel causes a heat flow from the tube wall into the fluid upstream from the heater, while creating an opposite heat flow downstream from the heater. As described in section 1.1.2, the resulting temperature difference $\Delta T = T_{down} - T_{up}$ is a function of the mass flow.

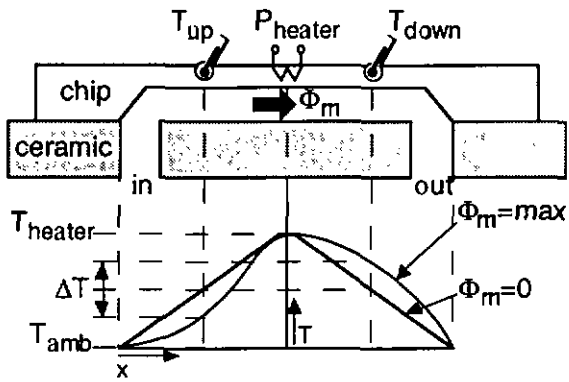

Figure 4.1: The principle of the calorimetric flow sensor.

A linear sensor model is derived showing that the sensitivity only depends on the heat capacity of the fluid and the heat conductance of the measurement tube. Additional model considerations are discussed to explain the improved sensitivity and the small dependence of the sensitivity on the ambient temperature.

4.2.1 Linear Model

The sensor model considers the temperature distribution along the sensor, which is created by the heat transport through the capillary tube and the heat transport by the fluid. The temperature difference between the fluid and the tube wall can be neglected by assuming that the heat diffusion from the tube wall into the fluid that is much larger than the heat transport by the fluid. This is achieved by using a tube diameter that is at least one order of magnitude smaller than the length of the tube. A uniform tube thickness is assumed to restrict the model to one dimension. Figure 4.2 depicts a schematic cross section of the measurement tube upstream from the heater.
The temperature gradient along the tube wall can be found in the following way:

$$T_x - T_{x+dx} = \frac{dx}{A_w k_w} q(x) \quad \Rightarrow \quad \frac{dT}{dx} = -\frac{q(x)}{A_w k_w} \tag{4.1}$$

with A_w, k_w and $q(x)$ respectively the cross-sectional surface, the heat conductivity and the local heat flow in the tube. For small mass flows the heat added to the tube, q_{fluid}, can be described with the specific heat of the fluid c_p and the mass flow ϕ_m:

$$q_{fluid} = q_{x+dx} - q_x = c_p \phi_m (T_x - T_{x+dx}) \quad \Rightarrow \quad \frac{dq}{dT} = -c_p \phi_m \tag{4.2}$$

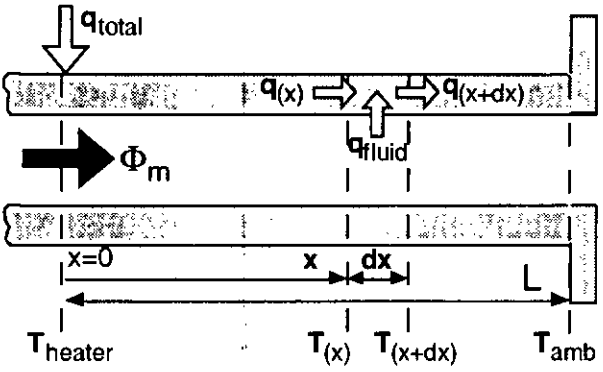

Figure 4.2: Schematic cross section of the measuring tube upstream from the heater.

Here, a constant temperature for a cross section of the tube is assumed as stated above. By combining equation 4.1 and 4.2, the heat flow through the measurement tube is found:

$$\frac{dq}{dx} = \frac{c_p \phi_m}{A_w k_w} q(x) \quad \Rightarrow \quad q(x) = C \exp\left(\frac{x c_p \phi_m}{A_w k_w}\right) \tag{4.3}$$

The constant C is found by solving the following equation by substituting equation 4.3 with T = T_{amb} at $x = L$ (half the tube length) and T = T_{heater} at $x = 0$:

$$\int_0^L q(x)dx = \int_{Theater}^{Tamb} -A_w k_w dT = A_w k_w (T_{heater} - T_{amb}) \tag{4.4}$$

Now the temperature T_{up} at $x = L/2$ can be expressed by solving the following integrals and substituting equation 4.3 and the constant C calculated from equation 4.4:

$$\int_0^{L/2} q(x)dx = \int_{Theater}^{Tup} -A_w k_w dT \quad \Rightarrow \quad \frac{T_{up}}{T_{heater}} = 1 - \frac{1 - \exp\left(\frac{L c_p \phi_m}{2 A_w k_w}\right)}{1 - \exp\left(\frac{L c_p \phi_m}{A_w k_w}\right)} \tag{4.5}$$

A similar expression is found for T_{down} by changing the sign of ϕ_m. By rearranging the latter expression for T_{down} and T_{up}, the following expression for the sensor response is found:

$$\frac{\Delta T}{T_{heater}} = \frac{2\sinh\left(\frac{Lc_p\phi_m}{2A_wk_w}\right) - \sinh\left(\frac{Lc_p\phi_m}{A_wk_w}\right)}{1-\cosh\left(\frac{Lc_p\phi_m}{A_wk_w}\right)} \tag{4.6}$$

where ΔT equals T_{down} -T_{up}. The derivative of equation 4.6 to ϕ_m is almost constant for small flows. Therefore, this equation can be approximated by the following linear function which has a slope that equals the derivative of equation 4.6 for $\phi_m \rightarrow 0$:

$$\phi_m \approx \frac{4A_wk_w}{Lc_p} \cdot \frac{\Delta T}{T_{heater}} \tag{4.7}$$

This approximation is precise within 1 % in case the modulation of the signal ΔT does not exceed 20% of the heater temperature. However, not only the approximation 4.7, but also equation 4.6 is not valid anymore for such high flows, since the assumption that no temperature difference is present between the wall and the fluid does not hold anymore for signals beyond this range.
For small flows the sensor signal is linear proportional to the mass-flow. In contrast with other silicon sensors, the proportionally constant of the sensitivity only depends on the specific heat c_p of the fluid. Since the fluid heat diffusion does not appear in the model, the sensor is not sensitive to the fluid viscosity and the fluid heat conductivity. The sensitivity is also proportional to the channel heat conductivity. Since this conductivity depends on the ambient temperature, a temperature dependent sensitivity is expected. However, compensation can be achieved by modulation of the heater temperature by the ambient temperature.
Equation 4.7 is presented in a different way by equation 4.8, to demonstrate the similarity of the calorimetric flow sensor with an electrical Wheatstone bridge as presented in section 1.2.2. When used for a pressure sensor, the Wheatstone bridge produces a differential voltage V_{out}, which is linear proportional to the pressure P with the sensitivity factor α. The bridge is supplied with a constant voltage V_{bridge} and when no pressure is applied, its total resistance equals R_o. Similar to the electrical Wheatstone bridge, the calorimetric flow sensor produces ΔT, which is linear proportional to ϕ_m with the sensitivity factor β which equals $c_p/2$. The bridge is supplied with the temperature T_{heater} and when no flow is present, the total heat conductance equals G_o.

$$\begin{aligned} &\textit{Flowsensor:} && \frac{\Delta T}{T_{heater}} = \beta\frac{\phi_m}{G_o} \quad \textit{with} \quad G_o = \frac{2A_wk_w}{L} \\ &\textit{Pressuresensor:} && \frac{\Delta V}{V_{bridge}} = \alpha\frac{P}{R_o} \end{aligned} \tag{4.8}$$

The similarity with the conventional Wheatstone bridge is striking. Hence, this sensor can be regarded as a thermal Wheatstone bridge and differential measurement is exploited to minimise offset and offset drift. Since the comparison of the two temperature signals already takes place in the thermal domain, an intrinsic compensation is effected, as discussed in section 1.2.2.

4.2.2 Additional Model Considerations

Experiments showed that the sensitivity is larger and the temperature dependence of the sensitivity, TCS, is smaller than was expected from the model. The model defines the sensor sensitivity proportional to the ratio of the heat capacity of the fluid and the heat conductance of the tube. The heat conductance is proportional to the heat conductivity of silicon which measures -0.35 %/°C, as is shown in figure 3.18. Since the heat conductivity of the sensor tube appears in the nominator of the linear model, a TCS of 0.35 %/°C was expected. This section argues that both the sensitivity and TCS are better than expected because the effective cross-sectional area that contributes to the sensor transfer function is smaller than the total cross-section A_w of the sensor tube, as assumed by the model. This effective cross-sectional area is determined by the asymmetry of the cross-section of the measurement tube. By taking into account this asymmetry, the determination of the sensor transfer would result in a three dimensional numerical flow problem, requiring too much computer power for our facilities. Hence, the influence of this asymmetry is discussed qualitatively.
The cross-section of the sensor can be divided in a thin membrane section and two thick sensor sides, as depicted in figure 4.3. If the entire measurement tube would have a thickness that equals the membrane thickness, a much smaller effective area has to be taken into account for the model, resulting in a much higher sensitivity. On the contrary, a much lower sensitivity would be found if the entire tube would have a thickness that equals the thick sides. Hence, the temperature change at the membrane is higher than predicted, whereas at the sensor sides, the temperature change is smaller than predicted. Since the temperature sensors are placed at the middle of the membrane, the measured sensitivity is larger than predicted by the model.

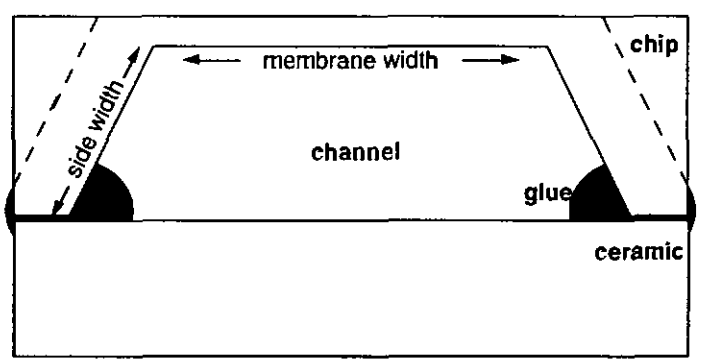

Figure 4.3: Schematic cross-section of the measuring tube.

A second reason for the enhanced sensitivity is the presence of an effective depth at the sides. This effective depth is explained in the following way: The heat transfer between the fluid and the tube wall causes a temperature gradient in the wall which is inversely proportional to the tube thickness and perpendicular to the inner tube surface. The heat flowing out of (or into) this surface is delivered by (or added to) the conductive heat flowing from the heater along the tube and the closer to the inner tube surface, the more is contributed to the heat exchange at this surface. Hence, the temperature gradient perpendicular to the inner surface has its maximum at this surface and decreases towards the outer surface. The effective depth is reached when the gradient approaches zero. For very thick tube walls, this depth is smaller than the distance to the outer tube surface and the temperature at the outer tube surface will not change anymore with the flow. The effective depth defines an effective inner cross-sectional area that contributes to the heat exchange. The temperature is independent of flow beyond this area. The dotted lines in figure 4.3 represent the effective tube area at the sensor sides which is smaller than the total chip cross-section. Hence, by replacing the entire cross-sectional area A_w by the effective inner area, a higher sensitivity is anticipated by the model.
Introduction of an effective area not only results in a higher predicted sensitivity, but also in a smaller TCS. A TCS of 0.35 %/°C was expected from the linear model taking into account the entire cross-section of the tube. The small TCS is explained by the presence of an effective inner area, through which the heat flows that contributes to the heat exchange with the fluid. When the heat conductivity of the tube decreases by an increase of ambient temperature, less heat becomes available in that area for the heat exchange with the fluid. To provide more heat that is necessary for the exchange, the heat flow beyond the effective inner area starts to contribute as well. Hence, the effective depth increases with the ambient temperature and the product of the effective area and the heat conductivity remains constant at the thick sensor sides, independently of the temperature dependence of the silicon heat conductivity. Therefore, the silicon heat conductivity only has an effect in the membrane. Hence, the TCS is much smaller than the temperature dependence of the heat conductivity of the sensor tube, due to the thick sides of the sensor tube.

4.3 Realisation

The design and the packaging of the sensor is discussed. Both the sensor chip and the ceramic substrate with the thick-film circuit were produced by industrial fabrication processes. Not only the heater and the temperature sensors were integrated on-chip, but also the current sources to supply the temperature sensors and the heater regulation.

4.3.1 Low-Cost Hybrid Design

Original calorimetric sensors consist of a metal capillary tube which is heated in the middle by a platinum heat resistor. The temperature difference upstream and downstream from the heater are measured by platinum resistors also. The ends

of the tube are clamped in a metal block which assures that the temperature of both tube ends are kept at ambient temperature.
For the design presented here, a 7.0 mm long and 0.8 mm wide flow channel was micro-machined in a silicon die of 8.0 mm x 1.5 mm by using an anisotropic etch to form a 50 µm thick membrane over an 350 µm high flow channel. The heater was placed in the middle of this channel and the temperature sensors were placed at one fourth the channel length from each end of the channel to obtain a maximal output signal. Temperature sensors were also placed in the heater area and at the rim of the chip in order to control the heater to a fixed temperature, relative to the ambient temperature. The circuitry was fabricated using the same fully industrial bipolar process described in section 3.3.1.4. The chip was glued to an aluminium oxide ceramic substrate in which two inlet-outlet holes of 0.7 mm diameter were laser-drilled. Furthermore, slits were drilled in the substrate next to the chip in order to achieve maximal thermal insulation of the flow channel. The ceramic substrate served as an excellent heat sink to assure ambient temperature at both ends of the chip. A thick-film circuit printed on the ceramic provided electrical connection with the chip. Thick-film trim resistors set the heating temperature and cancelled offsets. Figure 4.4a shows the thick film substrate for six sensors.
For characterisation the sensor was clamped to an aluminium block which provided a 6 mm fluid interconnect. Sealing between the block and the ceramic was achieved by O-rings with an inner diameter of 0.7 mm. The block also provided a good heat sink for the sensor. Figure 4.4b shows a photograph of one completed sensor mounted to the aluminium block.

4.3.2 On-Chip Electronics

Figure 4.5 shows a block diagram of the circuitry which is used to drive the flow sensor. The temperatures T_{heater}, T_{amb}, T_{up} and T_{down} are each measured by a string of four diodes that are supplied by a constant current of 100 µA in order to obtain four temperature dependent voltage sources of about 7.00 mV/°C. In series with the temperature sensing diodes, small resistors are connected: By adjusting R_{up} and R_{down} V_{out} is set to zero when no flow is present. The heating temperature of the heater is set by adjusting R_{center}.
The calorimetric flow sensor was realised with two different on-chip circuits. The first version was fabricated by ASCOM Microelectronics, whereas the second version was produced by H.E.G. in Frankfurt a.d. Oder, Germany. For the first version heating was provided by means of a 300 Ω resistor in the middle of the sensor tube, that was driven by an external instrumentation amplifier which was built of three op-amps of a standard LM 324 circuit on a PCB. The resistor R_{up} was realised on-chip by the base-diffusion. This resistor showed an important temperature dependence of about 0.2 %/°C that resulted in offset drift. Hence, for the second version, these resistors were all realised on the ceramic, since thick-film resistors have a negligible temperature dependence. In addition, the heat resistor was replaced by two Darlington transistors. The dissipated heat in these transistors is given by the product of the collector current and supply voltage. The amplifier driving these transistors, was integrated on-chip.

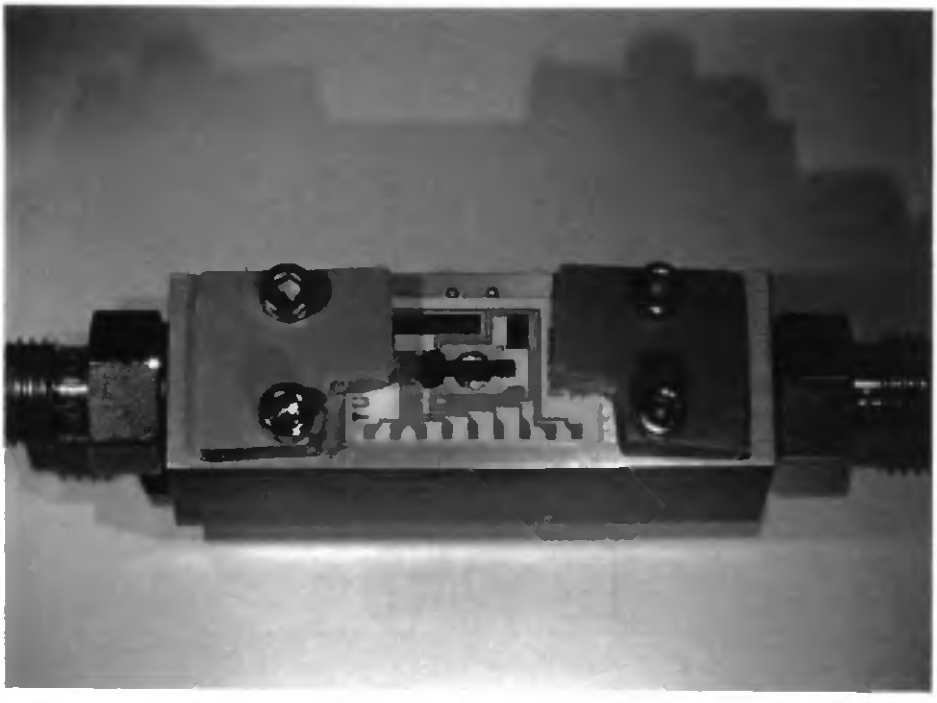

Figure 4.4a: The completed calorimetric flow sensor of the first series mounted on the aluminium block.

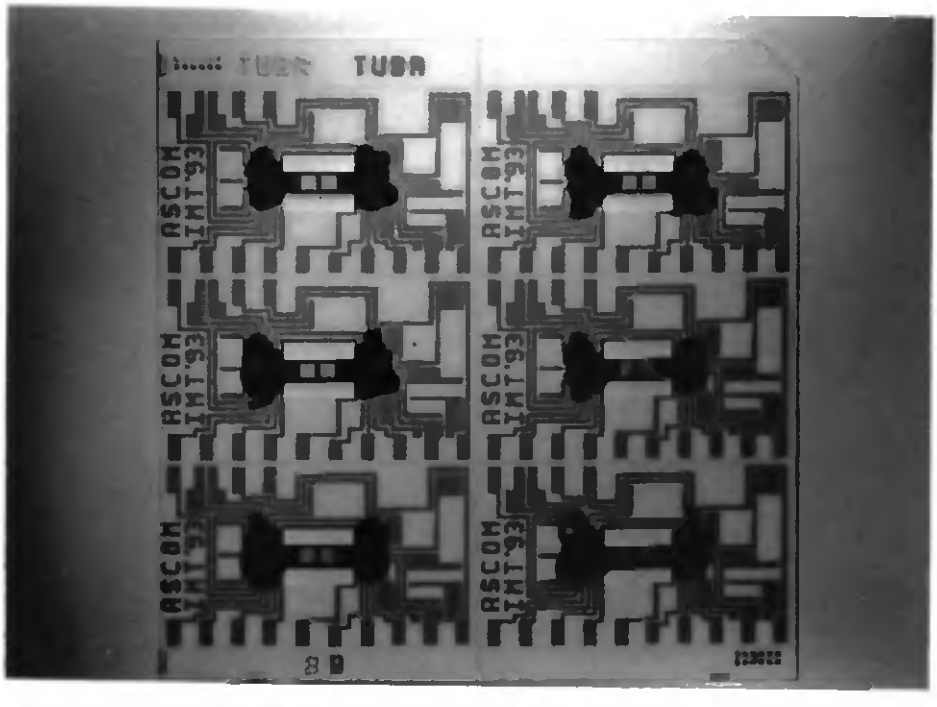

Figure 4.4b: The ceramic substrate with mounted chips and thick film interconnect for six sensors of the second series.

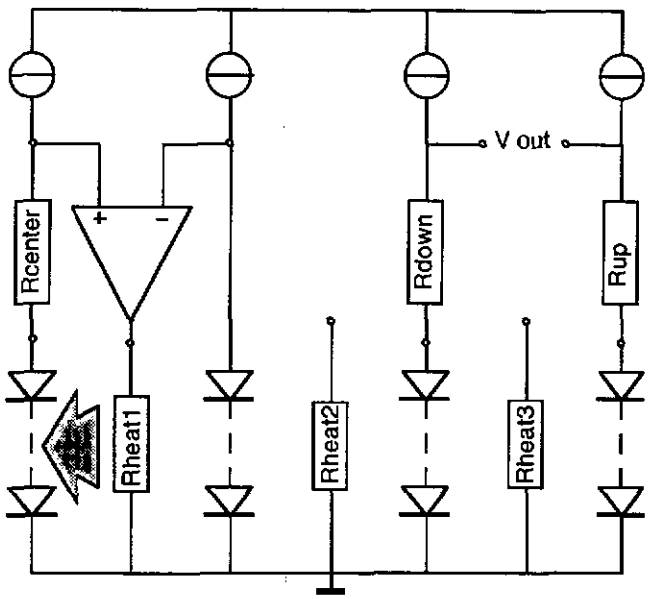

Figure 4.5: Block diagram of the sensor driving circuit.

Two additional heat resistors were integrated upstream and downstream from the middle to be able to maintain the temperature at both sides at a constant value by using a Sigma-Delta controller for the current fed to the two heaters. Figure 4.6 depicts the circuit diagram of the bipolar circuitry integrated on the second version. The reference current I_{ref} is generated by the voltage across R_3 and copied by the Wilson current mirror *1* to the four temperature sensing strings. A second Wilson current mirror 2 assures that the currents are equal in all temperature sensing strings by using a closely matched transistor layout in a common centroid geometry. Mirror *1* also copies I_{ref} to the Zener-connected transistor T_1. The Zener voltage V_{zener} determines the voltage across the resistors R_3-R_1. The voltage across the resistors R_2 and R_1 is proportional to the base-emitter voltage V_{be} of T_2. Hence, the proper choice of the ratio R_2/R_1 can be used to cancel first order temperature effects and I_{ref} can be expressed as:

$$I_{ref} = \frac{\frac{R_5}{R_5+R_4}V_{zener}(T) + \left(1 - \frac{R_2}{R_1} - \frac{R_5}{R_5+R_4}\right)V_{be}(T)}{R_3(T)} \qquad (4.9)$$

Transistor T_3 was not implemented on the first version which resulted in a meta-stable condition. The current through the resistors R_4 and R_5 was equal to I_{ref}, although the voltage across these resistors was 3 V smaller than V_{zener}. This resulted in a current of only 23 µA for the current sources. To prevent the circuit from being locked in this condition, an external capacitor was connected between the emitters of mirror 2 and V_{cc}. This caused the voltage across the Zener to reach its breakdown voltage when the circuit was switched on. This condition was effectively eliminated by adding transistor T_3.
Figure 4.7 depicts the measured temperature dependence of one of the current sources of the first version. The parabolic temperature dependence indicates the

cancelling of first order temperature effects. The use of Wilson current mirrors increased the output impedance of the current mirrors, resulting in a measured power supply dependence of the current sources of only 0.15 %/V.

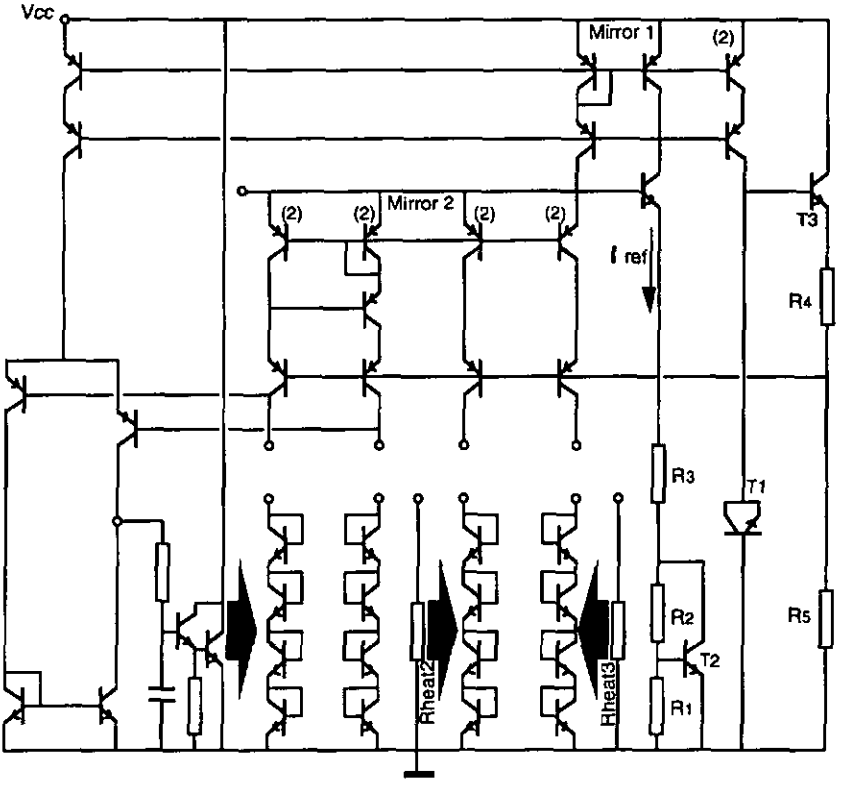

Figure 4.6: Circuit diagram showing the circuitry integrated on-chip.

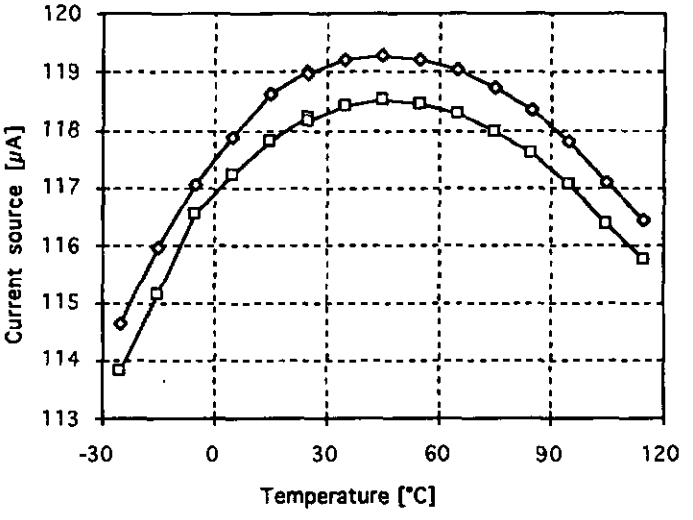

Figure 4.7: Measured temperature dependence of the on-chip current sources.

The integrated heat controller consists of a differential amplifier. Its output current is directly fed to the base of the Darlington transistors. An external resistor of 100 KΩ was connected in-between the base of the Darlington and the supply voltage to provide a bias current for the Darlington transistors. A capacitor was integrated on-chip between the base and ground to prevent oscillation. It consisted of an 1.1 mm^2 aluminium square connected to the base of the Darlington which was realised above a grounded emitter diffusion.
Figure 4.8 depicts the deviation of the heater temperature as function of the ambient temperature for two different devices operating at a different heating temperatures. For both devices the heater temperature changed with 0.024 °C per 1 °C ambient temperature, for both water and air. This value was caused by a difference in sensitivity of 0.2 mV/°C of the heater temperature sensor and the ambient temperature sensor. The difference is explained by the fact that for the second version, current mirror 2 was implemented without a buried layer. Therefore, only 15 % of the current injected by the double emitters arrived at the collectors, whereas 85 % disappeared into the substrate. This is caused by the fact that a buried layer between the epitaxial layer and the substrate would block the current to the substrate by recombination of all the minority carriers that are now able to cross the epitaxial layer. The ratio of the currents reaching the collector and the substrate depends on the voltage across emitter and collector which is 2 V_{be} for all transistors, except for the transistor connected as a diode. This one has an emitter-collector voltage of only 1 V_{be} and the current that reaches the collector of this transistor is only 45 - 55 % of the current that reaches each of the other collectors. Hence, the sensitivity of the temperature sensor connected to this branch is 0.2 mV/°C less than for the other branches.

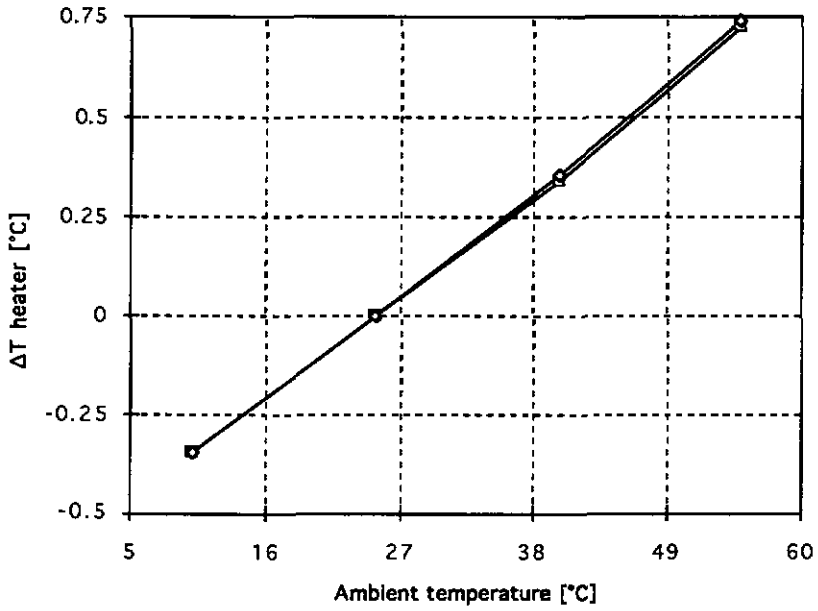

Figure 4.8: Measured heater temperature shift as function of the ambient temperature.

It is concluded that the temperature dependence of the heater temperature is caused by the lack of the buried layer of current mirror 2. This layer was left out unintentionally and has to be added in further versions of the design. The measurements taken with the temperature controller, were all corrected for this dependence.

4.4 Characterisation

Two different ways of signal treatment were used to characterise the sensor. The first method was based on differential temperature measurement for which the temperature in the middle of the chip was regulated by the on-chip temperature controller. The second method was based on maintaining a certain constant temperature upstream and downstream from the middle by regulating the currents in the resistors at one third and two thirds of the measurement tube. Since for this arrangement two temperature controllers were used with two thermal feedback signals in one single chip, a special Sigma-Delta modulator was used to guarantee a stable sensor signal. Measurements were taken for both water and air with the measurement set-up that was described in section 2.4.1.

4.4.1 Differential Temperature Measurement

The first measurement method for sensor characterisation was based on differential temperature measurement upstream and downstream from the heater. The temperature in the middle of the sensor tube was kept constant by the on-chip heat controller discussed in section 4.3.2. In this way, an open-loop measurement of the flow was realised. Since the heater temperature controller depends on the ambient temperature with a gradient of 0.024 °C/°C, all output voltages are normalised for a heater temperature of 1 °C, although the heater temperature was set at a temperature of about 12 - 18 °C above ambient.

4.4.2 Differential Current Measurement

The second measurement method for sensor characterisation was based on differential measurement of two heating currents with a Sigma-Delta converter. In contrast with the former method, a closed-loop measurement arrangement is realised by controlling the temperature upstream and downstream from the middle of the sensor tube to a same temperature above ambient. The magnitude of the flow is represented by the current difference.
A straight forward solution to provide such a feedback could not be implemented due to thermal cross talk. The heat resistors and temperature sensors of the calorimetric flow sensor are realised on one single chip. Therefore, the thermal cross talk of the two feedback controllers is very high. By using analog temperature regulators, a stable sensor output is obtained, since no heat flows from the upstream sensor to the downstream sensor when these sensors are once at the same temperature. However, Sigma-Delta conversion is based on regulation of the *average* temperature by using of heat pulses that cause temperature variations. Since the temperature controllers trigger each other by their heat pulses, the sensor output becomes unstable. This problem

was successfully solved by using one Sigma-Delta temperature controller in combination with an analog controller, as depicted in figure 4.9.

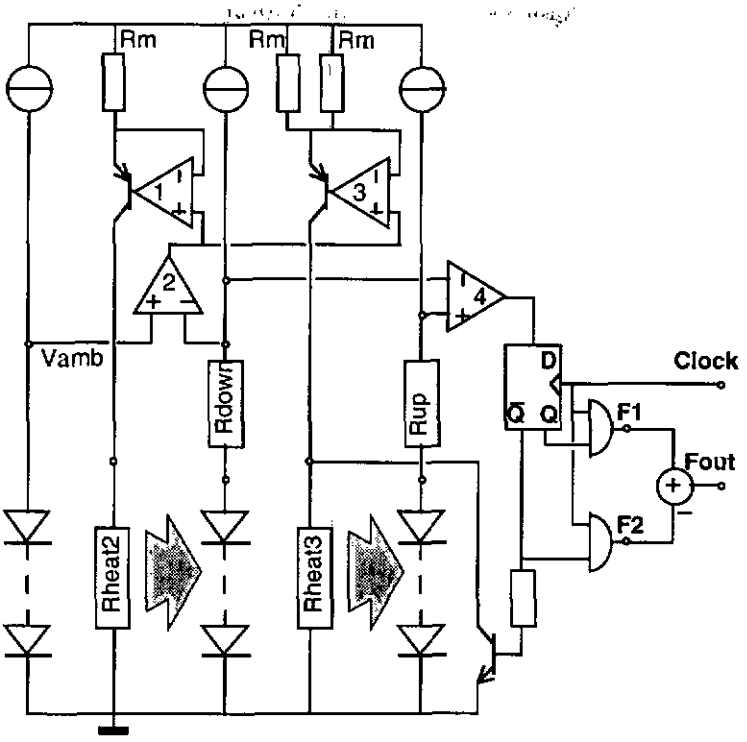

Figure 4.9: Differential power measurement based on Sigma-Delta conversion.

The heater downstream from the middle is depicted on the left of the circuit diagram and is supplied with a heating current from the current source that is realised with op-amp *1* and resistor R_m. The high gain amplifier 2 regulates this current in such a way that downstream from the middle a constant temperature above ambient is set by the trim resistor R_{down}. The voltage across this resistor represents the regulated heater temperature. A second heating current, about twice as large as the first heating current, is created simultaneously with op-amp *3* and two resistors R_m. This current is either switched to the heating resistor upstream from the middle of the sensor or to ground through the npn transistor. This transistor acts as a switch which is regulated by comparator *4* in combination with the clock triggered flip-flop, to regulate the temperature upstream to the same value as the temperature downstream from the middle. The pulse-width of the current pulses in this heat resistor is then F_1/F_{clock}. As shown in section 1.3, the ratio F_1/F_2 is an expression of the current difference upstream and downstream from the middle. Hence, this difference of heating current is a measure for flow. If no flow is present, F_1 can be set equal to F_2 by trimming one of the resistors R_m. Trimming the resistor R_{up} would cause a temperature offset and results in offset drift, as is explained in the next paragraph. The frequency ratio can be measured directly with the low-cost circuit depicted in figure 1.6. The total circuit consists of the on-chip current sources, heat resistors and temperature sensors in combination with a PCB

'eurocard' with standard op-amps and TTL logic. The frequency F_1 was counted by a HP frequency counter which was triggered after 2^{14} pulses of F_2. This trigger pulse was generated by a programmable frequency divider built of the integrated circuit SN74292. A clock frequency of 50 kHz was used for triggering. The clock period was about 100 times shorter than the sensor relaxation time.
In principle, the circuit described above can by simplified by replacing the analog temperature regulation, realised with op-amp *2*, with a constant heating current. Omitting op-amp *2* and applying a constant voltage on the positive inputs of the op-amps *1* and *3* will result in a constant heating current. Although this results in higher heating temperatures for higher ambient temperatures, the sensitivity, expressed by the ratio of F_1 and F_2, would not change. Experiments with such a constant heating current resulted indeed in a sensitivity independent of ambient temperature, However, a large offset drift for the output frequency was found which was linear proportional to the heating temperature. Apparently, the heat conductance upstream from the middle of the sensor was modulated in a different way by the heater temperature than downstream from the middle. This mismatch was probably caused by parasitic heat flows such as free convection. However, the modulation of the conductance by the heating temperature was prevented by keeping the heater temperature constant by means of the regulation implemented with op-amp *2*.
The circuit depicted in figure 4.9 was not only used for the characterisation of the sensor for both air and water, but was also successful in providing a digital signal with a commercial flow sensor which consists of two platinum heat resistors mounted to a stainless steel tube [9]. For the latter application the platinum heat resistors also served as temperature sensors.

4.4.3 Sensor Response for Air

Figure 4.10 depicts the digital sensor response for different absolute fluid pressures at room temperature. The measurements were taken with the Sigma-Delta converter described in the previous section. Since a mass-flow was applied to the sensor, the fluid velocity in the sensor is inversely proportional to the fluid pressure. However, a significant change for the sensor response is not observed. Hence, the sensor acts as a real mass-flow sensor as was expected from the sensor model and the Reynolds number, which is proportional to the fluid velocity, does not affect the sensor response.
Figure 4.11 depicts the sensor response that was measured for different ambient temperatures with both the Sigma-Delta converter and the on-chip temperature controller. For both measurement methods, the sensitivity is constant for flows smaller than 0.4 mg/sec. Beyond this value the sensor response is not linear anymore, as boundary layers start to affect the sensor function.
In general, no offset drift is observed, although the offset shows a drift for the Sigma-Delta converter at 55 °C and for the temperature controller at 10 °C. These offset drifts are probably due to statistical measurement errors, since no repeatability of these offset drifts was found.

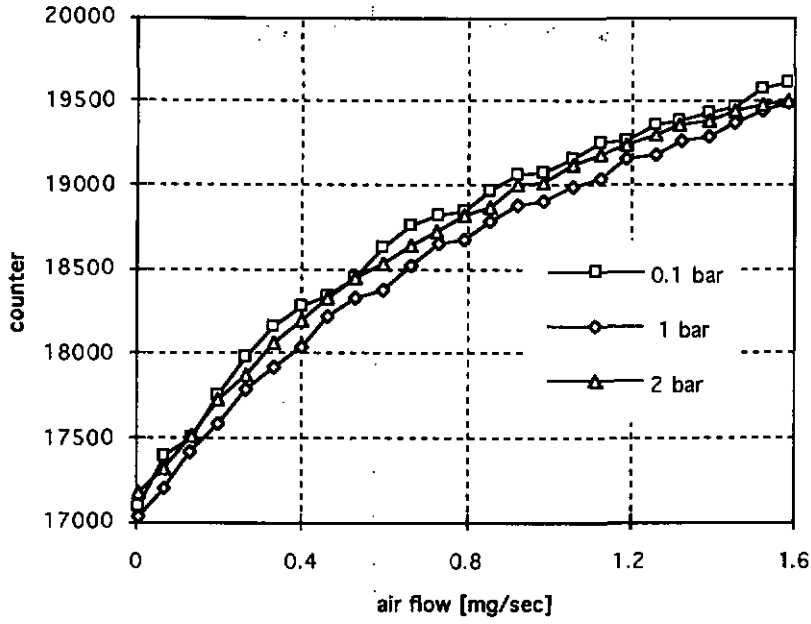

Figure 4.10: Measured digital response for air at different outlet pressures.

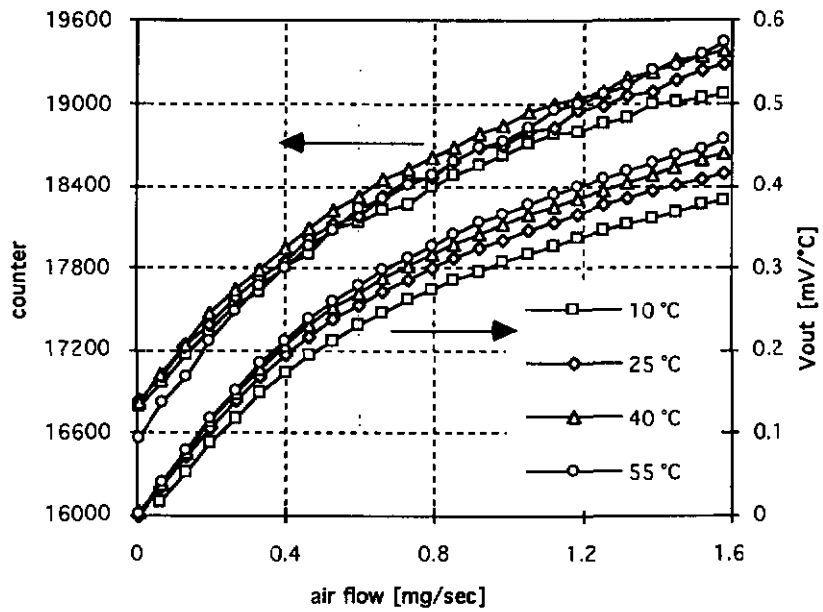

Figure 4.11: Measured digital response and differential temperature response for air at different ambient temperatures.

4.4.4 Sensor Response for Water

Figure 4.12 depicts the sensor response for the first version for different membrane thicknesses. A linear response is found up to 1 mg/sec for the three membrane thicknesses. The sensitivities were 60 % higher than expected from equation 4.7. As discussed in section 4.2.2, the high sensitivity was caused by the following effects: a) The membrane thickness which is much smaller in comparison with the sensor sides, and b) the presence of an effective inner area for the thick sensor rims. A slightly higher sensitivity was found for the 20 μm thick membrane, than for the sensors with a membrane thiekness of 40 μm and 80 μm, which showed a same sensitivity. Therefore, the first effect is only significant for a membrane thickness smaller than about 30 μm, whereas the second effect was present for all sensors.

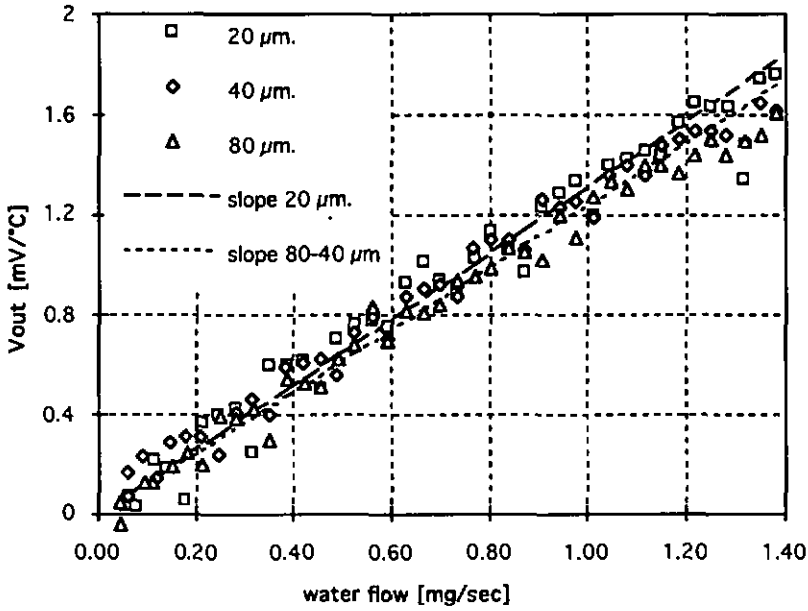

Figure 4.12: Measured response for water for different membrane thicknesses. (Normalised for a heater temperature of 1 °C and corrected for offset.)

Since a large random error was found on the measurements due to air bubbles, the measurement set-up was slightly changed by placing the sensor in-between a small water reservoir and the input of the flow controller. This water reservoir was placed in the climate chamber and a pressure of 300 mbar was supplied to the reservoir in order to achieve a stable flow. This change greatly reduced the influence of air bubbles, resulting in much more stable measurements.
Figure 4.13 depicts the sensor response for the Sigma-Delta converter and the open loop response for different ambient temperatures. A linear response was found up to about 1.3 mg/sec, independent of temperature. Offset drift was not observed and the sensitivity is only slightly temperature dependent. Hence, the temperature dependence of the silicon heat conductivity is effectively suppressed by the shape of the tube cross-section as discussed in section 4.2.2.

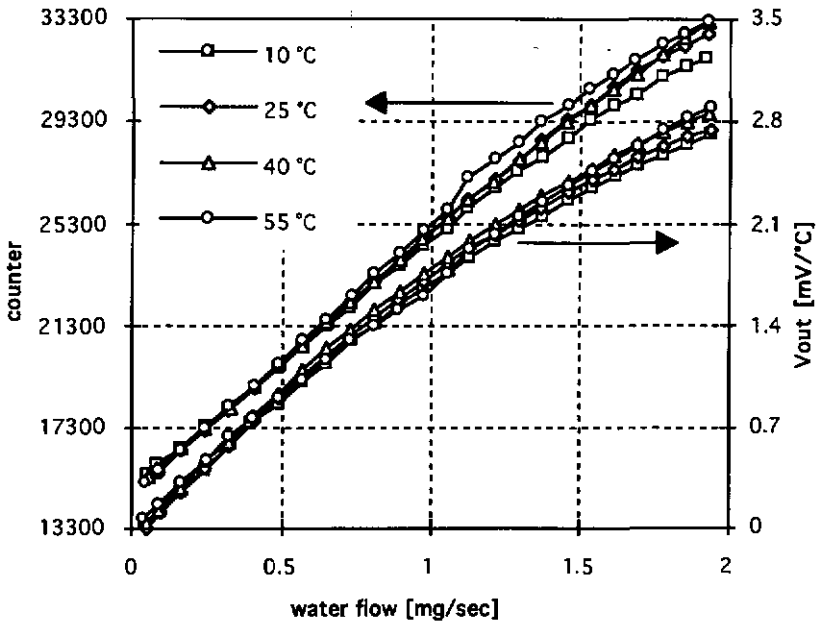

Figure 4.13: Measured digital response and differential temperature response for water at different ambient temperatures.

Figure 4.14 shows the differences between the two measurement methods for both air and water. Each curve represents the average output of the four measurements at different ambient temperatures of the previous graphs. This graph shows that the signal modulation for water is four times higher than for air. This ratio equals the ratio of the heat capacities of water and air. Hence, if the sensor is calibrated once for a certain fluid, it can be used for other fluids also by multiplying the output with the ratio of heat capacities of the actual fluid and the calibration fluid.

For water the power modulation and the temperature modulation is exactly the same. However, figure 4.13 shows that the counter offers a larger linear range than the differential temperature difference. This can be explained by the fact that the power modulation is represented by $(F_1-N_o)/(F_1+N_o)$ whereas the counter output represents (F_1-N_o). N_o represents the offset of the converter and equals F_1 if no flow is present. The difference of these functions can be regarded as a non-linearity of the Sigma-Delta read-out and was depicted in figure 1.5. This non-linearity compensates for the non-linearity of the sensor response.

For air, the power modulation is higher than the temperature modulation for flows higher than 0.4 mg/sec. This is explained by the fact that the temperature distribution is different for the two measurement methods. The Sigma-Delta modulator maintains a constant temperature from one third to two third of the sensor tube, whereas for the differential temperature measurement the temperature is only kept constant at the middle of the sensor. For this method the fluid is not heated completely anymore for flows higher than 0.4 mg/sec. This effect is not only caused by the limited heat conductivity of air, but also boundary layers start to have an effect at higher flows. Hence, the sensitivity

drops for high flows. However, for the Sigma-Delta converter a third of the sensor tube is kept at a constant temperature. Therefore, a better heat transfer from the tube to the fluid is achieved at higher flow velocities. Hence, the loss in sensitivity is much less. Boundary layers do not affect the sensor response for water, since the flow velocity for water is about 900 times lower than for air and the heat conductivity 30 times higher.

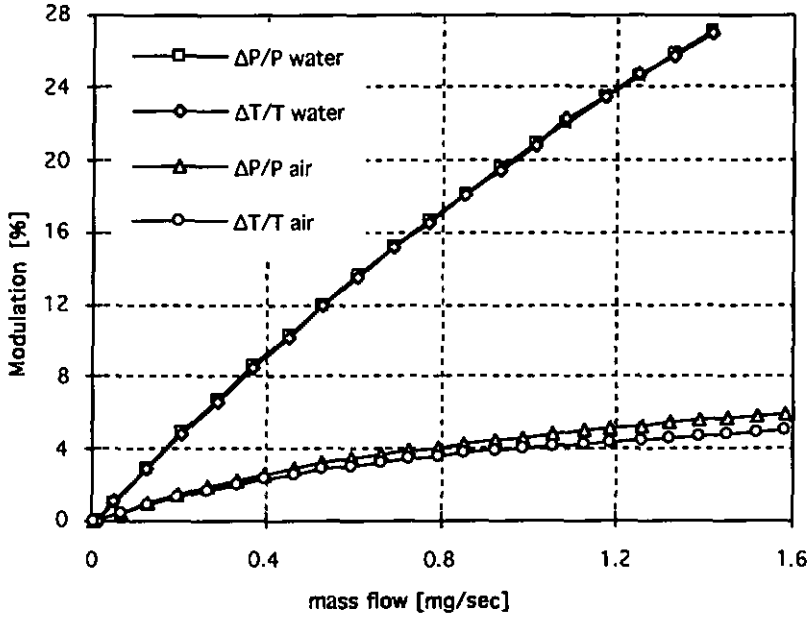

Figure 4.14: Measured sensitivity for water and air with Sigma-Delta conversion and constant heater temperature.

4.5 Summary

A linear silicon calorimetric mass-flow sensor for both liquids and gases has been realised using an industrial bipolar process in combination with an industrial thick-film process. By presenting the flow to the back of the sensor chip, the response was not affected by contamination. A temperature controller and current sources were realised on-chip, in addition to four temperature sensors and two heating resistors.

An analytic sensor model has been found that predicts a linear relation between sensor output and mass-flow. Furthermore, it is shown that the sensor sensitivity only depends on the heat capacity of the fluid and the sensor heat conductance.

A special Sigma-Delta converter (14 bit, 50 kHz) has been developed that offered stable digital measurement of heating current. In combination with the calorimetric sensor, an extended linear range up to 1.5 mg/sec for water with a sensitivity of 10000 counts/(mg/sec) was found. The sensitivity was in good agreement with the measurements with the on-chip temperature controller. Offset and drift were easily eliminated for both measurement methods. Furthermore, the sensor is independent of fluid pressure, fluid velocity and ambient temperature.

5 DISCUSSION

This chapter compares the sensors presented in the previous three chapters. Section 5.1 discusses the different measurement principles of the sensors and the parameters determining the sensor transfer functions whereas section 5.2 discusses the performance of the sensors. Section 5.3 gives an overview of possible applications and section 5.4 presents a summary of this thesis.

5.1 Flow Measurement Concepts

Table 5.1 lists the characteristics of the different physical principles of the three sensors that have been developed. The table shows the intermediate quantities and the parameters which determine the sensor transfer functions. The orifice flow sensor detects a flow dependent pressure drop, whereas the other sensors detect flow dependent temperature changes. However, the hot-wire sensor and the calorimetric sensor are basically different since the hot-wire sensor is based on heat transfer from one spot into the fluid, whereas the calorimetric one is based on a fluid dependent temperature gradient along the entire measurement tube. Conversion from the intermediate quantity to the electrical information signal is also realised in different ways: Piezoresistors measure the pressure drop for the orifice flow sensor, whereas diodes measure the temperature differences in the hot-wire and the calorimetric sensor.
The sensor transfer functions depend on fluid and sensor properties, which each has its own impact on the sensor behaviour. The fluid properties are determined by the choice of the measurement principle, whereas the sensor properties depend on the choice of the sensor material. By choosing the right materials, conventional sensors are optimised for high sensitivity and small influence of perturbing quantities. However, silicon is normally not chosen because of its properties, but because it allows for batch processing and realisation of on-chip electronics. As a consequence, the properties of silicon might perturb the sensor function more than conventional sensors, which have more freedom in the choice of materials.

5.1.1 Fluid Parameters

Four fluid properties that contribute to the sensor transfer functions can be distinguished: density, viscosity, heat conductivity and heat capacity. The transfer function of orifice flow sensors (equation 2.8), depends on the square root of the fluid density. Hence, the gas pressure has to be known for precise measurement. Since the correction factor β depends on the Reynolds number, the gas viscosity has an influence on the sensor behaviour too. The transfer

function of hot-wire flow sensors, (equation 3.10), depends on the Reynolds number and the Prandtl number. Therefore, the sensitivity of these sensors is determined by the heat conductivity, the heat capacity and the viscosity of the fluid. If gas flow is measured, the fluid pressure also appears in the transfer function. The transfer function of calorimetric flow sensors, (equation 4.7), is linear proportional to the fluid heat capacity. Only the heat capacity of the fluid defines the sensor transfer function and furthermore, a linear response is obtained if the fluid heat transport is smaller than the fluid heat conduction. For high flows, the response becomes non-linear and dependent on the Reynolds number. The calorimetric principle is the best principle, since it only depends on one fluid parameter that hardly varies with perturbing quantities. For the other principles the fluid parameters are not constant, but vary with ambient temperature and fluid pressure.

Sensor	*Orifice*	*Hot-wire*	*Calorimetric*
Intermediate Quantity	*Pressure Drop*	*Heat Convection*	*Temperature Gradient*
Fluid Heat Conductivity		•	
Fluid Heat Capacity		•	•
Fluid Viscosity	•	•	
Fluid Density	•	•	
Silicon Heat Conductivity		•	•
Silicon Piezo Resistivity	•		

Table 5.1: Physical background of the silicon flow sensors and the parameters determining the sensor transfer function.

5.1.2 Sensor Dimensions and Material Properties

Not only the fluid parameters, but also the sensor dimensions and the material properties determine the sensor output. The sensitivity of silicon flow sensors is determined by the membrane size as well as the positioning of the temperature sensing diodes, piezo resistors and heat resistors. These dimensions are much better controlled for silicon sensors than for conventional sensors due to the application of IC-technology. For example, the heat resistors and the

temperature sensing diodes have to be carefully positioned for calorimetric flow sensors in order to achieve differential measurement without offset and drift. This positioning is guaranteed within 2 µm for the silicon calorimetric sensor by the photolithography of the fabrication process. Such a precision is not possible for conventional calorimetric flow sensors using platinum resistors that are wound around a stainless steel tube.
In contrast to the dimension control, the properties of silicon are not always better than the materials used for conventional sensors. The silicon heat conductivity and piezoresistivity are the main material properties which appear in the transfer functions of the silicon flow sensors.
The heat conductivity of silicon is for both the hot-wire and the calorimetric sensor a major parameter. However, for the hot-wire sensor this parameter appears in the bias component, whereas for the calorimetric sensor it appears in the sensitivity. Therefore, the temperature dependence of -0.35 %/°C of the silicon heat conductivity causes offset drift for the hot-wire flow sensor and sensitivity drift for the calorimetric flow sensor, although the shape of the cross-section eliminates the drift almost entirely for the calorimetric sensor.
The piezoresistivity of silicon is a major parameter for the orifice flow sensor which determines the sensor sensitivity for the pressure drop that is created by flow. The temperature dependence is about 0.25 %/°C for silicon resistors with a high piezoresistive effect. However, it can easily be compensated by using dedicated sensor read-out.
A remarkable difference between these two silicon properties is that the heat conductivity of silicon contributes to the first transfer function from flow to the intermediate quantity, whereas the piezoresistivity only contributes to the second transfer function from the intermediate quantity to the information signal. Hence, the piezoresistors can be replaced by other sensing elements to overcome disadvantages of the silicon piezoresistivity. Optical and capacitive detection could be exploited to measure the pressure drop across the silicon cantilevers in the orifice. However, temperature measurement with thermocouples or SAW devices does not avoid the influence of the silicon heat conductivity in the hot-wire and the calorimetric sensor.

5.1.3 Compensation Methods

Compensation is necessary for many applications to cancel the temperature and pressure dependence of flow sensors. Compensation methods that improve the responses of the silicon sensors are discussed in detail. The sensors are all indirect sensors which convert the magnitude of the flow into an information signal y, by means of an intermediate quantity z. Figure 5.1 shows the block diagram of an indirect flow sensor, as was presented in figure 1.1 in a general way. The possible influence of ambient temperature and fluid pressure are indicated by T and P.

5.1.3.1 Compensation for the Orifice Flow Sensor

The orifice flow sensor is an indirect sensor with two totally different transfer functions which need different approaches for compensation of ambient

temperature and fluid pressure. The first sensor function f of the orifice flow sensor converts the magnitude of flow into a pressure difference. This function is of the self-generator type and shows no offset and drift [14,15]. Hence, the function O_1 equals zero and can be omitted. However, the sensitivity S_1 shows a large temperature dependence of 0.93 %/°C and a pressure dependence of -0.15 %/mbar.

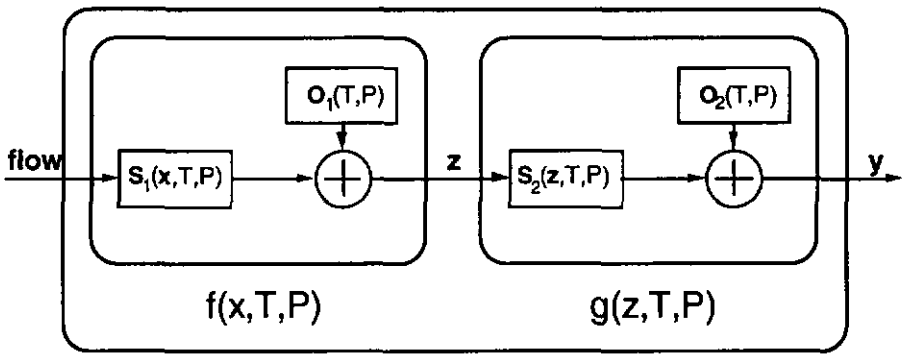

Figure 5.1: General block diagram of an indirect flow sensor with z the intermediate quantity and y the output signal. T and P denote the influence of ambient temperature and fluid pressure.

The second sensor function g converts the pressure difference into an electrical signal by means of silicon piezoresistors. This function is of the modulation type and both the functions O_2 and S_2 are affected by the ambient temperature, but not by the fluid pressure. The sensitivity function S_2 has a negative temperature dependence, which can partially compensate for the positive temperature dependence of S_1. A standard method to compensate for the temperature dependence of O_2 and S_2, is extending the Wheatstone bridge configuration with thick-film resistors that can be laser-trimmed. The values of these thick-film resistors can be calculated as function of the bridge current and output voltage for two pressures at two temperatures [29]. This method can also be used for the orifice sensor to cancel drift, since O_1 equals zero. However, it cannot create a high enough temperature dependence for S_2 that can compensate for the temperature dependence of S_1. Hence, external compensation has to be applied to cancel the temperature dependence of the sensitivity. To achieve such an external compensation, the output signal has to be modulated with the ambient temperature. Hence, the ambient temperature has to be measured by an additional temperature sensor. Also an additional pressure sensor is needed to compensate for the fluid pressure.

5.1.3.2 Compensation for the Hot-Wire Flow Sensor

The hot-wire sensor is an indirect sensor with two different transfer functions. The transfer function f converts the magnitude of flow into a temperature difference, whereas g converts the temperature difference into an electric output signal. The transfer function g is realised by a differential temperature sensor with sensitivity S_2, which is linear within 0.5 % full scale from 0 to 100 °C. The offset O_2 is effectively controlled by a potentiometer, as shown in figure 3.13.

Hence, drift and offset at the output y of the hot-wire sensor are totally determined by the first sensor function f. The function S_1 defines the modulation of the heat flow from the membrane into the fluid as function of the fluid velocity. The bias component O_1 is created by a constant heat flow in the membrane and is determined by the silicon heat conductivity which has a temperature dependence of -0.35 %/°C. The sensor can be regarded as a flow dependent heat conductance defined by O_1 with a large temperature coefficient that is supplied by the heater temperature T_{heat}. This heat conductance is modulated by the flow by means of S_1. Hence, King's law was written as $z = P_{diss} = (O_1 + S_1)\cdot T_{heat}$. Note the similarity with the absolute sensor for pressure, which consists of a single piezoresistor as is shown in figure 1.3a, where R_o equals O and ΔR equals S. For the same reasons, modulation of the heater temperature cannot be applied to keep O_1 at a constant value, since S_1 is also proportional to the heater temperature. Modulation of O_1 would transfer the temperature dependence from the bias component O_1 to the sensitivity S_1.
Application of differential measurement can cancel the temperature dependence of the first transfer function f. In order to achieve differential measurement, a second signal y_{ref}, has to be created which shows the same temperature dependence as y, but does not depend on the flow: $y_{ref} = g(O_1)$. Subtraction of y_{ref} from y then results in a final output signal y_{fin} that does not depend on O_1: $y_{fin} = y - y_{ref} = g(O_1 + S_1) - g(O_1) = g(S_1)$.
Three different ways are considered to determine the reference y_{ref} that has to be subtracted from the output signal y: a), measurement of y_{ref} with a second hot-wire sensor which is not exposed to the flow, b), Calculation and generation of y_{ref} as function of the parasitic quantities and c), measurement of y_{ref} with the same sensor by exposing the sensor alternately to the flow to be measured and a (zero) reference flow. The most straight forward solution for this requirement is given by the first method where a second flow sensor is used that is not exposed to the flow. In general, silicon sensors show excellent matching since their dimensions are extremely well defined by the photolithography process of IC-technology. Hence, by use of differential measurement implemented with two sensors, mismatch is reduced to a minimum, even if the response is non-linear for the ambient temperature and fluid pressure. The efficiency of this method is shown in figure 3.20. Application of the second method requires the implementation of a sensor which gives an output as function of the perturbing quantities P and T. Since this response has to equal exactly the response of the flow sensor in case no flow is present, calculation and generation of y_{ref} should only be used if implementation of a second flow sensor is too costly or if it would dissipate too much power. The third method exposes the sensor to different flows. This does not only acquire mechanical interaction for changing the sensor alignment, but it also cancels the advantage of the very short response time of hot-wire sensors. Furthermore, the mechanical interaction has to be extremely precise since a small variation in sensor positioning will cause a large sensitivity drift, as is concluded from figure 3.12. Also thermal drift is introduced when the boundary layers are not equal for both sensor positions. Hence, this method should only be considered if the first two methods fail. In case the sensor is bi-directional, the flow to be measured can be used as reference by mechanically alternating the sensor alignment to the flow. This

method was introduced as the 'Alternating Direction Method' [20].
The sensitivity of hot-wire sensors depends on many temperature dependent parameters (Factor O_1 of King's Law, equation 3.10). Therefore, the sensitivity has to be compensated for ambient temperature in many practical applications. For differential measurement, compensation can be achieved by modulating the heater temperatures of both sensors by the ambient temperature. As a result, the sensitivity S_1 becomes dependent on the ambient temperature whereas the bias components still will be cancelled, since they remain common mode for both sensors. An uncomplicated implementation of this compensation can be realised by supplying the temperature sensors on the membranes with a bias current that is different from the current supplied to the temperature sensors on the edge of the chips. This will result in different sensitivities for the temperature sensors. Hence, the heater temperature becomes a linear function of the ambient temperature and the sensitivity can be set by the choice of the supply currents of the temperature sensors.

5.1.3.3 Compensation for the Calorimetric Flow Sensor

The calorimetric flow sensor consists of a measurement tube that can be divided into two sections with a same heat conductance. Each section can be regarded as a sensor of which on end is kept at a certain heater temperature, whereas the other end of the tube section is maintained at ambient temperature. Hence, the calorimetric sensor can be regarded as a combination of two complementary sensors that are realised in one single chip. The output z of each sensor is given by the tube temperature in the middle of each tube section. Hence, both sensors have and equal bias component O_1 that equals half the heater temperature. However, the modulation S_1 of these complementary sensors is in anti-phase, since the output z decreases upstream from the heater, whereas it increases downstream, when a flow is present. The bias components O_1 are equal and cancelled by differential sensing of the output temperatures of the complementary sensors. This differential signal is measured with the same differential temperature sensor as is used for the hot-wire sensor which has excellent offset and drift features. The efficiency of the differential arrangement depends on the matching of the two heat conductance's of the sensor. These conductance's are not only determined by the silicon sensor tube, but also by the positioning and gluing of the sensor die onto the ceramic. Also the free convection of air outside the tube contributes to mismatch. Mismatch leads to offset drift of the thermal output signal of the sensor, although the mismatch is much smaller for the silicon sensor than for conventional calorimetric sensors. However, offset can easily be regulated by adjustable resistors in series with the temperature sensing diodes. Hence, mismatch of the bias components O_1 are compensated with an imposed mismatch on O_2. Experiments demonstrated that offset drift is effectively suppressed by controlling the heater temperature to a fixed value, as shown in the graphs 4.11 and 4.13. The measurements with the Sigma-Delta converter show a constant offset. However, this offset can easily be cancelled by using adjustable resistors in parallel with the heat resistors.
The sensitivity depends slightly on ambient temperature and fluid pressure. If these small deviations are not acceptable, external compensation can be applied by modulating the sensor output signal with the perturbing quantities.

5.2 Sensor Performance

Table 5.2 lists the performance of the different sensors that have been realised. The calorimetric flow sensor is the only one that can be used for both gases and liquids. The hot-wire sensor is not sensitive enough for gases and the output signal of the orifice flow sensor drifts when the sensor is exposed to water.
The maximum flow range of the calorimetric flow sensor is small, although the accurate measurement range is much larger than that of the other sensors. Variation of the sensitivity is not possible, since the dimensions of the silicon chip determine the sensitivity. The sensitivity of the orifice flow sensor can be varied by a factor 3, as the fabrication process allows for different apertures. However, the flow range of the hot-wire sensor depends on the external conduit diameter which allows for large variation.

Sensors	*Orifice*	*Hot-wire*	*Calorimetric*
Fluid	*gases*	*liquids*	*gases & liquids*
Measurement Range	*1:10*	*1:10*	*1:30*
Max. Flow Range in mg/sec	*25 - 75*	*100 - 1 000 000*	*1.5*
Sensitivity	*quadratic*	*square root*	*linear*
Response Time in msec	*1*	*5*	*40*
Power Consumption	*0.3 mW/V_{bridge}*	*18 mW/°C*	*42 mW/°C*
Robustness	*fragile*	*encapsulation dependent*	*excellent*
Contamination	*sensitive*	*sensitive*	*insensitive*
Temperature Dependence	*moderate*	*large*	*negligible*
Pressure Dependence	*large*	*moderate*	*negligible*

Table 5.2: Comparison of the performance of the fabricated sensors.

A linear response is only found for the calorimetric flow sensor. The measurement concepts that are practised for the other sensors result in non-linear responses. The orifice flow sensor shows a quadratic response to the flow, whereas the response of the hot-wire flow sensor is proportional to the square root of the fluid velocity. Hence, the application of orifice and hot-wire flow sensors is difficult for feedback controllers, as a linear response is preferable for proper operation of these systems.
The response time of the orifice flow sensor is determined by the inertia of the cantilevers, whereas the response time for the hot-wire and the calorimetric flow sensor is determined by the heat capacity of respectively the membrane and the entire chip. Hence, the response time of the hot-wire and the orifice flow sensor are extremely short, whereas the response time of the calorimetric sensor is an order of magnitude larger. However, this silicon sensor is still much faster than conventional calorimetric flow sensors.
The power consumption of silicon sensors that exploit heating, is normally large because of the high thermal conductivity of silicon. Therefore, the power consumption for the hot-wire chip is an order of magnitude larger than for the orifice flow sensor. For a same heater temperature, the consumption of the calorimetric sensor is larger than for the hot-wire sensor, as for the calorimetric sensor the whole chip is used as a heat conductor. However, the efficiency is not lower, since its sensitivity is much larger than the sensitivity of the hot-wire sensor, allowing the calorimetric sensor to operate at much lower heater temperatures.
Robustness is important for applications in hostile environments. Only the calorimetric flow sensor will survive under extreme conditions, since the flow is presented to the back side of a thick membrane which can be coated with a protection layer for aggressive fluids. Protection for high fluid pressures can be achieved by application of a moulded package. The orifice flow sensor is fragile, since the cantilevers break when the flow becomes too high and when particles hit the cantilevers. Epoxy glue is used to encapsulated the hot-wire sensor and forms the weak point of the hot-wire sensor. Since it absorbs water, it causes either leakage currents or broken bond wires due to swelling.
Protecting the sensors from contamination is difficult, since fluids are never totally clean. The sensitivity of the calorimetric flow sensor is rather insensitive to such contamination, since the diameter of the flow channel is not a parameter of the sensor function. However, the sensitivity of the hot-wire sensor is strongly affected by contamination, since it not only changes the boundary layer across the chip, but it also decreases the heat conduction from the membrane to the surface of the contamination. The sensitivity of the orifice flow sensor is increased when dust particles partially block the sensor aperture.
The temperature dependence of the hot-wire flow sensor and the orifice flow sensor needs compensation, even when the ambient temperature changes a few degrees. However, the response of the calorimetric flow sensor does not drift.
The pressure dependence of the orifice flow sensor is very large and needs compensation. If the hot-wire is used for incompressible liquids, a small pressure dependence is observed that is probably due to bending of the membrane. However, a change of fluid pressure will result in a moderate change of sensitivity when such sensors are used for gas flows. Since the calorimetric

flow sensor is a mass-flow sensor, fluid pressure does not affect the sensor response at all. Possible compensation methods for ambient temperature and fluid pressure have been discussed in the previous section.

5.3 Sensor Applications

Applications for the orifice flow sensor are pressure control and maximum flow detection. As this sensor is very sensitive to differential pressure, it can be exploited in air conditioning systems when pressures up to a few mbar have to be measured. Furthermore, the sensor response suits well for maximum flow detection since it is quadratic. However, flow control is difficult since the response depends on ambient temperature and fluid pressure. A filter should be used in series with the sensor in order to avoid breaking and contamination of the fragile silicon cantilevers.
Applications for the hot-wire sensor are flow and turbulence detection and air bubble counting. In contrast to the orifice flow sensor, the sensitivity of this sensor is proportional to the square root of the signal and shows maximum sensitivity for the lower part of the measurement range. Therefore, this sensor detects whether a flow is present or not. Due to its short response time of only 5 msec, distinct pulses are created by air bubbles that pass the sensor and disorder the boundary layer. Hence, this device can be used as an air bubble counter. The RMS output voltage can be used as a no-flow indicator in large conduits: The turbulence of the flow is indicated by the large RMS output voltage of the sensor, which becomes zero when no flow is present.
Applications for the calorimetric mass-flow sensor are low-cost flow control and flow measurement for both gases and liquids, since it has a linear response which is independent to fluid pressure and ambient temperature. Furthermore, this sensor is very robust and insensitive to contamination. Although the precision is a little less than conventional calorimetric flow sensors because of sharp corners inside the sensor, production and calibration costs are much lower than for conventional sensors, since the sensor control circuit is entirely integrated on the device. The Sigma-Delta converter can easily be integrated on-chip as well.

5.4 Summary

A new classification for sensors is presented that distinguishes direct sensors from indirect ones and absolute sensors from relative ones. Direct sensors are better than indirect sensors, since the latter group fulfils two functions by conversion of the magnitude of the desired quantity into an information signal through an intermediate quantity. Relative sensors are better than absolute sensors, since for the latter group the stability of the transfer function determines the accuracy, whereas the stability of a reference source defines the accuracy for relative sensors. Differential measurement is a relative concept which is used in Wheatstone bridge configurations. Offset and drift are cancelled by using a second sensor as an active reference, which has an opposite or zero response for the desired quantity, but a same response for perturbing quantities.

The relevance of this classification has been demonstrated with three different flow sensors that have been designed and fabricated with standard bipolar wafer processing and standard packaging. Digital sensor read-out with high resolution has been realised for all sensors with Sigma-Delta conversion. All sensors have been tested at ambient temperatures ranging from 10 °C to 60 °C and at fluid pressures ranging from 0.1 bar to 2 bar for both water and air.

The bi-directional orifice flow sensor measures the differential pressure caused by a gas flow perpendicular to two silicon cantilevers suspended in an orifice. The bending of these cantilevers is measured by piezoresistors. According Bernoulli's law a quadratic sensor response is found that is affected by the fluid pressure and ambient temperature. However, the response is independent to the flow direction because of the symmetric design. The sensitivity measures 0.044 mV/V/(mg/sec)^2 or 5.7 counts/(mg/sec)^2 by using either a Wheatstone bridge or a Sigma-Delta converter. The temperature dependence is 0.93 %/°C and is reduced to 0.50 %/°C if the output is modulated by the temperature dependent bridge resistance. The sensitivity to the fluid pressure measures -0.15 %/mbar.

The hot-wire sensor measures the heat flow from a heated spot into water. The response is proportional to the square root of the fluid velocity, as predicted by King's Law. It is strongly affected by the sensor positioning and the temperature dependence of the fluid parameters, as the thermal boundary layer across the sensor determines the response. An effective compensation for temperature has been realised by using differential measurement with two sensors and a Sigma-Delta converter which resulted in a sensitivity of 115 counts/(mg/sec)$^{0.5}$.

The calorimetric flow sensor measures the temperature gradient along a conduit that is modulated by a gas or a liquid mass-flow. The response is linear and is only determined by the fluid heat capacity and the conduit heat conductivity. Measurement showed that the sensitivity is not affected by the fluid pressure and ambient temperature. A temperature controller and current sources have been realised on-chip along with temperature sensors. The sensor was made insensitive to contamination by presenting the flow to the backside of a 50-100 µm thick membrane. With a Sigma-Delta converter, a linear range up to 1.5 mg/sec and a sensitivity of 10000 counts/(mg/sec) has been realised. Hence, this sensor has several advantages for commercialisation: It is not only linear, but also independent of fluid pressure, ambient temperature and contamination.

References

1 S. Bouwstra, R. Legtenberg and H.A.C. Tilmans,'Resonating Micro-bridge Mass Flow Sensor, *Proc. 5th Int. Conf. Solid-State Sensors and Actuators (Transducers '89 & Eurosensors III), Montreux, Switzerland, 1989*, pp. 140 - 141.

2 A. van Herwaarden, Thermal Vacuum Sensors based on Integrated Silicon Thermopiles, *Ph.D. Thesis*, University of Delft, The Netherlands 1987.

3 M. Hohenstatt, Thermal Mass Flow Meters, *Sensors, a Comprehensive Survey*, VZH Weinheim, 1990, volume 4, pp. 323 - 343.

4 J.H. Huijsing, Signal Conditioning on the Sensor Chip, *Sensors and Actuators, 10* (1986) 219 - 237.

5 J.H. Huijsing, F.R. Riedijk and G. van der Horn, Developments in Integrated Smart Sensors, *Proc. 7th Int. Conf. Solid-state Sensors and Actuators (Transducers '93), Yokohama, Japan, june 7 -10, 1993*, pp. 320 - 326.

6 F.P. Incropera and D.P. De Witt, *Fundamentals of Heat and Mass Transfer*, Wiley, New York, 3rd edn., 1990, chapters 5,6,7 and 8.

7 R.G. Johnson and R.E. Higashi, A Highly Sensitive Silicon Chip Microtransducer for Air Flow and Differential Pressure Sensing Applications, *Sensors and Actuators, 11* (1987) 63 - 72.

8 W. Jouwsma, Marketing and Design in Flow Sensing, *Sensors and Actuators A, 37-38* (1993) 274 - 279.

9 W. Jouwsma and H.J. Boer, Private comminucation with Bronkhorst High-Tech, Ruurlo, The Netherlands, June, 1994.

10 W. Kalide, *Einführung in die Technische Strömungslehre*, Carl Hanser Verlag, München - Wien, 1980, pp. 173 - 179.

11 B. Kloeck, Design, Fabrication and Characterisation of Piezoresistive Pressure Sensors, including the Study of Electrochemical Etch-Stop, *Ph.D. Thesis*, Institute of Microtechnology, University of Neuchâtel, Switzerland, 1993.

12 T.S.J. Lammerink, M. Elwenspoek and J.H.J. Fluitman, Integrated Micro-liquid Dosing System, *Proc. IEEE MEMS, Fort Lauderdale, Florida, USA, 1993*, pp. 254 - 259.

13 Ch. Linder and D. Kerschbaumer, Evaluation von Sensoren für Klima Anlagen, Insbesondere von Fluss-Sensoren, *Internal report No. 208 EC 01/87*, Institute of Microtechnology, Neuchâtel, Switzerland, 1987.

14 S. Middelhoek and A.C. Hoogerwerf, Classifying Solid-State Sensors: the 'Sensor Effect Cube', *Sensors and Actuators, 10* (1986) 1 - 8.

15 S. Middelhoek and D.J.W. Noorlag, Signal Conversion in Solid-State Transducers, *Sensors and Actuators*, 2 (1982) 211 - 228.

16 D. Moser, CMOS flow sensors, *Ph.D. Thesis*, E.T.H., Zurich, Switzerland, 1993.

17 B.W. van Oudheusden and J.H. Huijsing, An integrated silicon flow-direction sensor, *Sensors and Actuators, 16* (1989) 109 - 119.

18 K.E. Petersen, J. Brown and W. Renken, High-precision, High-performance Mass Flow Sensor with Integral Laminar Flow Micro-channels, *Proc. 3rd Int. Conf. Solid-State Sensors and Actuators (Transducers '85), Philadelphia, USA, 1985*, pp. 830 - 833.

19 A.F.P. van Putten, Integrated silicon anometers. *Ph.D. Thesis*, University of Leuven, Belgium, 1988.

20 M.J.A.M van Putten, M.H.P.M van Putten and A.F.P. van Putten, Full Additive Drift Elimination in Vector Sensors using the Alternating Direction Method (ADM), *Sensors and Actuators, A 44* (1994) 13 - 17.

21 Rosemount Brooks Instrument Division, *Catalogue of Products for Flow Control, 1991-1992.*

22 D.M. Rowe and C.M. Bhandari, Preparation and Thermal Conductivity of Doped Semiconductors, *Prog. crystal growth and charact., 13* (1986) 254 - 257.

23 H. Schlichting, *Grenzschicht Theorie*, Verlag G. Braun, Karlsruhe 1963, pp. 552 - 558.

24 E.A. Schönbächler, A highly sensitive orifice flow and pressure sensor, *Masters Thesis*, E.P.F., Lausanne, Switzerland, 1993.

25 G. Stemme, A micromachined, silicon mass-air-flow sensor for automotive applications, *Proc. 6th Int. Conf. Solid-state Sensors and Actuators (Transducers '91), San Francisco, CA, USA, June 24-28, 1991*, pp. 30 - 33.

26 C.H. Stephan and M. Zanini, A monolitic gas low sensor with polyimide as thermal insulator, *IEEE Trans. Electron Devices, ED-33* (1986) 254 - 256.

27 O. Tabata, H. Inagaki and I. Igarashi, Monolithic pressure-flow sensor, *IEEE Trans. Electron Devices, ED-34* (1987) 2456 - 2462.

28 T. Tschan, N.F. de Rooij, A. Bezinge, S. Ansermet and J. Berthoud, Characterization and Modelling of Silicon Piezoresistive Silicon Accelerometers Fabricated by a Bipolar-compatible Process, *Sensors and Actuators, A25 - A27* (1991) 605 - 609.

29 A.J. van der Wiel, An exact Wheatstone bridge trimming procedure for zero offset and zero temperature drift for offset and sensitivity, *Internal report to ASCOM Microelectronics*, Dec. (1993).

30 W.C. Young, *Roak's Formulas for Stress & Strain*, McGraw-Hill, New York, 6th edn., 1989, pp. 93 - 107.

Acknowledgements

Many people encouraged me in various ways during this project.

Of these people I especially like to thank

N.F. de Rooij, for his stimulation and all the support I needed to carry out this work,

Christian Linder, Alex Bezinge and in particularly Arno Hoogerwerf, for their inspiring conversations, their successful collaboration and help with the publications,

Edgar A. Schönbächler, for the design and investigations of the orifice flow sensor,

My colleagues Marc Boillat and Stephan Trautweiler, for their discussions and help,

W. Jouwsma and H.J. de Boer of Bronkhorst High Tech, for their fruitful discussions and sensor characterisations,

All collaborators of ASCOM Microelectronics, especially D. Otter, J. Ardalan, L. Kendall, J.J. Vuillemier and W. Pfeiffer, for their work, interest and discussions,

My colleagues at the I.M.T, for their help and friendship,

Tjalf Ubbens, for his discussions in evenings and weekends,

M. De Grauwe, H.J. Huijsing and A.C. Hoogerwerf as a collaborator of ASCOM Microelectronics, for kindly agreeing to be co-examiners and

The Feldschlösschen Brewery, for lending me two beer kegs.

Furthermore the financial support of the Committee for the Promotion of Applied Scientific Research and the LESIT research program is greatly acknowledged.

P.S. In July 1994 ASCOM Microelectronics was taken over by Micronas Semiconductor S.A.

Appo van der Wiel,
November 1994.

Curriculum Vitae

Appolonius Jacobus van der Wiel was born in Ede, the Netherlands in 1964. In 1983 he started his study in Electrical Engineering at the Technical University of Twente. In 1988 he interrupted his study for one year to work as a teaching assistant at the University of Zambia. In 1989 he worked as a trainee at the Institute of Microtechnology in Neuchâtel on the fabrication of a high temperature pressure sensor with polysilicon piezoresistors. In 1990 he finished his masters project on the development of CAD analog tools. In the same year, he started at the Institute of Microtechnology in Neuchâtel his PhD. project of which a summary is given in this thesis. This project was carried out in close collaboration with ASCOM Microelectronics in Bevaix, Switzerland.

Publications

A.J. van der Wiel, C. Linder, A. Bezinge and N.F. de Rooij, A liquid Velocity Sensor based on the Hot-Wire Principle, *Sensors and Actuators, A37-A38*(1993) 693 - 697.

A.J. van der Wiel, A.C. Hoogerwerf and N.F. de Rooij, A Calorimetric Mass-Flow Sensor for Hostile Environments, *Proc. 7th Int. Conf. Solid-state Sensors and Actuators (Transducers '93), Yokohama, Japan, June 7 -10, 1993,* pp. 800 - 803.

A paper about the orifice flow sensor and a paper about the temperature and pressure characteristics of the calorimetric flow sensor are in preparation.